Mitochondrial Protein Import Motor PAM Reacts on Protein Misfolding Stress by Protein Import Reduction and Induction of PINK1-Mitophagy

Dissertation

zur Erlangung des Doktorgrades

der Naturwissenschaften

vorgelegt beim Fachbereich 14

der Johann Wolfgang Goethe-Universität

in Frankfurt am Main

von

Jonas Benjamin Michaelis

aus Frankfurt am Main

Frankfurt am Main, 2022

D30

vom Fachbereich 14 der
Goethe - Universität Frankfurt als Dissertation angenommen

Dekan: Prof. Dr. Clemens Glaubitz

Gutachter: Prof. Dr. Volker Dötsch

Dr. Christian Münch

Datum der Disputation: ……

Table of content

I List of abbreviations

ΔΨ	Mitochondrial membrane potential
µM	Micromolar
AAA	ATPases associated with diverse cellular activities
AD	Alzheimer's disease
ADP	Adenosine diphosphate
AMP	Adenosine mono-phosphate
Anti	Antimycin A1
AO	Combination of Antimycin A1 and Oligomycin
ATG	Autophagy-related
ATP	Adenosine triphosphate
BafA1	Bafilomycin A1
BAK	Bcl-2 homologous antagonist/killer (synonym BAK1)
BAX	Apoptosis regulator BAX
BCL2	B-cell lymphoma 2 gene (*implication* regulator protein of apoptosis)
BCL2L13	Bcl-2-like protein 13
BH3 domain	Bcl-2 homology 3 domain
BNIP3	BCL2/adenovirus E1B 19 kDa protein-interacting protein 3
BNIP3L	BCL2/adenovirus E1B 19 kDa protein-interacting protein 3-like (synonym NIX)
CALCOCO2	Calcium-binding and coiled-coil domain-containing protein 2 (synonym NDP52)
Cas9	CRISPR-associated endonuclease Cas9
CCCP	Carbonyl cyanide m-chlorophenyl hydrazone
cDNA	Coding deoxyribonucleic acid
CMA	Chaperone mediated autophagy
CRISPR	Clustered regularly interspaced short palindromic repeats
DFP	Deferiprone
DMSO	Dimethyl sulfoxide
DNA	Deoxyribonucleic acid
DRP1	Dynamin-related protein 1 or Dynamin-1-like protein (synonym DNML1)
E3	Enzyme 3 (ubiquitin ligases)
EDTA	Ethylenediaminetetraacetic acid
EGFP	Enhanced green fluorescent protein
ER	Endoplasmic reticulum
FACS	Fluorescence-activated cell sorting

FBS	Fetal bovine serum
Fe/S	Iron-sulfur
FIS1	Mitochondrial fission 1 protein
FUNDC1	FUN14 domain-containing protein 1
GO	Gene ontology
gRNA	Guide ribonucleic acid
HD	Huntington's disease
HeLa cells	Immortalized cell line based on primary samples from Henrietta Lacks
HSP	Heat shock protein
Hygro	Hygromycin
IMM	Inner mitochondrial membrane
IMS	Intermembrane space
KO	Knockout (gene deletion)
LC3	Microtubule-associated proteins 1A/1B light chain 3B
LIR	LC3-interacting region
MAM	Mitochondria-associated ER membranes
mePROD	Multiplexed enhanced Protein Dynamic
mePROD^{mt}	mitochondrial proteome-targeting mePROD
mKEIMA	Monomeric KEIMA
mPOS	Mitochondrial precursor over-accumulation stress
MS	Mass spectrometry
mt	Mitochondrial
mtDNA	Mitochondrial deoxyribonucleic acid
MTS	Mitochondrial targeting sequence
Neo	Neomycin
NIX	NIP3-like protein X (synonym BNIP3L)
nm	Nanometer
nM	Nanomolar
NPD52	Antigen nuclear dot 52 kDa protein (synonym CALCOCO2)
NTC	Non-targeting control
N-terminal	Amino-terminal end of polypeptide/ protein
Oligo	Oligomycin
OMM	Outer mitochondrial membrane
OPTN	Optineurin
p62	Sequestosome-1 (synonym SQSTM1)

PAM	Presequence translocase associated import motor
PARKIN	E3 ubiquitin-protein ligase PARKIN (gene *PARK2*, *PRKN*)
PARL	Presenilins-associated rhomboid-like protein, mitochondrial
PBS	Phosphate-buffered saline
PD	Parkinson's disease or disorder
PINK1	PTEN-induced kinase 1
PSM	Post-translational modificatio
RNA	Ribonucleic acid
RNAi	RNA interference
ROS	Reactive oxygen species
s.d.	Standard deviation
sgRNA	Single guide RNA
SILAC	Stable isotope labeling by/with amino acids in cell culture
siRNA	Small interfering RNA
TCA	Tricarboxylic acid
TIM	Translocase of the inner mitochondrial membrane
tM2	Thresholded Mander's coefficient 2 (comparing channel 2 to channel 1)
TMRE	Tetramethylrhodamine
TMT	Tandem Mass Tag
TOM	Translocase of the outer mitochondrial membrane
UPRam	Unfolded protein response activated by mistargeting of proteins
UPR^{mt}	Mitochondrial unfolded protein response
UPS	Ubiquitin-proteasome system
USP30	Ubiquitin-specific peptidase 30
WT	Wild type

II List of figures

III Summary

Mitochondria are important for cellular health and their dysfunction is linked to a variety of diseases, especially neurodegeneration. Thus, the renewal and degradation of dysfunctional mitochondria is crucial for the well-being of organisms. The selective digestion of damaged mitochondria via the lysosome (mitophagy), is the main pathway to do so.

In my dissertational work, I investigated the connection between protein misfolding, protein import into mitochondria and the degradation of mitochondria via mitophagy. Here, I present a new model for the initiation of mitophagy without collapse of the membrane potential. This model provides the link between protein import into mitochondria, stress signal transduction to the cytosol and the mitochondrial stress sensor PINK1. To comprehensively examine how mitophagy can be triggered, I performed a genome-wide CRISPR knockout screen utilizing the mitophagy reporter mitochondrial mKEIMA. Thereby, I observed numerous novel gene deletions that induce mitophagy. Prominently, I identified an accumulation of gene deletions of the protein import and of protein quality control factors. I validated several of those and examined HSPA9 (mitochondrial HSP70) and LONP1 (a mitochondrial matrix AAA protease) in more detail, regarding their effect on mitophagy and protein import. For this, I used an established fluorescence-based, mitochondrial-targeted EGFP, as well as a newly-developed pulsed-SILAC mass spectrometry approach (mePROD^{mt}). Depletions of both genes resulted in reduced protein import and PINK1-dependent mitophagy. Strikingly, I did not observe any loss of mitochondrial membrane potential, which was hitherto believed to be essential for activation of PINK1-mediated mitophagy. Literature shows that certain mitochondrial stressors can also induce mitophagy without mitochondrial membrane depolarization, which I confirmed with my assays. Next, I characterized the impact of *LONP1* and *HSPA9* depletion, which are involved in proteostasis maintenance, and the mtHSP90 inhibitor GTPP on mitochondrial protein folding in more detail. GTPP treatment and *LONP1* depletion both resulted in the accumulation of an insoluble protein fraction, as judged by proteomic analysis. This insoluble protein fraction enriched several components of the presequence translocase-associated motor PAM, including TIMM44. TIMM44 acts as a link between

the translocon, the import pore of the inner mitochondrial membrane (TIM) complex and the PAM complex. Thus, I hypothesized that TIMM44 dissociates from the TIM complex upon protein folding stress, when it becomes part of the insoluble protein fraction. To validate this model, I measured the TIMM44 interactome upon proteostasis disturbance using proximity labeling. Indeed, interaction of TIMM44 with the import pore was almost completely abolished, explaining the loss of matrix-targeted import upon protein folding stress. From these findings, I reasoned that an import reduction mediated by the PAM complex would likely also inhibit the degradation of PINK1. Consistent with this hypothesis, I observed that mitophagy induced by *HSPA9* or *LONP1* deletion was prevented when *PINK1* was genetically deleted. In comparison, non-processed PINK1 was stabilized on mitochondria in wild type cells when mitochondrial protein import was impaired. On this basis, I drew the conclusion that the loss of mitochondrial import was the stress signal, which leads to the stabilization of PINK1, as it could not be processed anymore via the inner mitochondrial membrane protease PARL. PINK1 auto-activates itself upon accumulation and signals to the cytosol that this mitochondrion is damaged. Mitophagy is subsequently initiated by the ubiquitin kinase activity of PINK1. As a result, the autophagy apparatus gets activated, damaged mitochondria are engulfed by a double membrane and removed via lysosomal digestion. This proposed model is, to the best of my knowledge, the first to provide an explanation for protein folding stress-induced and protein import inhibition-triggered mitophagy without mitochondrial depolarization. The model thus extends the PINK1/PARKIN-dependent mitophagy pathway to milder stresses and clears some of the open questions in the field. Furthermore, this work is also important, because protein misfolding stress and dysfunctional mitochondria are two hallmarks of neurodegeneration. In particular, mitochondrial protein import inhibition during Parkinson's and Huntington disease might be driver of mitochondrial dysfunction. Hence, I hope and anticipate that the newly developed protein import method, mePROD^{mt}, and the proposed model will be beneficial to further characterize underlying processes and to establish which factors prevent or drive these disorders on molecular level.

IV Zusammenfassung

Mitochondrien versorgen die Zelle mit Energie, Metaboliten und Eisen-Schwefel-Clustern, die essentiell für die zelluläre Gesundheit sind. Die Erneuerung und der Abbau dysfunktionaler Mitochondrien ist mithin entscheidend für die Funktion des Organismus. Mitochondriale Fehlfunktion wird daher auch mit einer Reihe von Krankheiten in Verbindung gebracht, insbesondere mit Neurodegeneration und Herzkrankheiten. Der zelluläre Selbstverdau, die sogenannte „Autophagie“ spielt hierbei eine wichtige Rolle. Geschädigter Mitochondrien werden dabei, durch eine Doppelmembran umschlossen und mittels Fusion mit dem Lysosom abgebaut werde. Diese Form der selektiven Autophagie wird bei Mitochondrien als Mitophagie bezeichnet. Sie ist der wichtigste Weg, um Mitochondrien abzubauen und der Akkumulation beschädigter Mitochondrien vorzubeugen.

In meiner Dissertation untersuchte ich den Zusammenhang zwischen Proteinfehlfaltung, Proteinimport in Mitochondrien und dem Abbau von Mitochondrien durch Mitophagie. Hier stelle ich ein neues Modell für die Einleitung der Mitophagie ohne Zusammenbruch des mitochondrialen Membranpotenzials vor. Dieses Modell erklärt die Verbindung zwischen dem Proteinimport in die Mitochondrien, der Weiterleitung von Stresssignalen an das Zytosol und wie der mitochondriale Stresssensor PINK1 auf Mitochondrien stabilisiert werden kann. Um umfassend zu testen, welche Faktoren Mitophagie auslösen können, führte ich einen genomweiten CRISPR-Knockout-Screen mit dem Mitophagie-Reporter mKEIMA durch. Hierbei konnten zahlreiche neue Gendeletionen identifizieren werden, die Mitophagie auslösen. Innerhalb dieser Gendeletionen beobachtete ich eine Anhäufung von Genen, die für Proteinimportfaktoren und für die Qualitätskontrolle von Proteinen kodieren. Zunächst validierte ich mehrere von diesen Kandidaten mittels individueller Gendeletion und untersuchte anschließend *HSPA9* (mitochondriales HSP70, ein Chaperon notwendig für Proteinimport in Mitochondrien und Proteinfaltung in der Matrix) sowie *LONP1* (eine mitochondriale AAA-Protease, notwendig für den Abbau von beschädigten Proteinen in Mitochondrien) genauer in Hinblick auf ihre Wirkung auf Mitophagie. Dabei interessierte mich vor allem, wie der Verlust dieser Proteine Mitophagie initiierte. Der aktuell bekannteste Mechanismus zur Mitophagie-Aktivierung resultiert aus

dem Zusammenbruch des mitochondrialen Membranpotentials, welches sich mittels der Atmungskette zwischen der Matrix und dem Intermembranraum aufbaut. Hierbei sorgt der Verlust des Membranpotentials dafür, dass der Mitophagiesensor PINK1 nicht mehr über die innere mitochondriale Membran transportiert werden kann, wo er unter Normalbedingungen durch die PARL Protease geschnitten und hierdurch destabilisiert würde. Anschließend würde destabilisiertes PINK1 im Zytosol durch das Proteasom, die Hauptprotease der Zelle, abgebaut werden. Bei verringerten Proteinlevel von HSPA9 oder LONP1 in Mitochondrien, sehe ich allerdings keinen Zusammenbruch des Membranpotentials, nichtsdestotrotz wird PINK1 unter diesen Bedingungen stabilisiert. In der Literatur wurden ebenfalls weitere Behandlungen beschrieben, bei denen das eben dargestellte Modell nicht erklären kann, wie der Abbau der Mitochondrien über PINK1 aktiviert werden konnte. Um diese offene Frage zu klären, untersuchte ich den mitochondrialen Proteinimport genauer. Hierzu verwendete ich zum einen ein etabliertes fluoreszenzbasiertes Untersuchungsverfahren bei dem mitochondriales grün fluoreszierendes Protein zusammen mit dem mitochondrialen Farbstoff Mitotracker Deep Red lokalisiert, falls mitochondriale Proteinimport vorhanden ist und schließe daraus auf Proteinimportdefekte, sowie zum anderen unser neu entwickeltes Massenspektrometrie-verfahren, mePROD^{mt}, welches auf gepulster *Stable Isotope Labeling by/with Amino acids in Cell culture* (SILAC)-Markierung basiert. Das letztgenannte Verfahren erlaubte es, neben der generellen Auswirkung auf den Proteinimport, auch Proteine individuell zu messen und festzustellen in wie weit diese noch in Mitochondrien aufgenommen werden. Mit dieser Methode untersuchten meine Kollegen und ich zusätzlich verschiedene Wirkstoffe, welche bereits Mitophagie-Induktion in anderen Studien gezeigt hatten, auf ihren mitochondrialen Proteinimport-Effekt. Diese Wirkstoffe zeigten auch in unseren Experimenten Mitophagy und sorgten gleichzeitig für eine Inhibition des Proteinimports. Daraus schlussfolgerte ich, dass wahrscheinlich nicht der Zusammenbruch des Membranpotentials für die PINK1-Stabiliserung verantwortlich war, sondern vielmehr der verlangsamte oder blockierte Proteinimport ausreichend war, so dass PINK1 nicht mehr über die innere mitochondriale Membran transportiert wurde und somit nicht durch die Intramembran-Protease PARL geschnitten werden konnte. Um zu zeigen, dass PINK1 tatsächlich nicht mehr durch PARL prozessiert wurde, isolierte ich

Mitochondrien von *HSPA9* oder *LONP1* RNAi-behandelten Zellen und wies die unprozessierte Form von PINK1 nach. Zusätzlich überprüfte ich mittels *PINK1* Knockout Zellen die PINK1-Abhängigkeit der Mitophagie-Aktivierung und stellte eine fast vollständige Inhibition gegenüber Wildtyp Zellen fest. Da HSPA9 ein essentieller Teil des Proteinimportmotors PAM ist, ist es naheliegend, dass der Verlust von *HSPA9* dafür sorgt, dass der Proteinimport in Mitochondrien inhibiert und somit weniger PINK1 prozessiert wird. Für *LONP1* RNAi und den mitochondrialen HSP90-Inhibitor GTPP hingegen ist es nicht direkt ersichtlich. Es ist allerdings bekannt, dass mitochondriales HSP90 sowie LONP1 für die Aufrechterhaltung des Proteingleichgewichts in Mitochondrien wichtig sind, weshalb ich deren Effekt auf die mitochondriale Proteinfaltung genauer untersuchte. Mittels Isolation von Mitochondrien aus Zellen und anschließendem Auflösen der mitochondrialen Membranen durch milde Detergenzien extrahierte ich eine unlösliche Proteinfraktion. In GTPP- als auch *LONP1* RNAi-behandelten Zellen, war eine Akkumulation dieser unlöslichen Proteinfraktion durch massenspektrometrische Analysen nachweisbar. Neben Bestandteilen aus der mitochondrialen Translationsmaschinerie und aus der Atmungskette waren mehrere Komponenten des PAM-Proteinimportmotors angereichert. Insbesondere TIMM44, HSPA9, sowie deren Ko-Chaperone GRPEL1 und 2 wurden detektiert. TIMM44 wirkt als Bindeglied zwischen dem Translokon, der Importpore der inneren mitochondrialen Membran (TIM Komplex) und dem PAM-Komplex. Es sorgt mithin für die Rekrutierung der weiteren PAM-Bestandteile und ist damit essentiell für einen funktionsfähigen Proteinimportmotor. Die gerade beschriebene Beobachtung, dass der PAM Komplex unter Proteinfaltungsstress ein Teil der unlöslichen Proteinfraktion wird, legt nahe, dass der Proteinimportmotor in diesem Zustand nicht mehr aktiv ist und vermutlich seine Lokalisation am TIM Komplex verliert. Um diese Hypothese zu überprüfen, untersuchte ich die TIMM44-Interaktionen mittels Nachbarschaftsmarkierung („proximity labeling“), eine Methode bei der die direkte Umgebung des Proteins mit Biotin markiert wird und anschließend über Streptavidin präzipitiert und nachgewiesen werden kann. Hierbei zeigte sich, dass TIMM44 fast vollständig den Kontakt mit der Importpore unter Proteinfaltungsstress verlor im Vergleich zu Kontrollbedingungen. Dies erklärte somit weshalb der Proteinimport in Mitochondrien unter Proteinfaltungsstress gestört war: Der Proteinimportmotor PAM löst sich unter der Akkumulation von

fehlgefalteten Protein von der Importpore und bindet die unlösliche Proteinfraktion oder entfaltet sich selbst und wird Teil von ihr. Das hat eine verringerte Konzentration an Proteinimportmotor-Komponenten am TIM Komplex zur Folge, wodurch, ähnlich wie bei *HSPA9* RNAi, der Proteinimport in Mitochondrien verlangsamt wird. Dies wiederum sorgt für geringe Prozessierung von PINK1 durch PARL und Mitophagie wird aktiviert. Zusammenfassend, haben ich damit einen neuen Mechanismus zur Mitophagie-Aktivierung entdeckt, der auf Proteinfaltungsstress reagieren kann und bereits ausgelöst wird bevor das mitochondriale Membranpotential zusammenbricht. Die darauffolgenden Schritte des Mitophagieprozesses sind aus der Literatur bekannt: PINK1 akkumuliert auf Mitochondrien in der mitochondrialen äußeren Membran und aktiviert benachbarte PINK1 Moleküle durch *trans*-Autophosphorilierung. Dadurch wird die Kinasefunktion von PINK1 aktiver und phosphoryliert Ubiquitin-Proteinreste auf der mitochondrialen Oberfläche. Dies wiederum rekrutiert die E3-Ubiquitin-Ligase PARKIN, welche das Mitophagie-Signal verstärkt und dadurch Mitophagie-Rezeptoren an das markierte Mitochondrium bindet. Diese Mitophagie-Rezeptoren sorgen nun für die Aktivierung des Autophagie-Apparats, welcher eine Vielzahl von Prozessen in Gang setzt, um das beschädigte Mitochondrium mit einer Doppelmembran zu umgeben. Das so eingeschlossene Mitochondrium, ein sogenanntes (Mito)-Autophagosom, fusioniert schließlich mit dem Lysosom. Lysosomale Enzyme bauen dann das Mitochondrium samt unlöslicher Proteinfraktion ab und schützen so die Zelle vor schädlichen Folgen. Mein Modell könnte also einen Früherkennungsmechanismus darstellen, der Mitophagie aktiviert, um durch Proteinfaltungsstress beschädigte Mitochondrien oder Mitochondrien mit defektem Proteinimport abzubauen, bevor diese eine dysfunktionale Atmungskette entwickeln, wodurch das mitochondriale Membranpotential mit der Zeit zusammenbricht.

Es wurde beobachtet, dass die Mitophagie im Alter nachlässt, wodurch dysfunktionale Mitochondrien die Zellen durch oxidativen Stress weiter belasten und zum Beispiel das Genom oder weitere Mitochondrien schädigen können. Letztlich kann dies zum intrinsischen Zelltod über die Permeabilisierung der äußeren mitochondrialen Membran führen und somit zum Verlust der Zelle. Im

Fall von Neuronen, die besonders anfällig für mitochondriale Schäden zu seien scheinen, trägt dieser fortschreitende Prozess zur Neurodegeneration bei. Im Fall von Parkinson wurden Formen, die eindeutig auf Mutationen in Mitophagie-Genen, zum Beispiel *PARK2*, *PARK6* oder *PARK7* (Synonyme für *PARKIN*, *PINK1* und *DJ-1*) zurückzuführen sind, festgestellt. Diese führten zu einer früh einsetzenden Parkinson-Krankheit. Des Weiteren, wurden unlösliche Proteinaggregate nachgewiesen, die den mitochondrialen Proteinimport inhibierten. Inwieweit diese Aggregate, den hier vorgestellten Mitophagie-Mechanismus verhindern, ist eine offene Frage. Doch die zuvor berichtete Korrelation zwischen Proteinfaltungsstress/ Proteinaggregation, Verlust an Mitophagie und inhibiertem mitochondrialen Proteinimport, deutet einen kausalen Zusammenhang an und bietet bei weiterer mechanistischer Forschung gegebenenfalls Ansatzpunkte für eine Therapie. So wurde in den letzten Jahren gezeigt, dass eine verstärkte Mitophagie, zumindest in neurodegenerativen Modellsystemen, für eine Verbesserung des zellulären Zustands sorgte. Die in dieser Doktorarbeit etablierte mitochondriale Proteinimport-Methode mePROD^{mt} wäre daher ein guter Ansatz um mittels Modell-Zelllinien oder mittels primärer Zellkulturen von Patientenproben ein besseres Verständnis der den Krankheiten zugrundeliegenden Mechanismen zu gewinnen.

1 Introduction

1.1 MITOCHONDRIAL FUNCTION

Mitochondria are intracellular organelles found in the eukaryotic cytoplasm. They were first described as such in 1886 by Richard Altmann (Altmann, 1894). According to the endosymbiont theory, mitochondria originated from the integration of an endosymbiotic α-proteobacterium into a host cell. During evolution, most genetic information was lost or transferred to the host nucleus (Zimorski et al., 2014; Roger et al., 2017). Remnant features of the endosymbiotic origin are still present in today's mitochondria: the double membrane, bacterial-origin cardiolipins and the presence of β-barrel proteins in the outer membrane, their own mitochondrial genome in form of cyclic chromosome and a separate mitochondrial translation machinery including mitochondrial ribosomes (W. Martin & Mentel, 2010; Tian et al., 2012; Pereira & Lupas, 2018).

Mitochondria contain two membranes with highly specialized phospholipid bilayers: The inner mitochondrial membrane (IMM), which contains the matrix, and outer mitochondrial membrane (OMM), surrounding the intermembrane space (IMS). The IMM forms curvy or folded membrane structures, called cristae, providing large surfaces for the respiratory chain and ATP-synthesis (Sjöstrand, 1953; Zick et al., 2009; Blum et al., 2019).

Mitochondria fulfill different roles for cell viability, including their important role in energy metabolism (Siekevitz, 1957). The tricarboxylic acid (TCA or citric acid, Krebs) cycle generates metabolites and reducing equivalents in the mitochondrial matrix, which are used as electron source in the respiratory chain (Kennedy & Lehninger, 1949, Bonora et al., 2012). The electrons are transferred to molecular oxygen, converting the freed energy to pump protons through the inner membrane into the IMS (Lodish et al., 2000). This proton gradient forms the mitochondrial membrane potential ΔΨ and is used by the F1FO-ATP-synthase to generate most of the cellular adenosine triphosphate (ATP), the main energy "currency" of the cell (Bonora et al., 2012). Besides energy production, metabolic enzymes in mitochondria enable the biosynthesis of amino acids, lipids, heme ring formation and iron-sulfur

clusters, all essential for cell function and proliferation (Paul et al., 2017; Dudek, 2017; Swenson et al., 2020). In addition, mitochondria are involved in apoptosis activation via permeabilization of the OMM and release of pro-apoptotic proteins (Crompton et al., 1998; Green & Kroemer, 2004). Furthermore, mitochondria are important for multiple steps of the innate immune response in higher eukaryotes by providing antibacterial, mitochondrial reactive oxygen species (ROS) or by regulating antiviral signaling (C. Wang & Youle, 2009; West et al., 2011; Song et al., 2021) (Figure 1).

Mitochondria form highly dynamic networks. They consist of vast spectrum of shapes, from small spheres, short or elongated tubules to highly branched, reticular networks, depending on the cell type or tissue (Galloway et al., 2012). By mitochondrial fission or fusion, its shape is defined and can be adjusted upon changing conditions. For communication, mitochondria form large contact sites with other organelles, especially the endoplasmic reticulum (ER) (Marchi et al., 2014). ER-mitochondria contacts are called mitochondria-associated ER membranes or MAMs. Via MAMs, the ER and mitochondria exchange lipids, regulate calcium release and act together to restore homeostasis, for example during inflammatory signaling (Poston et al., 2013; Vance, 2014; Vig et al., 2021).

This diverse set of functions and organization places mitochondria as one central organelle in maintaining cellular survival. As a consequence, mitochondrial impairment can lead to multiple age- or stress-associated diseases, such as cancer and neurodegenerative disorders (Y. Kang et al., 2018; Yablonska et al., 2019; Nicolas et al., 2019)

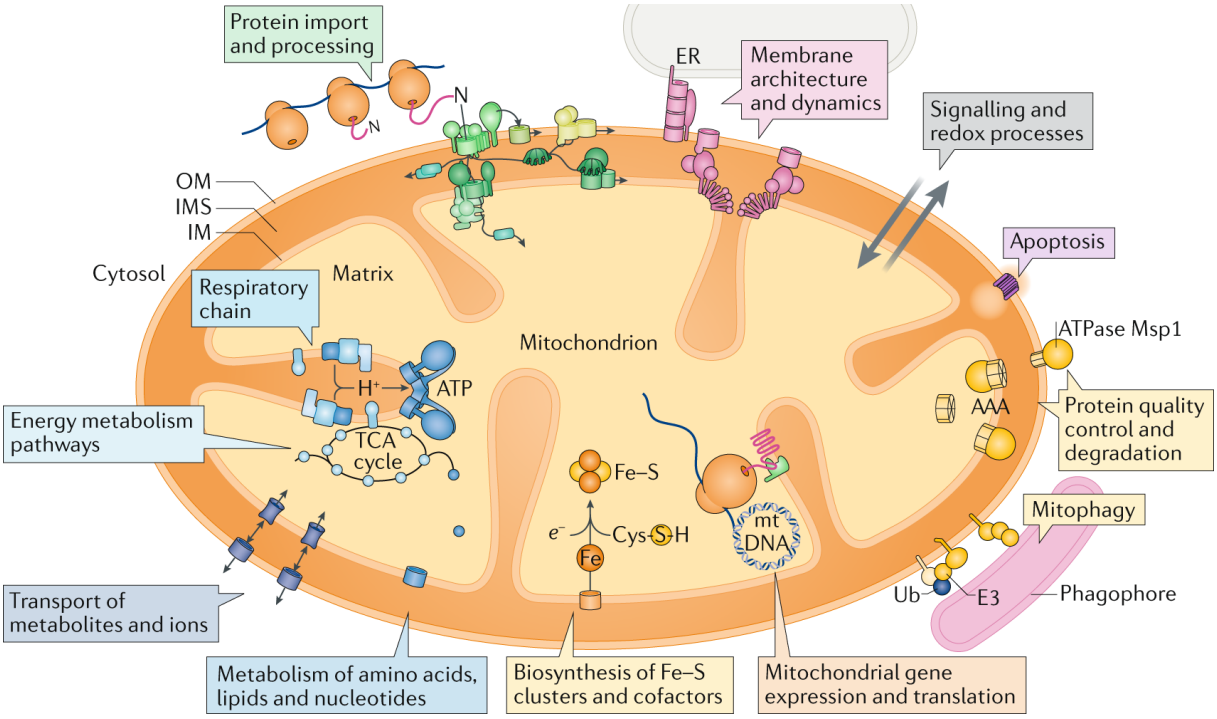

Figure 1: **Mitochondria structural and functional overview.** Mitochondria are composed of four compartments: outer membrane (here OM), intermembrane space (IMS), inner membrane (here IM), and matrix. Mitochondrial proteins and protein complexes are thought to have a variety of functions, as shown in the figure: Energy metabolism including the respiratory electron transport chain and ATP synthesis using the mitochondrial membrane potential; biosynthesis of iron-sulfur clusters (Fe/S) and heme; metabolism of small metabolites such as amino acids, lipids, and nucleotides; transcription and translation of mitochondrially-encoded genes from the mitochondrial genome; cellular quality control and degradation processes comprise mitophagy and the controlled cell death via apoptosis; signaling via protein processing and redox processes e.g. in the IMS are used to communicate with other cell compartments; and import and processing of precursor proteins synthesized at cytosolic ribosomes are necessary for a constant renewal of mitochondrial proteins (Figure from Pfanner et al., 2019).

In order to maintain protein homeostasis (proteostasis) in mitochondria, cells have adapted multiple quality control steps at several stages to monitor the mitochondrial proteostasis and to avoid mitochondrial dysfunction. The mechanism of proteostasis comprise everything that controls the turnover of a protein, including its synthesis, import or localization, folding and degradation.

First, by a continuous flux of proteins to the mitochondria, degradation of old or damaged proteins at the sub-compartments and release of peptides from the organelle, mitochondrial proteins are steadily renewed (Haynes et al., 2010). As only 13 proteins are encoded in the human mitochondrial genome and synthesized inside the matrix, the majority, more than 1,100 mitochondrial proteins, are

translated by cytosolic ribosomes and have to be taken up by mitochondria (Schmidt et al., 2010; Rath et al., 2021). The cytosolic translation products are generated as precursors and stabilized by cytosolic chaperones. Next, they are imported and transferred into the correct sub-compartment of the mitochondrion. For respiratory chain complexes, both mitochondrial and nuclear genomes are necessary. In this regard, it was found that in yeast, mitochondrial and cytosolic translation of these genes are synchronized processes, which serve to avoid formation of dysfunctional complexes in the electron transport chain (Couvillion et al., 2016). Additionally, co-translational protein import into mitochondria was observed for IMM proteins, which simplifies the protein import from the cytosol, as the nascent polypeptide chain is directly synthesized into the mitochondrial translocon (Williams et al., 2014; Lesnik et al., 2014). However, an in-depth understanding of co-translational mitochondrial protein import in mammalian cells still remains elusive (Avendaño-Monsalve et al., 2020) and it is assumed that this mechanism is only true for a minority of mitochondrial proteins.

1.2 MITOCHONDRIAL PROTEIN IMPORT AND FOLDING

Most mitochondrial proteins are translated in the cytosol and bound to heat shock proteins (HSP), such as HSP40 (DnaJ homolog subfamily B member DNAJB), HSP70 and HSP90, prior to import, maintaining them in an import-competent unfolded state (Young et al., 2003; Becker et al., 2019). These precursor proteins contain a mitochondrial targeting sequence (MTS), which is recognized by translocase of the outer mitochondrial membrane (TOM) receptors (TOMM20 and TOMM70) (Young et al., 2003). All mitochondrial imported proteins are transferred through the import pore of the TOM complex. It consists of the β-barrel TOMM40 channel and the small stabilizing TOM proteins, TOMM5, 6 and 7. Two TOMM40 channels (with stabilizing small TOMMs) cluster together with one central TOMM22 (Araiso et al., 2019; Tucker & Park, 2019; W. Wang et al., 2020). During or after transit through the OMM, mitochondrial proteins are sorted in the right sub-compartment with support of a network of proteins. For example, the sorting and assembly machinery (SAM) folds β-barrel proteins, which are integrated into the OMM (Höhr et al., 2015). Coiled-Coil-Helix-Coiled-Coil-Helix domain containing 4

(CHCHD4) and growth factor, augmenter of liver regeneration (GFER) bind and assist in oxidative folding of cysteine-rich IMS proteins via the formation of disulfide bridges (Finger & Riemer, 2020). Small translocase of inner mitochondrial membrane (TIMM) proteins support both aforementioned processes by stabilizing unfolded proteins during the transfer of OMM and IMM proteins that are inserted from the IMS or associate (see Figure 2) (Weinhäupl et al., 2018).

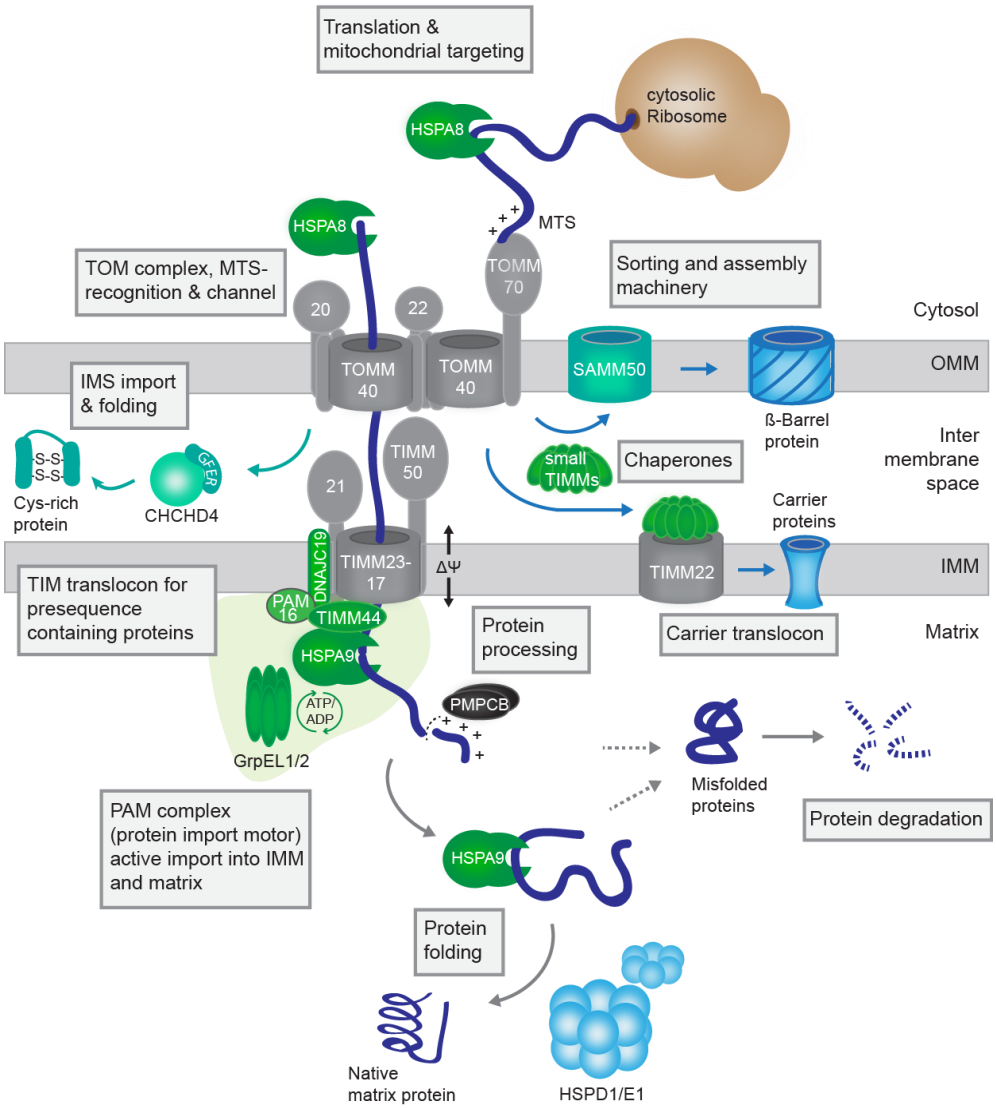

Figure 2: **Mitochondrial protein import is a complex, multistep process.** Mitochondrial precursor proteins with an amino (N)-terminal mitochondrial targeting sequence (MTS) are recognized by outer mitochondrial membrane (OMM)-based receptors TOMM20 and TOMM70 and are channeled through the translocon of the outer mitochondrial membrane (TOM), TOMM40. By direct contact of TOM with TIMM50 the intermembrane space (IMS) is crossed and the precursor transferred to the translocon of the inner mitochondrial membrane (TIM) complex. The positively charged MTS and the membrane

potential (ΔΨ) drives this movement. The ATP-driven presequence translocase associated import motor (PAM) complex pulls the precursor into the matrix, where PMPCA/B removes the MTS and allows the folding via chaperones/ chaperonins as HSPD1/E1. Figure based on Pfanner et al., 2019.

The majority (in yeast about 60%) of all mitochondrial proteins, contain a positively charged MTS and are targeted to the mitochondrial matrix and IMM (Vögtle et al., 2009). The positive charges of the N-terminal presequence thereby are driving the protein towards the negatively charged matrix, due to the membrane potential (ΔΨ). Thus, matrix-targeted proteins are channeled from the TOM through the TIM complex (Mokranjac et al., 2009; Schulz et al., 2011; Shiota et al., 2015). When the MTS reaches through the TIM, it is actively pulled through the translocon by the ATP-driven presequence translocase associated import motor (PAM) complex. The PAM complex is composed of mitochondrial import inner membrane translocase subunit TIM14, aka DnaJ heat shock protein family member C19 (DNAJC19), GrpE like 1 or 2, mitochondrial (GRPEL1/2), mitochondrial heat shock protein 70 (mtHSP70 aka HSPA9), presequence translocase associated motor 16 (PAM16 aka TIM16) and TIMM44. TIMM44 interacts with the TIM translocon, the IMM and acts as a platform to recruit the HSPA9, as well as its co-chaperone and nucleotide exchange factor GRPEL1/2. The PAM complex import activity is based on HSPA9's ability to bind and release stretches of newly imported proteins by circulating between its adenosine tri- and adenosine diphosphate (ADP)-bound state (Bukau & Horwich, 1998). This HSPA9 binding of substrate proteins, together with the Brownian movements, generate a pulling force, leading proteins efficiently through the import pore (De Los Rios et al., 2006; Schulz & Rehling, 2014; Schulz et al., 2015; Ting et al., 2017; Craig, 2018). ADP-bound HSPA9 has a high affinity to bind substrates, to release them ADP dissociation is needed. GRPEL1 triggers this release of folded proteins from HSPA9 by ATP rebinding and thus allows multiple cycles of HSPA9 to the imported protein (Goswami et al., 2010). DNAJC19 seems to stimulates the ATPase activity of HSPA9, while PAM16 inhibits DNAJC19; in yeast these activities are essential for a functional PAM complex and their combined function seems to drive efficient protein import to the matrix (Frazier et al., 2004). In human the understanding of this process is still vague, but it is assumed to follow a similar mechanism. During

or after import, the mitochondrial-processing peptidase PMPCB cleaves off the presequence of newly imported proteins, bringing them in their mature form and allowing them to find their native fold (Mossmann et al., 2012). Chaperones like HSPA9, chaperonins as 60 kDa heat shock protein, mitochondrial (HSPD1) and 10 kDa heat shock protein, mitochondrial (HSPE1), assist and tightly control folding and assembly of mitochondrial complexes, thereby minimizing the accumulation of non-functional proteins (Ostermann et al., 1989; Horwich et al., 2007; Böttinger et al., 2015; Zurita Rendón et al., 2018; Shin et al., 2021).

1.3 MITOCHONDRIAL PROTEIN QUALITY CONTROL

Mitochondrial protein homeostasis is critical for cellular health and function. In particular, correct mitochondrial protein import, protein sorting, assembly and folding to native, functional protein is essential. Therefore, all protein import steps are tightly controlled and assisted by chaperones and the import machinery. Nevertheless, during these processes, proteins can get stuck, can mislocalize to the wrong compartment or can misfold in general (Avendaño-Monsalve et al., 2020). Hence, as a countermeasure, in the cytosol, chaperones and the ubiquitin-proteasome system (UPS) ensure that only properly synthesized proteins are transported into the mitochondria, during which the proteins remain in a transport-competent unfolded state. However, when proteins get stuck in the TOM complex or misfold in the OMM, they can be removed via the UPS and transitional endoplasmic reticulum ATPase (VCP aka p97) (Xing Guo & Qi, 2017). If this happens inside of mitochondria, ATPases associated with diverse cellular activities (AAA) proteases, guard the IMS or matrix and remove damaged proteins (Figure 3). ATP-dependent zinc metalloprotease YME1L (YME1L) is one of the AAA proteases that regulates the protein import, lipid trafficking and mitochondrial dynamics from the IMM pointing to the IMS (Potting et al., 2013; Anand et al., 2014; Richter et al., 2019). AFG3-like protein 2 (AFG3L2) with paraplegin (SPG7) are also located in the IMM directed to the matrix. These AAA proteases guard mitochondrial ribosomes and Ca^{2+} uniporter assembly by degrading non-native assembled complexes and misfolded proteins in the IMM and its close proximity (König et al., 2016;

Hurst et al., 2019). Lon peptidase 1 (LONP1), as well as caseinolytic peptidase subunit P and X (ClpXP), locate to the matrix and degrade the majority of matrix-located proteins. They play a crucial role for mitochondrial genome (mtDNA) maintenance, mitochondrial transcription, translation and various other functions (Matsushima et al., 2010; Szczepanowska et al., 2016; Kunová et al., 2017; Deshwal et al., 2020). Together these AAA proteases ensure regular mitochondrial protein renewal, while degrading damaged proteins. Despite maintaining the mitochondrial proteome under steady state, protein quality control mechanisms adapt to cellular stress to maintain homeostasis.

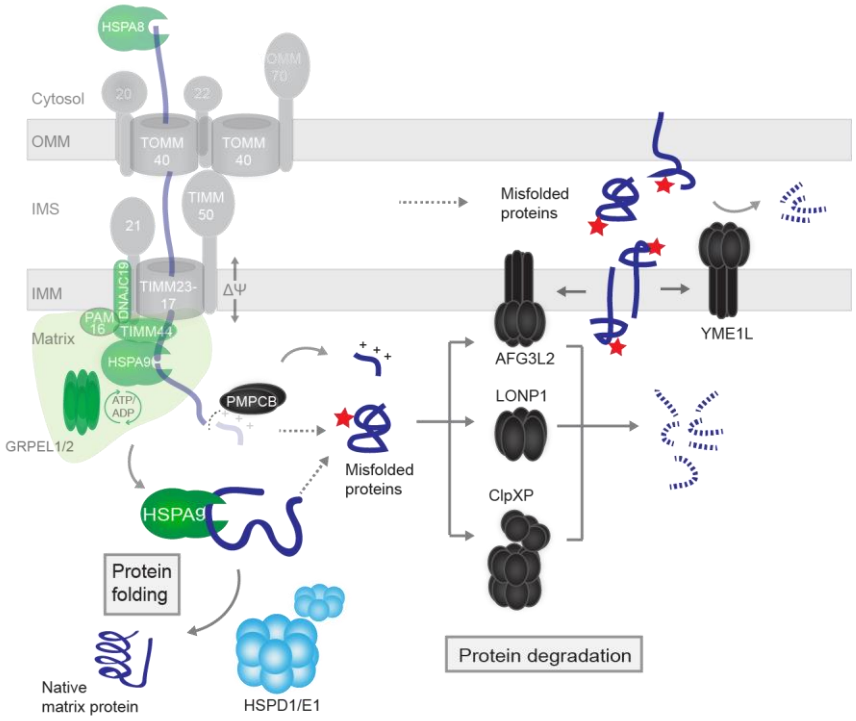

Figure 3: **Protein quality control in mitochondrial sub-compartments.** Precursor proteins are channeled from the cytosol trough the TOM and TIM translocon into the sub-compartments. The membrane potential and PAM complex drive the transfer over the IMM, where HSPA9 (synonym mtHSP70) and LONP1 support the folding of newly imported proteins. The mitochondrial processing peptidase MMP with its catalytic part PMPCB remove the mitochondrial targeting sequence. The chaperonins HSPD1 and HSPE1 further aid with matrix proteins to find their native fold. Impaired processing, chaperone function or obtained protein damage can lead to the formation of misfolded proteins (indicated by a red star). ATPases associated with diverse cellular activities (AAA) proteases have the function to remove these proteins before they accumulate. LONP1 and ClpXP remove misfolded proteins from the matrix. AFG3L2 and SPG7 are guarding the IMM directed to the matrix.

YMEL1 sits also in the IMM and is oriented to the intermembrane space (IMS) providing protein degradation in between the OMM and IMM. Figure inspired by Song et al., 2021.

1.4 MITOCHONDRIAL STRESS RESPONSES

The mitochondrial environment is sensitive to protein import and folding stress. Upon accumulation of misfolded proteins, mitochondria respond by activating cellular stress response pathways. A highly conserved stress signaling response, specific for accumulation of unfolded mitochondrial proteins was described, named mitochondrial unfolded protein response (UPR^{mt}). The key feature of UPR^{mt} is the increased transcription of nuclear-encoded mitochondrial chaperonins HSPD1 and HSPE1 (Martinus et al., 1996) as well as chaperone HSPA9. Furthermore, a decreased mitochondrial translation and increased transcription of mitochondrial matrix-based proteases was observed during UPR^{mt} (Fiorese et al., 2016; Münch & Harper, 2016). The underlying mechanism, however, how protein misfolding in the matrix is sensed and how it is signaled retrogradely from mitochondria to the nucleus remained so far unknown (Figure 4). What is known: there are two transcription factors which are essential for the UPR^{mt}-induced transcriptional response, cyclic adenosine monophosphate (AMP)-dependent transcription factor ATF-4 (ATF4) and DNA damage-inducible transcript 3 protein (DDIT3 aka CHOP) (Quirós et al., 2017; Kaspar et al., 2021). Both factors are already known from the integrated stress response (ISR), which downregulates protein synthesis and activates a transcriptional program upon intrinsic or environmental stresses (Novoa et al., 2003; Dey et al., 2010). Recently, two other factors, heat shock factor 1 (HSF1) and mitochondrial DAP3-binding cell death enhancer 1 (DELE1), were identified to play an important role for human mitochondrial stress signaling (Fessler et al., 2020; Katiyar et al., 2020; Xiaoyan Guo et al., 2020). Upon mitochondrial stress, DELE1 is processed by the mitochondrial metalloendopeptidase OMA1, thus it loses its membrane-bound domain, accumulates in the cytosol and activates heme-regulated inhibitor (HRI). HRI is an eukaryotic translation initiation factor 2 subunit 1 (eIF2α) kinase, which induces the ISR, resulting in a cap-dependent translation inhibition and transcriptional response via ATF4, CHOP and others (Xiaoyan Guo et al., 2020) (Figure 4). The transcriptional as well as translational response was further characterized, showing cross talk

between UPR^{mt} and ISR, however the sensing and signaling over the inner mitochondrial membrane by UPR^{mt} are still to be answered for mammals.

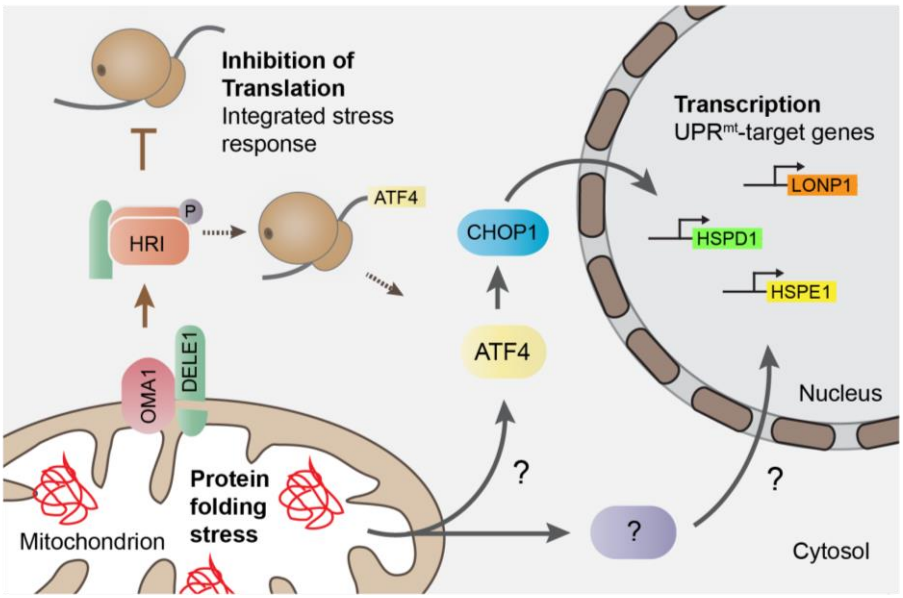

Figure 4: **The mitochondrial unfolded protein response UPR^{mt} and its crosstalk to the integrated stress response**. The accumulation of unfolded or misfolded proteins in the mitochondrial matrix applies a protein folding stress on the mitochondrial protein quality control machinery. (Right) This stress is sensed by a so far unknown mechanism and signaled to the cytosol. ATF4 and CHOP are activated in the cytosol and transition to the nucleus, where they drive the transcription of UPR^{mt}-target genes. (Left) Subsequent, the integrated stress response (ISR) can be co-activated at least by some protein folding stresses. Here, OMA1 cleaves the mitochondrial membrane domain of DELE1. Processed DELE1 then activates heme-regulated inhibitor HRI. HRI is a eIF2α kinase, its activity inhibits CAP-dependent translation and by that reducing most protein synthesis. CAP-independent translation as for ATF4 is still possible. Thus, the ISR supports the activation of the UPR^{mt}.

In *Caenorhabditis elegans*, e.g. an "elegant" molecular mechanism was uncovered (Priesnitz & Becker, 2018), explaining the transcriptional UPR^{mt} response by a dual-localized transcription factor, named activating transcription factor associated with stress 1 (ATFS-1). Under healthy conditions ATFS-1 is imported into the matrix and degraded by LONP1. However, under mitochondrial protein folding stress, ATFS-1 localizes to the nucleus, along with DVE-1 and UBL-5 and activates the transcription of UPR^{mt}-target genes (Benedetti et al., 2006; Haynes et al., 2007; Nargund et al., 2012, 2015). For

mammals, ATF-5 is suggested to have a similar role (Fiorese et al., 2016). However, this was not further supported since the initial study.

In yeast it has been seen that, upon decreased mitochondrial protein import, mitochondrial proteins mislocalize to the cytosol, inducing the mitochondrial precursor over-accumulation stress (mPOS). This leads to HSF1 activation and increased transcription of its target genes. As a result, the proteasomal capacities are expanded and mistargeted proteins degraded by proteasome, in a response called unfolded protein response activated by mistargeting of proteins (UPRam) (Wrobel et al., 2015; X. Wang & Chen, 2015; Coyne & Chen, 2019).

Overall, mitochondrial stress responses result in lower translation in the cytosol and mitochondrial matrix, leading to less folding load, while the transcription of protein quality control factors are increased. This increase in mitochondrial stress gene transcription is suggested to increase the folding capacity over time and make mitochondria more stress resistant, but especially for the mammal system many questions are so far unanswered.

1.5 AUTOPHAGIC MACHINERY

Another mechanism which resolves cellular stress besides transcriptional responses, is autophagy: the lysosomal removal of large damaged structures, organelles, aggregates or the unspecific digestion of cellular content during starvation. The mechanism of autophagy is based on the process of formation of a double membrane and the engulfment of cargo which shall be degraded in the lysosome. The complete process of autophagy consists of a series of subsequent steps with over 30 autophagic proteins or protein complexes (Ohsumi, 2014). Autophagy can be grouped into multiple sections: (a) Initiation by the Unc-51-like kinase 1 (ULK1) complex, (b) nucleation of a cup-shaped double membrane, called phagophore by the phosphoinositide 3-kinase (PI3KC) complex I, (c) cargo sequestration by microtubule-associated proteins 1A/1B light chain 3 (LC3) and/or gamma-aminobutyric acid receptor-associated protein (GABARAP) lipidation, (d) labeling of cargo in cases of

selective autophagy by ubiquitin or specific recognition by selective autophagy receptors, (e) expansion or elongation of the phagophore, (f) closure/sealing of the phagophore to form an autophagosome which traps the engulfed content, and (g) maturation and fusion with lysosomes forming an autolysosome. In those autolysosomes, (h) the cargo is degraded under an acidic pH by lysosomal hydrolases and (i) nutrients are released to the cytoplasm to be recycled (Yorimitsu & Klionsky, 2005; Dikic & Elazar, 2018). A comprehensive overview is provided in Figure 5.

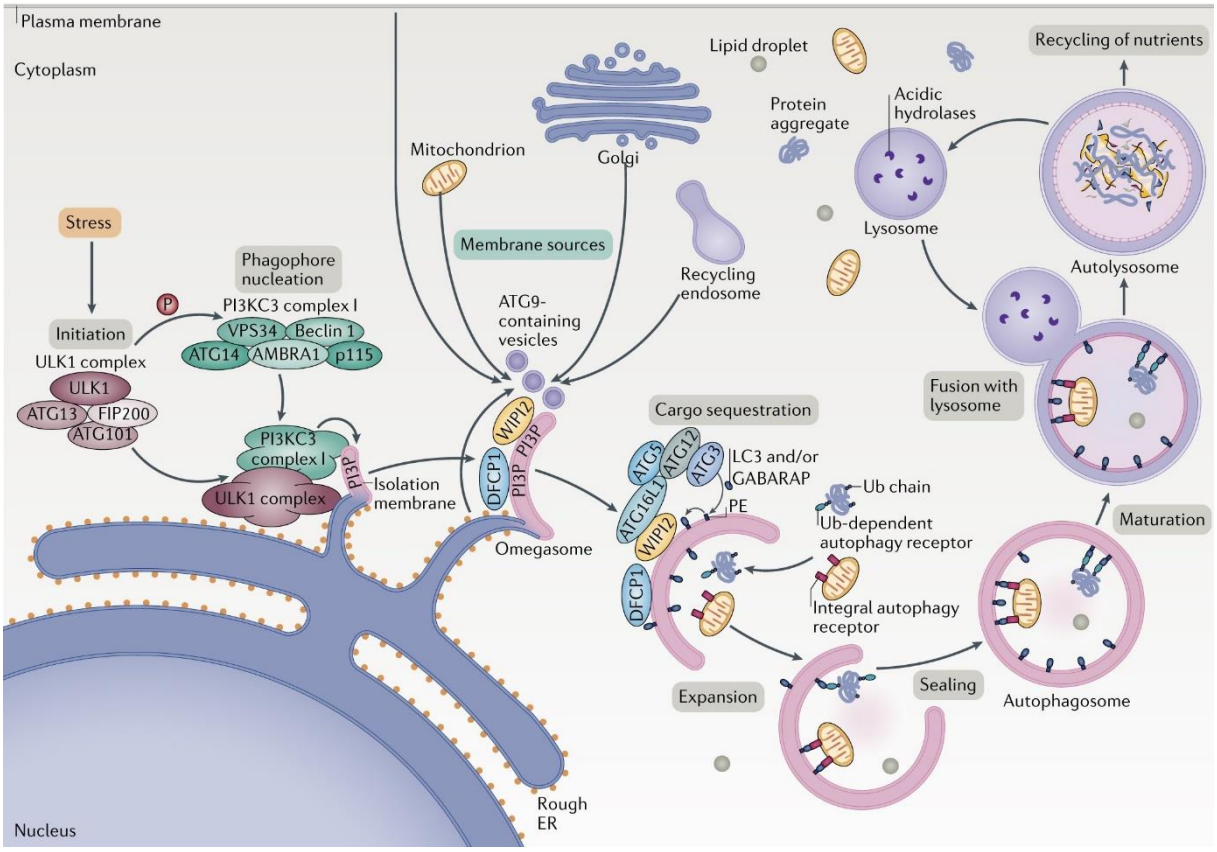

Figure 5: **Overview of macro autophagy machinery**. Various stress conditions such as starvation, hypoxia, oxidative stress, protein aggregation, endoplasmic reticulum (ER) stress and others can initiate autophagy. Unc-51-like kinase 1 (ULK1) complex (containing ULK1, autophagy-related protein 13 (ATG13), RB1-inducible coiled-coil protein 1 (FIP200) and ATG101) are the common targets of these signaling pathways, which trigger nucleation of the phagophore by phosphorylation of PI3K complex I (Phosphatidylinositol 3-kinase catalytic subunit type 3 (PI3KC3) , vacuolar protein sorting 34 (VPS34) class proteins, Beclin1, Beclin 1-associated autophagy-related key regulator (ATG14), activating molecule in Beclin1-regulated autophagy protein 1 (AMBRA1) and the general vesicular transport factor (p115)). PI3KC complex I activates the phosphatidylinositol-3-phosphate (PI3P) production locally at characteristic ER structures called omegasomes. PI3P recruits zinc-finger FYVE domain-

containing protein 1 (DFCP1) and WD repeat domain phosphoinositide-interacting proteins (here: WIPI2) to the omegasome. WIPI2 binds ATG16L1 and recruits the ATG12~ATG5–ATG16L1 complex, which enhances ATG3-mediated lipidation of ATG8 family proteins, like microtubule- associated protein light chain 3 (LC3) proteins and γ- aminobutyric acid receptor- associated proteins (GABARAPs) to membrane-resident phosphatidylethanolamine (PE). LC3-I is consequently converted into LC3-II — a typical characteristic of autophagic membranes. LC3-II is not only bound by LC3-interacting regions (LIR) motifs of autophagy receptors and thus critical for sequestration of cargo for many types of selective autophagy, but is also required for elongation of the phagophore and sealing. ATG9-containing vesicles originating from various sources contribute lipids to expand the phagophore until it completely engulfs the cargo forming a double-membraned, the autophagosome. During maturation the autophagosome loses the ATG proteins and finally fuses with the lysosome, which is then called an autolysosome. Acidic hydrolases of the lysosome degrade the autophagic cargo, and make the nutrients available again to be reused. (Figure from Dikic & Elazar, 2018)

Non-specific, bulk (macro-) autophagy is activated during deprivation of specific nutrients or energy (Shang et al., 2011). However, there are also selective autophagy pathways, which regenerate homeostasis by removal of potentially toxic, large structures. Cargo for selective autophagy are damaged organelles, like peroxisomes or mitochondria, or protein aggregates that have formed in the cytosol (Pankiv et al., 2007; Weidberg et al., 2011; Till et al., 2012; J. Lee et al., 2012). If the ubiquitin-proteasome system is unable to remove such large structures, the specific labeling, mainly with ubiquitin chains marks the cargo to be degraded via selective autophagy.

1.6 PINK1-/PARKIN-DEPENDENT MITOPHAGY

One focus of this study is the understanding of mitophagy, the selective autophagy pathway for the targeted degradation of damaged mitochondria. In the prevailing mitophagy model, mitophagy is activated by mitochondrial stress that causes a breakdown of the mitochondrial membrane potential. This loss of membrane potential serves as trigger for PTEN-induced kinase 1 (PINK1)/ E3 ubiquitin-protein ligase PARKIN (PARKIN)-dependent mitophagy, which then degrades the damaged mitochondrion (D. Narendra et al., 2008; D. P. Narendra et al., 2010). Thereby, PINK1 functions as key sensor for mitophagy. Looking at healthy mitochondria, PINK1 is partially imported through the mitochondrial translocons, processed by PMPCB and released in the IMM, where it is cleaved by the

presenilins-associated rhomboid-like protease (PARL). This processing leads to retrograde translocation of PINK1 to the cytosol and rapid degradation of PINK1 by the proteasome (Figure 6A) (Jin et al., 2010; Mossmann et al., 2012; Greene et al., 2012). In previous studies on mitophagy, compounds (protonophores, e.g. carbonylcyanide m-chlorophenylhydrazone (CCCP) or carbonylcyanide p-trifluoromethoxy-phenylhydrazone (FCCP) or inhibitors of the respiratory chain as well as ATP-synthase, like a combination of antimycin A1, inhibitor of complex III and oligomycin, inhibitor of F0 component of ATP-synthase (AO)), were established for depolarization of the IMM proton gradient (Vives-Bauza et al., 2010; Lazarou et al., 2015). This depolarization in turn prevents PINK1 import through the TIM translocon and its processing via PARL. Full length PINK1 is then stabilized on the OMM by TOMM7 (Hasson et al., 2013) and CHCHD4 in the presence of ROS (Gao et al., 2020).

Mitochondrial depolarization, facilitates PINK1 accumulation and *trans*-phosphorylation of nearby PINK1 molecules thereby activating PINK1's ubiquitin kinase function. PINK1 then phosphorylates ubiquitin at serine 65 on nearby ubiquitylated OMM proteins (Figure 6B). Phospho-ubiquitin accumulation results in the recruitment and activation of E3 ubiquitin ligase PARKIN (gene name *PRKN* or *PARK2*). PARKIN is further activated by phosphorylation of its ubiquitin-like domain via PINK1 (Vives-Bauza et al., 2010; Shiba-Fukushima et al., 2014; Kazlauskaite et al., 2015; Rasool et al., 2018; Sauvé et al., 2018).

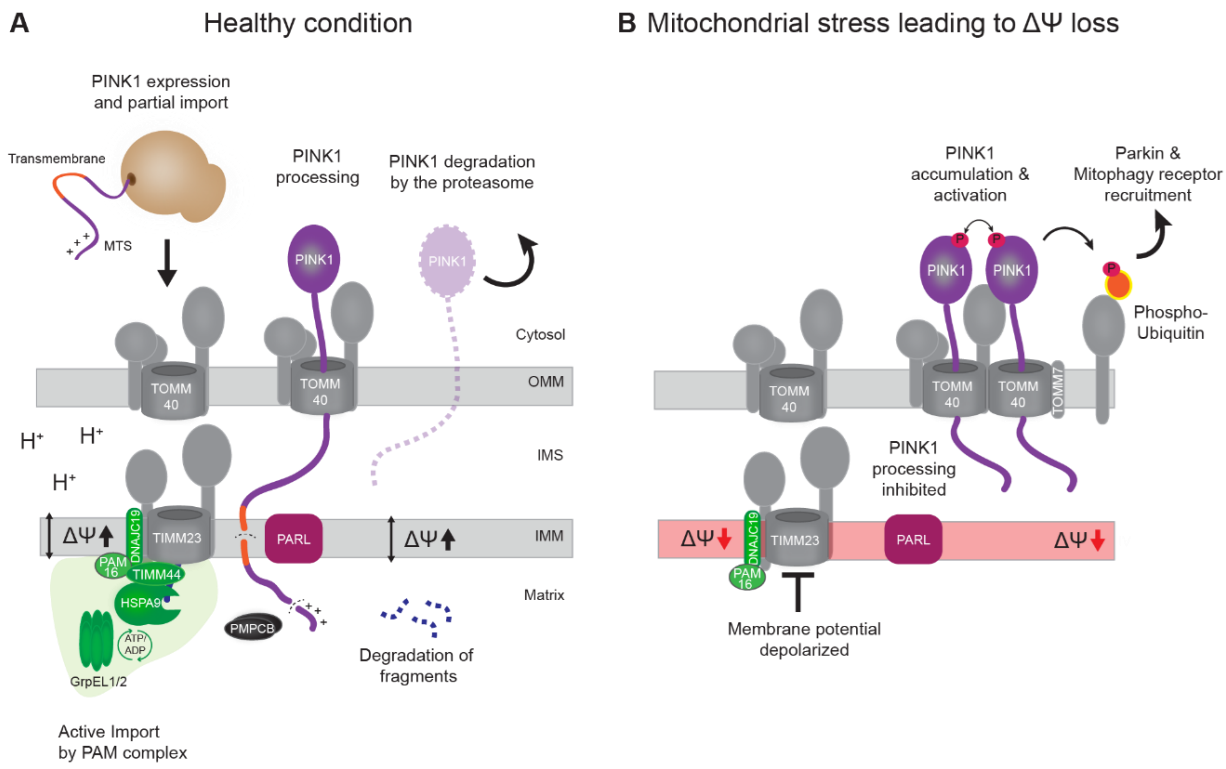

Figure 6: **PINK1-dependent mitophagy initiation.** (A) PINK1 is translated in the cytosol and recruited to the OMM. In healthy mitochondria, PINK1 is partially imported by its N-terminal MTS and processed in the IMM via the rhomboid-like protease PARL, resulting in a retro-translocation and rapid degradation via the proteasome. (B) Upon severe mitochondrial stress the mitochondrial membrane potential (ΔΨ) collapses and PINK1 import is blocked. This prevents PINK1 processing and leads to its accumulation in the OMM. PINK1 activates nearby PINK1-molecules and phosphorylates ubiquitylated OMM-proteins, resulting in the induction of mitophagy, which is further enhanced by the E3 ligase PARKIN.

During this process, PARKIN functions as signal enhancer, as it ubiquitylates more OMM proteins to increase the mitophagy signal and thus its efficiency (Ordureau et al., 2014). However, mitochondrial surface ubiquitylation does not exclusively rely on PARKIN, as other E3-ligases like mitochondrial ubiquitin ligase activator of NFKB 1 (MUL1), E3 ubiquitin-protein ligase ARIH1 (ARIH1), E3 ubiquitin-protein ligase SIAH1 (SIAH1), E3 ubiquitin-protein ligase SMURF1 (SMURF1) and E3 ubiquitin-protein ligase AMFR (AMFR aka Gp78), have been described to take over PARKIN activity or cooperate with it, downstream of PINK1 (Orvedahl et al., 2011; Lokireddy et al., 2012; Fu et al., 2013; Szargel et al., 2016; Villa et al., 2017; Garriga, 2019; Igarashi et al., 2020). When PINK1 and PARKIN are present and mitochondrial damage occurs, active PARKIN starts a feed-forward cycle resulting in phosphorylated

poly-ubiquitylation on the outer mitochondrial surface (Ordureau et al., 2014). These OMM protein modifications recruit autophagy receptors, such as optineurin (OPTN) and antigen nuclear dot 52 kDa (NDP52, synonym CALCOCO2) (Lazarou et al., 2015). These receptors bind phospho-ubiquitin on one domain and LC3 on another via its LC3-interacting region (LIR) motif. This results in tethering of a LC3-postitive double membrane to the damaged mitochondrion. Autophagy receptor binding to phospho-ubiquitin is further improved by TANK-binding kinase 1 (TBK1) activity. TBK1 phosphorylates OPTN and NPD52 to establish a second positive feedback mechanism (Heo et al., 2015). This phagophore expands and encloses around the organelle by the autophagy machinery, forming an autophagosome. The autophagosomes fuse with lysosomes, to generate autolysosomes , which then degrades depolarized mitochondria (Figure 7) (Marinković & Novak, 2015; Lazarou et al., 2015). Mitophagy thereby protects the cell from accumulation of dysfunctional mitochondria and prevents mitochondria-induced apoptosis and diseases caused by impaired mitochondrial function (Wanderoy et al., 2020).

As mitophagy removes whole parts from the mitochondrial network, there are mechanisms in place to reduce and prevent the removal of functional mitochondria. One mechanism being mitochondrial fission, where mitochondria are fragmented in smaller segments, separating healthy and damaged parts of the mitochondrion. This mechanism is largely mediated via dynamin-1-like protein (DRP1, synonym DNML1), mitochondrial dynamin-like 120 kDa protein (OPA1) and mitochondrial fission 1 protein (FIS1) or one of its orthologues (MFF/Mid49/Mid51) (Kraus et al., 2021). DRP1 is thereby not necessary for mitophagy, but rather rescues healthy parts of mitochondria from mitophagic degradation (Burman et al., 2017). Another mechanism to reduce mitophagy, is the deubiquitination of OMM proteins by the ubiquitin-specific peptidase 30 (USP30) (Bingol et al., 2014). USP30 was found to opposes PARKIN-driven mitophagy by removing poly-ubiquitin chains from mitochondria, hence rescuing mitochondria which recovered from the stress (Bingol et al., 2014).

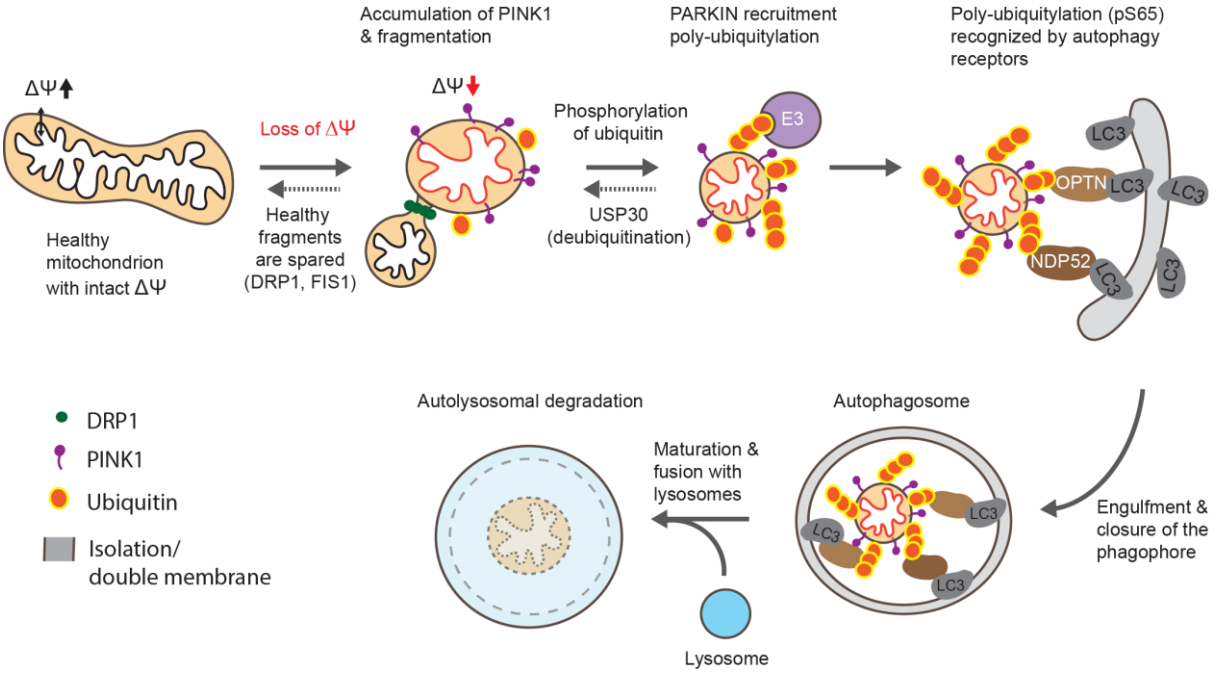

Figure 7: **PINK1/PARKIN-dependent mitophagy progression**. Break down of the membrane potential (ΔΨ↓) leads to stabilization of PINK1 and fragmentation of mitochondria by OPA1 degradation and DRP1, FIS1-dependent fission. PINK1 accumulates in the OMM and becomes activated phosphorylating ubiquitin-residues at serine 65 of OMM proteins. Phospho-ubiquitin recruits the E3 ubiquitin ligase PARKIN, which poly-ubiquitylates the mitochondrial surface. Autophagy receptors OPTN and NDP52 are recruited to the depolarized mitochondria by binding phosphorylated poly-ubiquitylation and trigger the formation and recruitment of a phagophore, a LC3 and GABARABL-positive double membrane. The phagophore engulfs the fragmented mitochondrion, forming an autophagosome, which fuses with lysosomes to degrade the autophagosomal cargo.

1.7 PINK1-/PARKIN-INDEPENDENT MITOPHAGY

In addition to the PINK1-PARKIN pathway, alternative proteins were identified as mediators for mitophagy (Allen et al., 2013; Hamacher-Brady & Brady, 2015; Dudek, 2017; Padman et al., 2019) and mitophagy can even occur independent of ubiquitin labelling of the mitochondrial surface (Padman et al., 2019). There are two different kinds: Receptor-based, where adaptor proteins directly bind to damaged mitochondria and recruit LC3-positive phagophore (BCL2/adenovirus E1B 19 kDa protein-interacting protein 3 (BNIP3), BCL2/adenovirus E1B 19 kDa protein-interacting protein 3-like (BNIP3L aka NIX), FUN14 domain-containing protein 1 (FUNDC1) or Bcl-2-like protein 13 (BCL2L13)), or there is the mitochondrial lipid cardiolipin, which changes its localization from the IMM to OMM during stress and binds LC3 (Figure 8) (Chu et al., 2013; Antón et al., 2016). It seems that some of these PINK1-

independent mechanisms are responsible for basal mitophagy, which is needed for continuous renewal of mitochondria during steady state conditions (McWilliams et al., 2018). PINK1 and especially PINK1 with PARKIN are known for its function in stress-induced mitophagy.

So far, there are only a few compound treatments known that induce PINK1-independent mitophagy, one for example are iron chelators, like deferiprone (DFP) and deferoxamine (DFO). DFP and DFO were found to function in a hypoxia-mimicking way, promoting hypoxia-inducible factor 1-alpha (HIF1α)-dependent mitophagy, via BNIP3 and BNIP3L, however with no or limited loss of mitochondrial membrane potential (Allen et al., 2013; Jin-Feng Zhao et al., 2020; Hara et al., 2020). Iron chelators for induction of mitophagy and their role in removing free or accumulated iron, are discussed and studied in first pilot trials to fight neurodegeneration (Rohani et al., 2018; Sian-Hulsmann & Riederer, 2020).

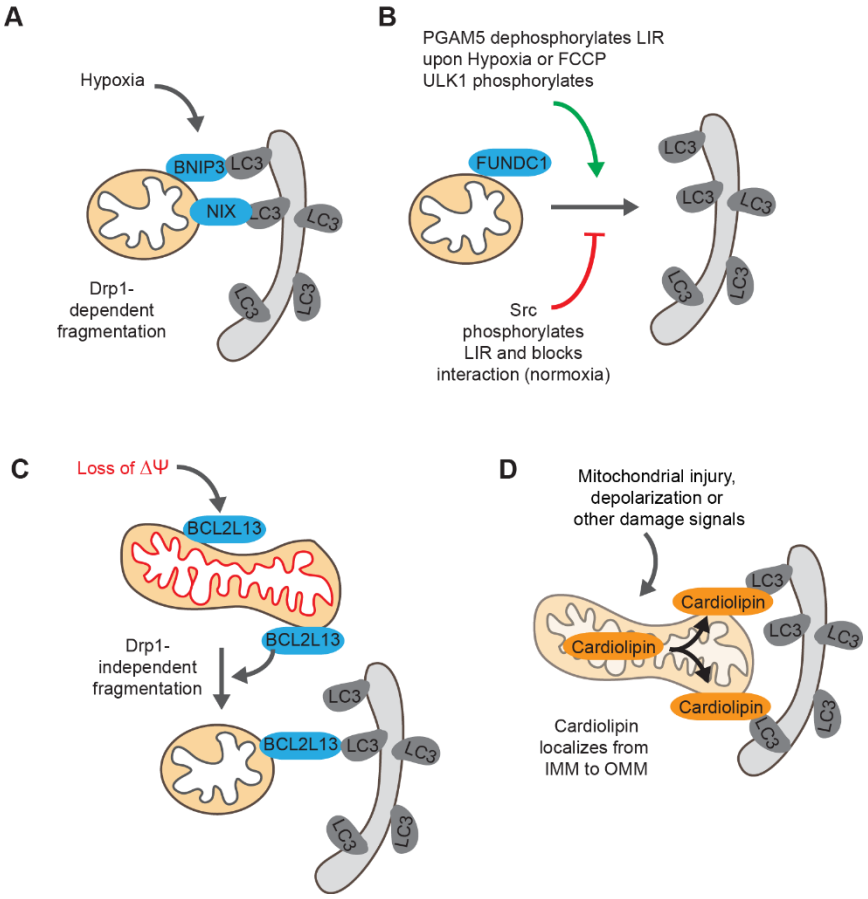

Figure 8: **Ubiquitin-/PINK1-PARKIN-idependent mitophagy an overview**. (A) BNIP3 and BNIP3L are induced upon hypoxic (low oxygen) conditions and localize to the OMM via a transmembrane region. They contain LIR motives and can supposedly be further enhanced via phosphorylation. (B) FUNDC1 contains three transmembrane domains that accomplish its OMM localization. During normoxia

(normal oxygen conditions), Src kinase phosphorylates tyrosine 18 and thereby inactivates FUNDC1's LIR motif. Hypoxia inactivates Src, allowing FUNDC1 LIR-mediated binding to LC3-positive double membrane (Hamacher-Brady & Brady, 2015). Mitochondrial serine/threonine-protein phosphatase PGAM5 antagonizes phosphorylation by CK2. During hypoxia and in response to depolarization ULK1 enhances LIR activity by phosphorylation at serine 17. (C) BCl2L13 induces DRP1-independent mitochondrial fragmentation and also binds LC3 via a LIR motif. (D) Cardiolipin, a IMM lipid, when localized to the OMM can directly bind LC3 and engage mitophagy (Chu et al., 2013; Antón et al., 2016). Illustration based on Hamacher-Brady and Brady, 2015.

1.8 NEURODEGENERATION AND MITOCHONDRIAL DYSFUNCTION

Dysfunctional mitochondria have been identified as a potential cause for neurodegenerative diseases (Y. Wang et al., 2019). They pose multiple threats to the cell, as damaged or dysfunctional mitochondria increase the cellular reactive oxygen levels, and damage proteins, lipids or the genome (Figure 9). Thus, it is not surprising that impaired mitophagy contributes to a wide range of human pathologies, including Parkinson's (PD) and Alzheimer's disease (AD), but also cancer and cardiomyopathies (Bernardini et al., 2017; Fivenson et al., 2017; Levine & Kroemer, 2019). By looking across clinical features in age- and autophagy-related disorders, overrepresentation of neurological diseases can be observed. This suggests that defects in autophagy often result in pathologies of the central nervous system. Remarkably, autophagy-related phenotypes show a significant overlap with phenotypes caused by mitochondrial diseases, indicating that mitochondrial dysfunction and a lack of mitophagy might be driving these disorders (Bakula & Scheibye-Knudsen, 2020). This hypothesis is further supported by disease studies on inherited PD patients. In this regard, studies on mitochondrial quality control have shown that mitochondrial dysfunction is an important contributor to the neurodegenerative phenotype in familial PD. Also, mutations in *PARK2* (*PARKIN*), *PARK6* (*PINK1*) or *PARK7* (*DJ-1*) have been identified to cause early-onset recessive PD. These clinical observations were further confirmed in animal studies, where deficient renewal or removal of mitochondria via mitophagy can lead to severe neurodegenerative diseases (Shimura et al., 2000; Valente et al., 2004). Hence, lack of mitophagy can be causal for PD development and understanding the molecular

mechanisms which are underlying mitophagy induction is essential for interpreting and modulating the processes leading to neurodegenerative diseases.

1.9 PROTEIN MISFOLDING AND NEURODEGENERATIVE DISEASES

The features of neurodegeneration protein aggregation and accumulation of misfolded proteins in cells of the neuronal system are well known (Ross & Poirier, 2004; Vaquer-Alicea & Diamond, 2019). In particular, it is accepted that accumulation of dysfunctional proteins cause disturbances in the cell or even lead to cell death (Figure 9) (Dikic & Elazar, 2018). In healthy cells, the ubiquitin-proteasome system and proteases in the organelles degrade misfolded or accumulated unfolded proteins. However, if the degradative capacities of this basal protein quality control are overloaded, the autophagic machinery becomes activated. As a consequence, in autophagy-deficient animals the major cause of death is neurodegeneration. In these cases, an accumulation of ubiquitiylated protein aggregates can be detected (Komatsu et al., 2006; Karsli-Uzunbas et al., 2014).

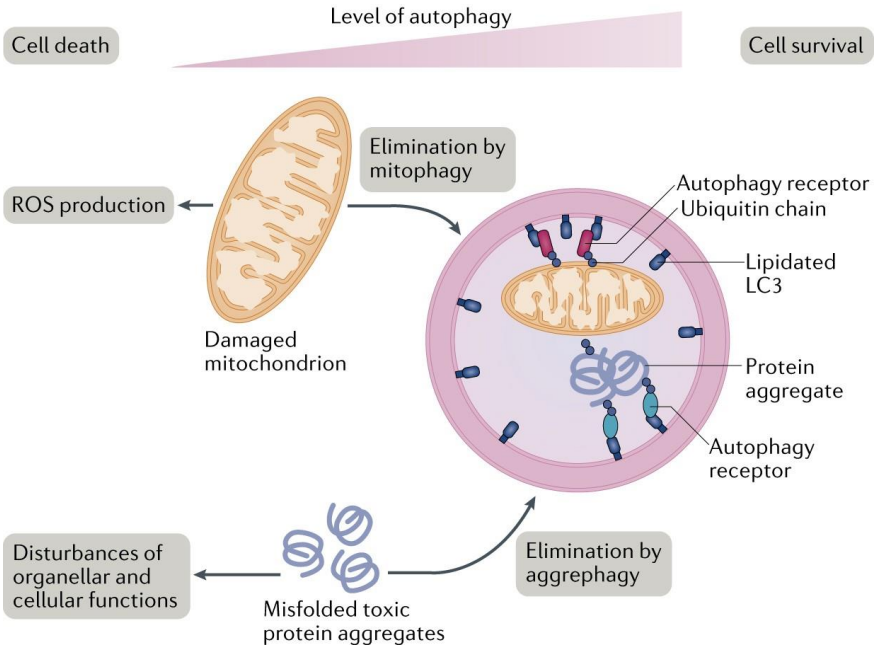

Figure 9: **Mitophagy and aggrephagy in neurodegeneration.** Selective autophagy protects against the accumulation of defective mitochondria or protein aggregates, being two hallmarks of

neurodegenerative diseases. Dysfunctional mitochondria can produce high levels of reactive oxygen species (ROS), posing a threat to cellular components, including proteins, lipids and the genome. Protein aggregates which are aggravated by ROS-mediated oxidative damage compromise the function of organelles and are considered particularly toxic for neurons. A reduced autophagic activity (for example during ageing or genetically caused) is therefore accompanied by the risk to development of a neurodegenerative disease (Figure from Dikic & Elazar, 2018)

For cytosolic oligomers of accumulated unfolded and misfolded proteins, the process that clears them is chaperone mediated autophagy (CMA). However, for aggregates, the selective macroautophagy machinery is required and it activates aggrephagy (Tan & Wong, 2017). Thereby, the autophagic cargo receptors sequestosome-1 SQSTM1/p62 and tax1-binding protein 1 (TAX1BP1) have a key role in clearing protein aggregates (Bjørkøy et al., 2005; Pankiv et al., 2007; Jackson et al., 2017; Sarraf et al., 2020). p62 helps to form aggregates in the cytosol, which can then be targeted by TAX1BP1 – which recruits the phagophore and facilitates the removal of these potential toxic protein accumulations (Sarraf et al., 2020).

At the mitochondrion, accumulation of misfolded proteins and possible aggregates can block the protein uptake, as for example for Huntington disease (HD) mutant huntingtin or for PD α-synuclein (Yano et al., 2014; Di Maio et al., 2016; Yablonska et al., 2019). Here, either mitophagy or aggrephagy should clear the dysfunctional mitochondria and aggregates, however in patients this seems to be inefficient (Martinez-Vicente et al., 2010; Martinez-Vicente, 2017). Besides, in regard of protein misfolding inside the matrix or IMM, mitophagy can be activated (Jin & Youle, 2013). A mechanistic model describing the mitophagy induction via mitochondrial protein misfolding however remains elusive.

1.10 OPEN QUESTIONS

Many mitophagy studies focused on compounds which quickly depolarized the mitochondrial membrane potential and by that trigger PINK1-PARKIN-dependent mitophagy. Under physiological stress conditions, there are two types of mitophagy: One is often referred to as programmed, basal or

PINK1-PARKIN-independent and the other stress-induced, PINK1-PARKIN-dependent mitophagy (Garriga, 2019). However, it is unclear for stress-induced mitophagy if and how the mitochondrial membrane potential would collapse *in vivo*; programmed mitophagy seems to rely mainly on pro-apoptotic proteins, such as BNIP3L, which seem to be mitochondrial membrane potential-independent. As stress-induced mitophagy caused by mitochondrial protein misfolding also seem to be mitochondrial membrane potential-independent (Jin & Youle, 2013; Burman et al., 2017; Fiesel et al., 2017), it is an outstanding question, during what conditions depolarized mitochondrial degradation plays a role or how PINK1 is stabilized upon these stressed conditions. To this end, I wanted to elucidate what induces mitophagy, how does protein misfolding induce mitophagy and propose a model filling the gap between acute compound-induced IMM depolarization and long term genetically-induced mitochondrial stresses without depolarization.

2 Aims

2.1 ESTABLISHING MITOPHAGY FLUX ASSAY AND IDENTIFICATION OF NOVEL MITOPHAGY FACTORS

For this study, I had to establish a sensitive, mitophagy detection method to analyze mitophagic flux during mild mitochondrial stress conditions or gene depletions. For this purpose, a HeLa FlpIn TRex cell line was genetically modified with inducible *PRKN* and mitochondrial m*KEIMA*, which reports the pH of the mitochondrial matrix and thereby provides information about healthy neutral or damaged mitochondria that localized in the acidic environment of the autolysosome. I combined it with inducible *PRKN* expression to further increase the sensitivity for mitophagy inducing reagents. This cell line was then used with the CRISPR/Cas9 Brunello library, which covers the whole coding genome, to search for novel mitophagy-driving or -inhibiting gene deletions. Several interesting candidates from the CRISPR/Cas9 screen were individually confirmed and set the basis for further characterization.

2.2 CHARACTERIZATION OF IMPORT DEFECT- / PROTEIN MISFOLDING-DRIVEN MITOPHAGY

As I found mitochondrial protein import-related and protein quality control gene depletions significantly enriched as drivers for mitophagy in my CRISPR/Cas9 screen, I further characterized the phenotype. The protein uptake into mitochondria, the membrane potential and the PINK1-dependency of mitophagy induction were tested. Furthermore, the formation of an insoluble protein fraction during protein quality control gene depletion or mitochondrial chaperone inhibition was investigated. Here, the protein import motor PAM was found enriched in the insoluble protein fraction and decreased in the soluble. This observation was confirmed and refined by proximity-labeling of one of the essential protein import motor's proteins.

2.3 DEVELOPMENT OF MITOCHONDRIAL PULSED-SILAC-BASED PROTEIN IMPORT MEASUREMENT

During the characterization of import-defective gene depletions, the need for a global unbiased method to study protein uptake into mitochondria awoke. The method my colleagues and I developed was based on mePROD (Klann et al., 2020), which measures protein translation in whole cell by pulsed SILAC proteomics. Here, I combined this method with the extraction of mitochondria from the cells, removing the labeling of extra-mitochondrial proteins and specifically only detecting proteins that have been imported into the mitochondrion. I further evaluated the method and used it for cells that were treated with mitochondrial stressors. As it is a global unbiased method, I also used it to look at global effects onto the cells, compared treatments and pathways affected with each other.

3 Material and methods

3.1 MATERIAL TABLE

3.1.1 Antibodies

anti-ATP5A1	Proteintech	Cat#14676-1-AP
anti-β-ACTIN	SantaCruz	Cat#sc69879
anti-GLRX5	Sigma-Aldrich	Cat#HPA063716
anti-GRPEL1	Proteintech	Cat#12720-1-AP
anti-Halo	Promega	Cat#G9211
anti-HSP60/ -HSPD1	Abcam	Cat#ab46798
anti-HSPA9	Abcam	Cat#ab2799
anti-LONP1	Proteintech	Cat#15440-1-AP
anti-PAM16	Proteintech	Cat#15321-1-AP
anti-phospho (S65)-Ubiquitin	Boston Biochem	Cat#A110
anti-PINK1	Cell Signaling Technology	Cat#6946, clone#D8G3
anti-TIMM23	Proteintech	Cat#11123-1-AP
anti-TIMM44	Proteintech	Cat#13859-1-AP
anti-TOMM20	SantaCruz	Cat#sc17764
anti-TOMM20 (IF)	Proteintech	Cat#11802-1-AP
anti-TOMM40	Proteintech	Cat#18409-1-AP
anti-TOMM40	SantaCruz	Cat#sc365467
anti-mouse-IgG-680RD	Li-Cor	Cat#926-68072
anti-mouse-IgG-800CW	Li-Cor	Cat#926-32210
anti-rabbit-IgG-680RD	Li-Cor	Cat#926-68073
anti-rabbit-IgG-800CW	Li-Cor	Cat#926-32213

3.1.2 Chemicals

Name	Company	Catalog number
0.25% Trypsin-EDTA mit phenolrot	Thermo Life Technologies	Cat#25200-056
2-Chloroacetamide	Sigma Aldrich	Cat#C0267
Antimycin A	Sigma Aldrich	Cat#A8674
Arginine 10	Cambridge Isotope Laboratories	Cat#CNLM-539-H-PK
Bafilomycin A1	Biomol / Cayman	Cat#Cay11038
Benzonase® Nuclease	SCBT	Cat#sc-202391
Biotin	Sigma Aldrich	Cat#B4639
Biotin HaloTag Ligand	Promega	Cat#G8281
Blasticidin (solution)	invivogen	Cat#ant-bl-1
Bolt 4-12% Bis-Tris Plus Gels, 12wells	Thermo Fisher Scientific	Cat#NW04122
Bolt 4-12% Bis-Tris Plus Gels, 15wells	Thermo Fisher Scientific	Cat#NW04125
Bolt MES SDS Running Buffer (20X)	Thermo Fisher Scientific	Cat#B0002
Bolt™ 12%, Bis-Tris, 12-well	Invitrogen	Cat#NW00122
Bortezomib	Biomol	Cat#Cay10008822
Bovine Serum Albumin	Sigma Aldrich	Cat#A7906
Carbonyl cyanide 3-chlorophenylhydrazone, CCCP	Sigma Aldrich	Cat#C2759
CELL CULTURE DISH 60x15 mm CELLSTAR	Greiner	Cat#628160 Sigma Cat#P7237
Chameleon® Duo Pre-stained Protein Ladder	Li-Cor	Cat#928-60000
cOmplete™, Mini, EDTA-free Protease Inhibitor Cocktail	Sigma Aldrich	Cat#11836170001
Deferiprone (DFP)	N/A	N/A
D-Mannitol	Sigma Aldrich	Cat#M9546-250G

Dulbecco's Modified Eagle Medium (DMEM)	Thermo Fisher Scientific	Cat#41966-029
DMEM, high glucose, no glutamine, no lysine, no arginine (for SILAC)	Thermo Fisher Scientific	Cat#A14431-01
DMSO for cell culture	AppliChem/VWR	Cat#A3672,0100
Doxycycline	Sigma Aldrich	Cat#D9891-10G
EBSS	Thermo Fisher Scientific	Cat#24010043
Fetal Bovine Serum, S.A.	Thermo Fisher Scientific	Cat#10270-106
Gamitrinib-triphenylphosphonium GTPP	N/A	https://doi.org/10.1172/jci44855
GenElute HP Plasmid Miniprep Kit	Sigma Aldrich	Cat#NA0160-1KT
High pH RP Peptide Fractionation Kit	Thermo Fisher Scientific	Cat#84868
Hydroxylamine solution, 50 wt. %	Sigma Aldrich	Cat#438227
Hygromycin B gold solution	invivogen	Cat#ant-hg-2
Intercept® (PBS) Blocking Buffer	Li-Cor	Cat#927-70003
Lipofectamine 2000	Thermo Fisher Scientific	Cat#11668027
Lipofectamine 3000	Thermo Fisher Scientific	Cat#L3000008
Lipofectamine RNAiMAX	Thermo Fisher Scientific	Cat#13778150
Lysine 8	Cambridge Isotope Laboratories	Cat#CNLM-291-H-PK
Methanol	Sigma Aldrich	Cat#32213-2.5L-M
MitoBloCK-6	Sigma Aldrich	Cat#5057590001
Mitotracker Red FM	Thermo Fisher Scientific	Cat#M22425
MitoTracker™ Deep Red FM	Thermo Fisher Scientific	Cat#M22426
N-Ethylmaleinimid (NEM)	Sigma Aldrich	Cat#E3876
Nitrocellulose Transfer Membrane	Thermo Fisher Scientific	Cat#EP4HY00010 Cat#1215471
Oligomycin A	Sigma Aldrich	Cat#75351

Pierce Streptavidin Magnetic Beads	Thermo Fisher Scientific	Cat#88816
Pierce™ BCA Protein Assay	Thermo Fisher Scientific	Cat#23228
Polybrene	Sigma Aldrich	Cat#TR-1003-G
Protein LoBind Tubes, 1.5 mL	VWR	Cat#525-0133 / 30108116
Protein LoBind Tubes, 2.0 mL	VWR	Cat#525-0134 / 30108132
Puromycin	InvivoGen	Cat#ant-pr-1
R110Direct	Promega	Cat#G3221
REVERT Total Protein Stain Kit	Li-Cor	Cat#926-11010
Roche PhosSTOP	Sigma Aldrich	Cat#4906837001
RPMI 1640 Medium (+L-Glutamine)	Thermo Fisher Scientific	Cat#21875-034
Tetramethylrhodamine, Ethyl Ester, Perchlorate (TMRE)	Thermo Fisher Scientific	Cat#T669
TMR 5mM	Promega	Cat#G8251
TMRDirect	Promega	Cat#G2991
TMT reagents	Thermo Fisher Scientific	Cat#A44520
TMT11 reagents	Thermo Fisher Scientific	Cat#A34808
Tris(2-carboxyethyl)phospine Hydrochloride solution	Sigma Aldrich	Cat#646547
TWEEN® 20	Sigma Aldrich	Cat#P1379
Whatman® Chromatography paper	Sigma Aldrich	Cat#WHA3030931
Cellculture dish Cellstar	Greiner	Cat#639160
Zeocin™ (solution)	Invivogen	Cat#ant-zn-1
Z-Leu-Leu-Leu-al, MG-132	Sigma Aldrich	Cat#C2211

3.1.3 Guide RNAs CRISPR Cas9

Guide RNA PINK1 for test screen	fwd ACATCATCTTGATGGCCAAG	Doench et al.,2016 Broad institute, GPP, doi: 10.1038/nbt.3437 , https://portals.broadinstitute.org/gpp/public/analysis-tools/sgrna-design
	fwd AGCACTGCAGCCCTTACCAA	
	fwd CCTCATCGAGGAAAAACAGG	
	fwd GCTGGTCCCAGCGAGCCGAG	
Guide RNA PINK1 clonal KO cell line	fwd GCCTCATCGAGGAAAAACAGG	GPP sgRNA Designer, Doench et al.,2016
	rev CCTGTTTTTCCTCGATGAGGC	GPP sgRNA Designer, Doench et al.,2016
Guide RNA GRPEL1-1	fwd GAGGCATTCAAGCCTTCTGCA	GPP sgRNA Designer, Doench et al.,2016
	rev TGCAGAAGGCTTGAATGCCTC	GPP sgRNA Designer, Doench et al.,2016
Guide RNA GRPEL1-2	fwd GGTGGCTGTGCACAACAACCG	GPP sgRNA Designer, Doench et al.,2016
	rev CGGTTGTTGTGCACAGCCAC	GPP sgRNA Designer, Doench et al.,2016
Guide RNA HSPA9_1	fwd GACAAATGCTCCAATCTGACT	GPP sgRNA Designer, Doench et al.,2016
	rev AGTCAGATTGGAGCATTTGTC	GPP sgRNA Designer, Doench et al.,2016
Guide RNA HSPA9_2	fwd GTCGCCGGCCAATGAGACGCT	GPP sgRNA Designer, Doench et al.,2016
	rev AGCGTCTCATTGGCCGGCGAC	GPP sgRNA Designer, Doench et al.,2016
Guide RNA PMPCB-1	fwd GATCTTAACTAGATTCGTGTG	GPP sgRNA Designer, Doench et al.,2016
	rev CACACGAATCTAGTTAAGATc	GPP sgRNA Designer, Doench et al.,2016
Guide RNA PMPCB-2	fwd GTCCAGATACAATCTGTCTCA	GPP sgRNA Designer, Doench et al.,2016
	rev TGAGACAGATTGTATCTGGAc	GPP sgRNA Designer, Doench et al.,2016
Guide RNA LONP1-1	fwd GTCTGGGC GTCCCCGTG	GPP sgRNA Designer, Doench et al.,2016
	rev CACGGGGACGTTTGCCCAGAc	GPP sgRNA Designer, Doench et al.,2016
Guide RNA LONP1-2	fwd GTGGCTCACGTCCATCCCTTG	GPP sgRNA Designer, Doench et al.,2016
	rev CAAGGGATGGACGTGAGCCAc	GPP sgRNA Designer, Doench et al.,2016
non-targeting sgRNA	fwd GACCACTAATGAGATTCTTGT	BRDN0001148474 was a gift from John Doench & David Root Addgene # 80247
	rev ACAAGAATCTCATTAGTGGTC	

3.1.4 Recombinant DNA constructs

pOG44 Flp-recombinase expression vector	Thermo Fisher Scientific	GenBank#X52327, Cat#V600520
MTS-EGFP (*Su9-EGFP*)	Chen et al., 2003	Addgene #23214
lentiCRISPRv2	Sanjana et al.,2014	Addgene #52961
pCHAC-mt-*mKEIMA*	Richard Youle	Addgene #72342
pHAGE C-TAP	Wade Harper	https://doi.org/10.1016/j.cell.2015.06.043
pHAGE *mKEIMA* (cytosolic)	This study	N/A
pHAGE *Su9-EGFP Hygro*	This study	N/A
pEGFP-*PARKIN* WT	Trempe et al.,2013	Addgene #45875
pCMV-Sport6 *TIMM44*	Horizon	Cat#MHS6278-202802023
pCDNA5 FRT/TO *GRPEL1-TurboID*	This study	N/A
pCDNA5 FRT/TO *PRKN*	This study	N/A
pCDNA5 FRT/TO *PRKN* IRES *PINK1*	This study	N/A
pCDNA5 FRT/TO *TIMM44-TurboID*	This study	N/A
pHAGE mt-*mKEIMA Neo*	This study	N/A
Human CRISPR Knockout pooled Library (Brunello)	Doench et al.,2016, gift from David Root and John Doench	Addgene #73178, https://doi.org/10.1038/nbt.3437.

3.1.5 Enzymes

BSMBI	NEB	R0580
EcoRI-HF	NEB	R3101S
Hot Start Taq 2X Master Mix	NEB	M0496L
NEBNext® High-Fidelity 2X PCR Master Mix	NEB	M0541
NEBuilder® HiFi DNA Assembly Master Mix	NEB	E2621L
NotI-HF	NEB	R3189S
Proteinase K solution	Qiagen	19133
Q5® High-Fidelity DNA Polymerase	NEB	M0491L
Q5® Site-Directed Mutagenesis Kit	NEB	E0554S
Quick Ligation Reaction Buffer	NEB	B2200S
T4 DNA Ligase	NEB	M0202

3.1.6 Experimental models: cell lines

Hek 293T	ATCC	N/A
HeLa	ATCC	N/A
HeLa FlpIn Trex	Le Guerroué et al.,2017	https://doi.org/10.1016/j.molcel.2017.10.029
HeLa FlpIn TRex *PRKN*	This study	N/A
HeLa FlpIn TRex *PRKN mt-mKEIMA*	This study	N/A
HeLa FlpIn TRex *PRKN mt-mKEIMA PINK1* KO	This study	N/A
HeLa FlpIn TRex *PRKN PINK1*	This study	N/A
HeLa FlpIn TRex *mKEIMA* (cytosolic)	This study	N/A
HeLa FlpIn TRex *PRKN Su9-EGFP*	This study	N/A

3.1.7 Machines

FACSAria III cell sorter	BD Biosciences	N/A
FACSymphony™ A5 Cell Analyzer	BD Biosciences	N/A
LSRFortessa™ Cell Analyzer	BD Biosciences	N/A
Orbitrap Fusion Lumos Tribrid MS	Thermo Fisher Scientific	Cat#IQLAAEGAAPFADBMBHQ
QExactive HF Orbitrap MS	Thermo Fisher Scientific	Cat#IQLAAEGAAPFALGMBFZ
Odyssey® CLx Imaging System	LiCor	https://www.licor.com/bio/odyssey-clx/

3.1.8 Software and algorithms

Bowtie2 2.3.0	Langmead and Salzberg 2012	https://doi.org/10.1038/nmeth.1923
ClueGo + Cluepedia v1-v2	Bindea et al., 2009, Bindea et al., 2013	https://doi.org/10.1093/bioinformatics/btp101 https://doi.org/10.1093/bioinformatics/btt019
CQ1 Software	Yokogawa	N/A
cutadapt 2.8	Marcel Martin 2011	https://doi.org/10.14806/ej.17.1.200
Cytoscape 3.5.1	Shannon et al., 2003	https://cytoscape.org/
Excel 2016	Microsoft	Cat#KB4011684
FACS Diva	BD Biosciences	Cat#910723
FlowJo software V10	Treestar	https://www.flowjo.com/
ggplot2	Wickham et al., 2016	https://ggplot2.tidyverse.org
ggridges	Wilke, 2020	https://CRAN.R-project.org/package=ggridges
Illustrator CS6	Adobe	Illustrator-CS6-Win-GM
ImageJ 1.53c	Schneider et al., 2012	https://doi.org/10.1038/nmeth.2089
MAGeCK v0.5.6	Li et al., 2014	https://doi.org/10.1186/s13059-014-0554-4
MaxQuant 1.6.17	Cox and Mann 2008	https://doi.org/10.1038/nbt.1511
pandas 0.23.4	McKinney, 2010	https://scipy.org/

Perseus 1.6.5.0	Tyanova et al., 2016	https://doi.org/10.1038/nmeth.3901
Prism 6	GraphPad	https://graphpad-prism.software.informer.com/6.0
Proteome Discoverer 2.4	Themo Fisher Scientific	Cat#OPTON-30957
Python 3.6	Python Consortium	https://www.python.org/
R studio 1.2.5033	RStudio Team, 2020	http://www.rstudio.com/
R version 3.6.1	R Core Team	https://www.r-project.org/
SciPy	Virtanen et al, 2020	https://doi.org/10.1038/s41592-019-0686-2
statsmodels 0.12.2	Seabold, Perktold 2010	https://pypi.org/project/statsmodels/
tidyverse	Wickham et al., 2019	https://doi.org/10.21105/joss.01686
Tune 2.9	Thermo Fisher Scientific	N/A
Xcalibur 4.0	Thermo Fisher Scientific	Cat#OPTON-30965

3.2 METHODS

The method section is largely based on Schäfer, Bozkurt, Michaelis et al., 2022 and Michaelis et al. 2022 (in revision). The experiments were performed for the publications as well as for the here presented thesis and mostly overlap.

3.2.1 Cell culture

Human cell lines used for this study are listed at the experimental models: cell lines in the material table. Human epithelial cervix-adenocarcinoma (HeLa) cells (female), HeLa FlpIn TRex cells were cultured at 37°C and 5% CO2 in a humidified incubator in RPMI1640 medium (GIBCO 21875034) with 10% heat inactivated and sterile fetal bovine serum (FBS) (GIBCO 10270-106), supplemented with 4 µg/ml Blasticidine (Invitrogen) and 150 µg/ml Zeocin (Invitrogen). After transfection with pCDNA5 FRT/TO with insert and co-transfection (1:9 ratio) with pOG44 Flp-recombinase expression vector (Thermo Fisher Scientific), cells were selected after 2 days for at least 14 days in 50 µg/ml Hygromycin B Gold (Invitrogen). For the mitophagy assay, HeLa FlpIn TRex *PRKN* cells were transduced with pHAGE mt-*mKEIMA* Neo and fluorescence sorted for KEIMA-positive cells. Hek-293T cells were cultured in Dulbecco's modified Eagle's medium (DMEM, Invitrogen). CRISPR/Cas9 knockout cell lines were generated with lentiviral particles containing plentiCRISPRv2 with the gRNA of choice, transduced in the presence of 8 µg/ml Polybrene (TR-1003, Merck Millipore) and selected with 2 µg/ml puromycin (P8833, Sigma) for 11 days. Clonal depletions were individualized in 96-well plate and verified by immunoblotting. *C. elegans* strain maintenance: Strains were maintained on standard Nematode Growth Media (NGM) as previously described (Brenner, 1974) and cultured at 20–25 ^{o}C.

3.2.2 Construct

MTS-EGFP was a gift from David Chan (Addgene #23214) and pCHAC-mt-*mKEIMA* from Richard Youle (Addgene #72342). *MTS-EGFP* was cloned into pLD-puro-2A-rtTA-TcVA (Addgene # 24592) by

NEBuilder® HiFi DNA Assembly. mt-*mKEIMA* was cloned from pCHAC-mt-*mKEIMA* into the lentiviral over-expression vector pHAGE C-TAP and puromycin resistance replaced by neomycin to generate stable cell lines. Two gRNA per gene from human Brunello CRISPR were used and cloned individually via *BSMBI* restriction into lentiCRISPRv2 (Addgene #52961).

PRKN was amplified from pEGFP-*PARKIN* WT (Addgene #45875) and cloned via Gibson cloning into pCDNA5 FRT/TO to generate doxycycline-inducible HeLa FlpIn TRex cell lines. *TIMM44* cDNA was amplified from pCMV-Sport6 *TIMM44* (Horizon MHS6278-202802023), *GRPEL1* from HeLa cDNA and cloned in frame with *GS-linker-TurboID-FLAG* in a pCDNA5 FRT/TO backbone. All cloned constructs were verified by SANGER sequencing.

HaloTag fusion constructs were cloned into the lentiviral over-expression vector pHAGE C-TAP (gift of Dr. Richard C. Mulligan, Harvard Medical School, Boston, MA). Human gene of interest sequences were amplified from HeLa ATCC cDNA and the RPL28-HaloTag7 plasmid from An et al. 2020 was used for the HaloTag sequence (An et al., 2020). Gene of interest- HaloTag fusion genes were integrated with Gibson cloning in pHAGE C-TAP in between *EcoRI* and *NotI* restriction sites.

3.2.3 siRNA knock-down

Gene knock-down was achieved by transfecting HeLa FlpIn TRex cell lines with small double-stranded interfering RNAs (siRNA). Either Dharmacon ON-TARGETplus Human SMARTPool siRNA for *HSPA9*, *PAM16* or individual siRNA against *LONP1* were compared with pooled non-targeting control (NTC) or individual NTC siRNA against firefly luciferase *GL2*. SiRNA was transfected with Lipofectamine RNAiMAX (Thermo Scientific, 13778150), according to manufacturer's recommendations. Cells were cultured for 96 h after transfection until harvesting. Successful gene silencing was controlled by monitoring protein levels using immunoblots.

3.2.4 Lentiviral particle production

To generate lentiviral particles, HEK293T cells were seeded to a density of 80% confluence and transfected with media containing 1/10 of culture volume Opti-MEM I (Thermo Fisher Scientific, 31985-047), 10.5 µl Lipofectamine 2000 (Thermo Fisher Scientific, 11668019), 1.65 µg/ml gRNA pooled library in plentiCRISPRv2 (Brunello vector) (Addgene #73178), 1.35 µg/ml pPAX1 (Addgene #12260), 0.5 µg/ml pMD2.G (Addgene #12259), and 1% FBS. Lentiviral particle containing supernatant was harvested 48 h after transfection and stored at -80°C. Human Brunello CRISPR knockout pooled library was a gift from David Root and John Doench (Addgene #73178).

Lentiviral titer was determined using HeLa FlpIn TRex cells, plated at 70% confluence in a 6-well plate. After transduction with 8 µg/ml polybrene (Sigma, H9268) and dilution series over six powers of magnitude, cells were incubated for 48 h at 37°C and selected for an additional 14 days with 2 µg/ml puromycin. After selection, established colonies were counted for each dilution and the number of colonies in the highest dilution was normalized to the volume to determine the lentiviral titer.

3.2.5 CRISPR mitophagy screen

Fluorescence-sorted HeLa FlpIn TRex mt-*mKEIMA PRKN* cells were transduced with Human Brunello CRISPR knockout pooled library, using 8 µg/ml polybrene and a multiplicity of infection (MOI) of 0.2. In total 4 * 10^6 cells at 70% cell confluence were transduced yielding a coverage of 100x. Starting two days after transduction, cells were selected by maintaining 2 µg/ml puromycin and washed a minimum of five times before harvest. Cells were collected and sorted eight days after transduction as mitophagy-positive cells or pooled as total for comparison. The mitophagy-positive gate was set to include the population of cells showing an increased 561 nm/405 nm mt-mKEIMA ratio similar to what is observed after a 6 h treatment with 10 µM antimycin A and oligomycin (AO), while the main population of untreated cells (DMSO) or autophagy-inhibited cells, bafilomycin A1 (BafA1)-treated were excluded (gating is shown in Figure 11A). The gate for sorting mitophagy-incompetent knockouts

was set by including BafA1- and DMSO-treated control cells, while excluding the shifted AO-treated cell population. The collected cells were lysed and genomic DNA extracted by GeneJet DNA purification kit (Thermo Scientific, K0721).

3.2.6 Mitophagy flux mt-mKEIMA assay

Flow cytometry was performed on a BD LSRFortessa, as previously described (Meyer et al., 2018) or with BD FACSymphony A5. In brief, events were preselected for viable, single cell populations which showed KEIMA fluorescence, dual-excitation at 405 (pH 7) nm and 561 (pH 4) nm with 582/15 nm emission filters for BD LSRFortessa or 610/20 nm for BD FACSymphony A5 and 610/20 nm in both cases for 561 nm excitation. The percentage of lysosomal mt-mKEIMA was calculated by analysis of the 561 nm/405 nm ratio. Data processing was done with FlowJo (v10, Tree Star). Fluorescence-activated cell sorting for individual knockout cell lines or the genome-wide CRISPR screen were performed on a BD FACSAria™ III Cell Sorter and either collected in mixed populations or individual cells were collected in single wells of 96-well plates. Mt-mKEIMA localization in HeLa FlpIn TRex mt-*mKEIMA PRKN* cells was controlled by live cell microscopy on a Yokogawa CQ-1 with 405 nm excitation and 617/73 nm emission wavelength for neutral mt-mKEIMA and 561 nm and 617/73 nm for acidic mt-mKEIMA fluorescence. A 40x or 60x magnification and 96-well plates for live cell microscopy (Greiner Cat#655090) were used.

3.2.7 Next-generation sequencing

Polymerase chain reaction (PCR) was performed with NEBNext® High-Fidelity 2X PCR Master Mix (M0541). Thermal cycler parameters were set to: initial denaturation for 5 min at 98°C, 20 cycles of denaturation at 98°C for 30 s, annealing for 30 s at 58°C, extension for 40 s at 72°C, and final extension for 5 min at 72°C. PCR products were purified via 1% agarose gel electrophoresis and QIAquick Gel Extraction Kit (Qiagen, 28706). All samples were denatured and diluted according to the Illumina

NextSeq system denature and dilute libraries guide (document # 15048776 v09, illumina.com) and sequenced on an Illumina NextSeq 500. Custom Python scripts, cutadapt 2.8 and Bowtie2 2.3.0 were used to deconvolute the raw data and determine the abundance of individual gRNAs in each sample (M. Martin, 2011; Langmead & Salzberg, 2012).

3.2.8 MAGeCK analysis

To identify significantly enriched/depleted gRNAs, the respective samples were analyzed with MAGeCK v0.5.6 using standard parameters and median normalization (W. Li et al., 2014). The robust ranking aggregation score provides information about significant difference between treatment and control.

3.2.9 Live imaging of *C. elegans*

Appropriately staged worms in PF127, as described before (Lesanpezeshki et al., 2019), were imaged as previously reported (Dutta et al., 2019) using a VisiScope spinning disk confocal microscope system (Visitron Systems, Puchheim, Germany) consisting of a Leica DMi8 inverted microscope, a Yokogawa CSU X1M Dual Camscan head, and Hamamatsu sCMOS ImagEM EC- CCM cameras. Z-sectioning was performed with a Piezodriven motorized stage (Applied Scientific Instrumentation, Eugene, OR, United States). All acquisitions were performed at 20–23 ^{o}C using a Leica HC PL APO 63X/1.4-0.6 oil objective. Most analysis were done in collected z-sections of 21 focal planes (1mm apart) with 1 min intervals with a 488 and 561 nm laser at an exposure of 100 ms, for a total of 20 min. Experiments were performed by Ludovico Alves (Pohl/Eimer group, Goethe Universität Frankfurt).

3.2.10 RNA interference in *C. elegans*

RNAi experiments were performed by feeding as previously described (Kamath & Ahringer, 2003; Dutta et al., 2019). RNAi feeding bacteria were grown overnight (around 16–18 h) in 1 ml Luria broth with ampicillin at a concentration of 100 mg/ml and 500 ml of this culture was used to inoculate 10 ml

of LB ampicillin and grown at 37 °C for 6–8 h. This culture was then pelleted and resuspended in 300 ml of the same media, which was plated and kept for drying and induction on feeding plates (NGM agar containing 1 mM IPTG and 100 mg/ml ampicillin). Worms were kept on these feeding plates for 8 h, and the animals laid on these plates were analyzed 2 days later. All clones were available from the Vidal library (Rual et al., 2004). Experiments were performed by Ludovico Alves.

3.2.11 Fluorescence intensities in *C. elegans* and data analysis

All quantifications of fluorescence intensities of proteins were performed on maximum intensity projection. For all measurements, background intensities were subtracted from the integrated intensity of the signals. Two-channel matching and co-localization scoring by Pearson's correlation was used. The scatter plots represent the pixel information and were scored by Costes et al. method (Costes et al., 2004). Experiments were performed by Ludovico Alves.

3.2.12 MTS-EGFP mitochondrial fluorescence import assay

HeLa FlpIn TRex cells with doxycycline inducible MTS-*EGFP* and *PRKN* were treated with RNAi for 96 h, while 0.25 µg/ml doxycycline was added 24 h prior to microscopy. For GTPP treated cells, doxycycline was added only during the 6 h treatment. The cells were then stained by 50 nM Mitotracker Deep Red FM (Cell signaling 8778) for 20 min in pre-warmed RPMI 10% FBS medium. Cells were washed with PBS and incubated in RPMI 10% FBS during measurements. The Yokogawa CQ-1 with 40x or 60x magnification and automated focus was used to take live cell images with 488 nm excitation 525/50 nm emission for EGFP and 640 nm excitation 685/40 nm emission for Mitotracker Deep Red FM. 8 images with minimum 100 cells per biological replicate in total were analyzed by JACoP ImageJ plugin (Bolte & Cordelières, 2006). The co-localization between MTS-EGFP and Mitotracker Deep Red FM was determined by thresholded M2 (tM2) Manders coefficient (Manders et al., 1993) and gave an estimate to the amount of protein import into the matrix. The tM2 value was used as the inducible

MTS-EGFP cell line contained cells without visible *EGFP* expression to receive a sufficient dynamic range.

3.2.13 Stable HaloTag-protein cell line generation

Lentiviral particles were generated in HEK 293T cells by transfection with pHAGE HaloTag fusion vectors, containing a mitochondrial gene of interested cloned in frame with *HaloTag7*. In addition, following helper vectors were co-transfected: pHDM-VSVG, -HGPM2, -tatIB and pRC-CMV-revIB. Lipofectamine2000 (Thermo Fisher Scientific, 11668019) was used with Opti-MEM I (Thermo Fisher Scientific, 31985-047) according to manufacturer protocol, including a medium exchange after 6 h. Lentiviral particle containing supernatant was harvested 48 h after transfection, subjected to centrifugation at 1000xg for 3 min and added 1/10 together with 8 µg/ml polybrene (Sigma, H9268) to HeLa cells. HaloTag fusion-positive cells were selected by addition of 2 µg/ml puromycin for 11 days. Each cell line was checked by HaloTag TMR ligand (Promega, G8252) labeling and fluorescence microscopy for correct mitochondrial localization of the HaloTag-fusion protein.

3.2.14 HaloTag-protein uptake assay

Cells stably expressing HaloTag-fusion protein were seeded in 10-cm dishes and, on the same day of seeding and after cells had attached, 5 µM HaloTag® empty ligand (gift of Müller group, Institute of biochemistry II, Goethe Universität Frankfurt) in 5 ml RPMI 10% FBS medium was added to the cells overnight. This saturated all previous synthesized HaloTag fusion protein. The next morning cells were washed twice with prewarmed PBS (37°C) for 1 min each, and once with prewarmed RPMI 10% FBS medium for 5 min at 37°C. Two more 10 min-washes with prewarmed RPMI 10% FBS medium with 0.1% DMSO or 10 µM CCCP were done. This started the treatment time. For the last hour of the treatment 5µM HaloTag® Biotin Ligand (Promega, G8282) (in 2 ml medium) was added to the cells to label during the treatment synthesized HaloTag fusion protein. After 5:50 h treatment the cells were

washed twice for 1 min with 1x PBS (37°C) and once for 10 min with 0.1% DMSO or 10 µM CCCP-containing 10% FBS medium. The cells were harvested by 1 ml 0.25% Trypsin/EDTA and resuspended in 7 ml 4°C 10% FBS RPMI medium. Then, the cells were washed twice with ice-cold 1x PBS, pelleted by 800xg for 5 min and transferred into 2-ml low binding tubes.

3.2.15 TMRE membrane potential measurements

The mitochondrial membrane potential, the proton gradient over the inner mitochondrial membrane, was measured by tetramethylrhodamine (TMRE) (Perry et al., 2011; Crowley et al., 2016). 200 nM TMRE was used to stain cells for 30 min at 37°C in medium. Cells were then harvested by trypsinization with 0.25% Trypsin and EDTA, washed with cold PBS, hold on ice and subjected to flow cytometric analysis. TMRE was measured with excitation at 488 nm and a 582/15 nm emission filter. At least 10,000 cells were measured and categorized by gating according to DMSO or siRNA negative and a positive control, depolarized via CCCP treatment during TMRE staining.

3.2.16 Mitochondrial isolation

Cells were harvested by trypsin/EDTA treatment and washed with PBS. Cells were then resuspended in ice-cold MTE buffer pH 7.4 (270 mM D-mannitol, 10 mM TRIS, 0.1 mM EDTA) supplemented with 1x cOmplete, EDTA-free protease inhibitor cocktail (Roche, 11836170001) and lysed by sonication (25% maximum amplitude, 3x 10s pulse, 10s pause, Sonic Vibra Cell). For phospho-S65-ubiquitin immunoblot samples, PhosStop (Roche, 4906837001) and 10 mM N-ethylmaleimide (NEM) were added to the lysis buffer. Cell debris was removed by 10 min 1,400 xg 4°C centrifugation and the supernatant subjected to 10 min 15,000 xg 4°C to receive crude mitochondria, as previously described in more detail (Williamson et al., 2015). The pellet was washed once with MTE buffer and used or stored at -80°C.

3.2.17 Organelle-specific pulsed-SILAC MS sample preparation

Cells were treated for the indicated time, while the last two hours the medium was exchanged with prewarmed heavy SILAC medium consisting of RPMI160 medium for SILAC (GIBCO 88365) supplemented with 100 µg/mL Arg10 (Cambridge Isotope Laboratories), 100 µg/mL Lys8 (Cambridge Isotope Laboratories) and 10 % FBS. Crude mitochondria were isolated and samples prepared as previously described (Kulak et al., 2014). In brief, proteins were denatured, reduced and alkylated, and then purified by methanol/chloroform precipitation. Proteins were resuspended in 8 M urea, 10 mM EPPS pH 8.2 and the protein concentration measured via bicinchoninic acid (BCA) protein assay kit (ThermoFisher Scientific 23225). 20 µg protein were digested with 0.4 µg (1:50) LysC (Wako Chemicals) and 0.2 µg (1:100) Trypsin (Promega) 15 h at 37°C. Peptides were purified over Empore C18 (Octadecyl) resin material (3M Empore). 10 µg were labelled with tandem mass tag TMT11 (Thermo Scientific, A34808), quenched and pooled for fractionation. Pierce high pH reversed phase peptide fractionation kit (Thermo Scientific 84868) was performed accordingly to manufacturer's instructions. The fractions were dried by vacuum centrifugation for mass spectrometric measurement.

3.2.18 Insoluble protein fraction sample preparation

40 µg crude mitochondria, resuspended in MTE buffer with protease inhibitor cocktail were incubated for 10 min at room temperature with 1% digitonin, if not indicated otherwise. The insoluble protein fraction was sedimented at 20,000 xg 15 min 4°C. The supernatant was collected, containing the soluble protein fraction and the insoluble one was resuspended in SDS-buffer, for MS in 2% SDS, 50 mM Tris-HCl pH 8, 150 mM NaCl, 10 mM TCEP, 40 mM chloroacetamide, for immunoblotting in 4x reducing SDS-sample buffer and boiled at 95°C for 10 min.

3.2.19 TurboID proximity biotinylation

HeLa FlpIn *TIMM44-TurboID* cells were cultured for 3 d in biotin-free medium (DMEM with 10% dialyzed FBS). The *TurboID*-fusion gene was expressed by 0.25 µg/ml doxycycline addition 24 h prior to treatment. Proximity-labelling was induced by a 20 min incubation with 0.5 mM biotin-containing pre-warmed medium. Biotinylation was stopped by placing the cells on ice and washing 5x with ice cold PBS. Cells were scraped off in 5 ml PBS supplemented with protease inhibitor cocktail, sedimented at 800 xg for 3 min at 4°C, snap frozen in liquid nitrogen and stored at -80°C for further processing (Branon et al., 2018).

3.2.20 Streptavidin pull down and MS sample preparation

All buffers were prepared freshly on the day of the streptavidin pull-down experiments. Frozen cell pellets were thawed on ice and incubated for 15 min in lysis buffer (8 M Urea, 100 mM sodium phosphate pH 8, 100 mM ammonium bicarbonate, 1% (w/v) SDS, 10 mM TCEP, 40 mM chloroacetamide and 1x cOmplete, EDTA-free protease inhibitor cocktail (Roche, 11836170001)). Lysates were sonicated on ice three times for 30 s at 45% amplitude with 2 s rest between the cycles. For trichloroacetic acid precipitation, an equal volume of 40% ice cold trichloroacetic acid was added to the lysate and incubated for 1 h on ice. Precipitated proteins were sedimented at 20.000 x g at 4°C for 10 min. Pellets were washed 3 times with 90% ice cold acetone, air-dried and dissolved in resuspension buffer (8 M Urea, 100 mM sodium phosphate pH 8, 100 mM ammonium bicarbonate and 1% SDS) by shaking for 1 h at room temperature. After determination of the protein concentrations using the BCA protein assay kit (Thermo Fisher Scientific), same protein amounts were diluted with an equal volume of mili-Q water and subject to Streptavidin pull down. For Streptavidin pull down 15 µl of streptavidin magnetic beads (Thermo Fisher Scientific) were prepared by washing 3 times with washing buffer (4M urea, 0.5 % SDS (w/v) and 100 mM sodium phosphate pH 8). The protein lysates were mixed with streptavidin beads and gently rotated 15h at 4°C. The beads were washed 5 times

using washing buffer and 10 times using washing buffer without SDS (Kulak et al., 2014; Meier et al., 2018).

For on-beads digestion, Streptavidin beads were resuspended in elution buffer (2 M urea, 200 mM EPPS pH 8.2, 8% ACN) and incubated with 1 µg LysC protease per 20 µl beads for 2-3 h at 37°C. Afterwards, the samples were dilute 1:2.5 in 200 mM EPPS pH 8.2 and digested with 0.25 µg Trypsin (Promega) 15 h at 37°C. The supernatant was mixed with ACN (final concentration 20%) and eluted peptides were labelled with TMT10. Samples were pooled and dried by vacuum centrifugation for further processing. Streptavidin pull down and MS sample preparation was performed by Melinda Brunstein (Münch group, Goethe Universität Frankfurt).

3.2.21 Mass spectrometry

Dried peptides were resuspended with 0.5 µg/µl in 2 % (v/v) acetonitrile / 1 % (v/v) formic acid solution. Samples were shot with settings similar to previously studies (Klann et al., 2020). Protocol is provided as in Bojkova et al., 2020: First, peptides were separated on an Easy nLC 1200 (ThermoFisher Scientific) and a 22 cm long, 75 mmID fused-silica column, which had been packed in house with 1.9 mm C18 particles (ReproSil-Pur, Dr. Maisch), and kept at 45-50°C using an integrated column oven (Sonation). Peptides were eluted by a non-linear gradient from 5%–38% acetonitrile over 120 min and subsequently sprayed into a QExactive HF mass spectrometer equipped with a nanoFlex ion source (ThermoFisher Scientific) at a spray voltage of 2.3 kV. Full scan MS spectra (350-1400 m/z) were acquired at a resolution of 120,000 at m/z 200, a maximum injection time of 100 ms and an AGC target value of $3x\ 10^6$. Up to 20 most intense peptides per full scan were isolated using a 1 Th window and fragmented using higher energy collisional dissociation (normalized collision energy of 35). MS/MS spectra were acquired with a resolution of 45,000 at m/z 200, a maximum injection time of 86 ms and an AGC target value of $1x\ 10^5$. Ions with charge states of 1 and > 6 as well as ions with unassigned charge states were not considered for fragmentation. Dynamic exclusion was set to 20 s to minimize

repeated sequencing of already acquired precursors. Mass spectrometry machine handling was done by Georg Tascher (SFB1177 Z01 proteomics unit, Goethe Universität Frankfurt).

3.2.22 Mass spectrometry data analysis

Mass spectrometric raw data was analyzed using Proteome Discoverer 2.4 (ThermoFisher Scientific) as described in (Klann et al., 2020). Files were recalibrated using the Homo sapiens SwissProt database (TaxID = 9606, v. 2017-10-25) with methionine oxidation (+15.995) as dynamic modification and carbamidomethyl (Cys,+57.021464), TMT6 (N-terminal, +229.1629) and TMT6 (+229.1629) at lysines as fixed modifications, in organelle-specific pulsed-SILAC experiments, also TMT6+K8 (K, +237.177), Arg10 (R, +10.008) were set for dynamic modifications. Spectra were selected using default settings and database searches performed using SequestHT node in Proteome Discoverer. Database searches were performed against a trypsin digested Homo sapiens SwissProt database and FASTA files of common contaminants (`contaminants.fasta` provided with MaxQuant) for quality control. Fixed modifications were set as TMT6 at lysine residues, TMT6 (N-terminal) and carbamidomethyl at cysteine residues. As dynamic modifications acetylation (N-terminal) and methionine oxidation were set. After search, posterior error probabilities were calculated and peptide-spectrum matches (PSMs) filtered using Percolator using default settings. The Consensus Workflow for reporter ion quantification was performed with default settings. For the organelle-specific pulsed-SILAC experiments, peptide files were exported and heavy SILAC-labelled peptides extracted (Klann et al., 2020). Mitochondrial proteins were annotated using the human MitoCarta2.0 (Calvo et al., 2016). Reactome pathway network analyses were performed with PANTHER 15.0 and visualized with R studio (version 1.2.5033) in combination with the ggplot2 and stringr packages (Thomas et al., 2003; Gómez-Rubio, 2017; Wickham, 2019). Density plots were produced also with R studio using ggridges and tidyverse packages (Wickham et al., 2019; Wilke, 2020). To analyze proteomic data on individual protein level R studio using the heatmap2 function or the Perseus platform was utilized, via the hierarchal clustering

and heat map representation (Tyanova et al., 2016), common clusters over several experiments were identified.

3.2.23 Network analysis

Reactome pathway network analysis was performed with Cytoscape (version 3.8.0) in combination with the plugins ClueGO (version 2.5.7) and CluePedia (version 1.5.7) (Shannon et al., 2003; Bindea et al., 2009, 2013).

3.2.24 Immunoblotting

Protein samples in reducing SDS sample buffer were separated by SDS-PAGE with 4-12% or 12% Bolt Bis-Tris Plus Gels (Thermo Scientific). Gels were generally run between 120-160 V until the blue (bromophenol) running front reached the bottom of the SDS gel and the Chameleon® Duo Pre-stained Protein Ladder (LI-COR, 928-60000) showed a good separation. Proteins were transferred to 0.45 µM nitrocellulose membranes by using the Mini Trans-Blot® Cell system (Bio-Rad, 1703930) with 60 min 350 mA at room temperature with an installed -20°C cooling unit or 15 h 30V at 4°C. The blotting membrane was subsequently dried between two blotting papers, blocked for at least 1 h with Intercept® (PBS) Blocking Buffer (LI-COR, 927-70001) and incubated with a primary antibody diluted in 5% bovine serum albumin PBS 0.05% Tween under gentle shaking for 15 h. Blots were washed 3x for at least 5 min with PBS 0.1% Tween. Secondary antibodies were used as 1:15,000 in PBS 0.05% Tween and incubated for 1h, room temperature during gentle shaking in an opaque incubation box. Blots were washed 3x for at least 5min with PBS 0.1% Tween and rinsed with PBS. Near-infrared secondary antibodies were imaged using an Odyssey CLx imager (LI-COR) with 169 µm resolution and low to medium quality settings. Colorimetric measurement, image adjustments and quantification were done with Image Studio Lite v5.2 (LI-COR).

3.2.25 Quantification and statistical analysis

C. elegans experiments: The number of replicates per condition is mentioned for each condition or experiment individually. For each RNAi experiment, at least five biological replicates were carried out and technical replicates of these pooled. Animals and embryos with clear developmental problems or improperly mounted were excluded from our analysis.

Statistical significance for immunoblot, FACS results or global import rates were determined by two-sided unpaired or paired t-tests as stated in the figure legends, and performed with GraphPad Prism 6 or Microsoft Excel 2016. For multiple t-testing statistical significance was determined using the Holm-Sidak method, with α=5%, without assuming a consistent s.d.. Reactome pathway analyses were performed with PANTHER 15.0, used corrections for multiple testing are stated individually in the figure legends. ClueGo network analysis was performed with Bonferroni step-down correction. No statistical methods were used to predetermine sample size. For quantified data, if not stated otherwise, mean and standard deviation (s.d.) are indicated.

3.3 DATA AVAILABILITY

The mass spectrometry and CRISPR datasets generated during these studies can be found presented and as supplementary tables in Michaelis et al. *Nat Comm* 2022 (in revision, see 7 Publication list) and Schäfer, Bozkurt and Michaelis et al. 2022. All raw data will be made available in context of the publication.

4 Results

4.1 ESTABLISHING OF MITOPHAGY READ OUTS AND PERFORMING A GENOME-WIDE MITOPHAGY SCREEN

4.1.1 Mitochondrial mKEIMA assay sensitively detects mitophagic flux

To monitor mitophagy, i.e. mitochondrial degradation via the lysosome, I established the mitochondrial (mt)-mKEIMA as flow cytometric assay in our lab (Meyer et al., 2018) (Figure 10A). mt-mKEIMA shifts its excitation maximum in the low-pH environment of autolysosomes allowing ratiometric analysis of mitophagy flux (Violot et al., 2009). Therefore, HeLa Flp-In TRex cells, which lack endogenous *PRKN* (protein PARKIN) expression, were transduced with a steady mt-*mKEIMA* construct and further modified with inducible *PRKN* expression (Figure 10A).

Using live cell imaging, I looked at the localization/ morphology of the 405 and 561 nm channel. The 405 nm channel representing neutral mt-mKEIMA in healthy mitochondria, showed the typical mitochondrial network. The 561 nm channel representing autolysosomal mt-mKEIMA showed dot like structures as expected (Figure 10B). By the broad absorbance and fluorescence spectrum range of mKEIMA, a double staining with Mitotracker Red FM, Deep Red or green Lysotracker resulted in overlapping signal with the mKEIMA fluorescence and could not be used.

To test the mt-*mKEIMA PRKN* cell line specificity, I treated it with a combination of the inhibitors for complex III, antimycin A1, and for the ATP-synthase (complex V), oligomycin and followed the fluorescence of both channels via live cell imaging (Figure 10B) and via flow cytometry (Figure 11A). This combination (antimycin A1 and oligomycin, AO) is known to depolarize the mitochondrial membrane potential and give a strong PINK1-/PARKIN-dependent mitophagic reaction (Lazarou et al., 2015).

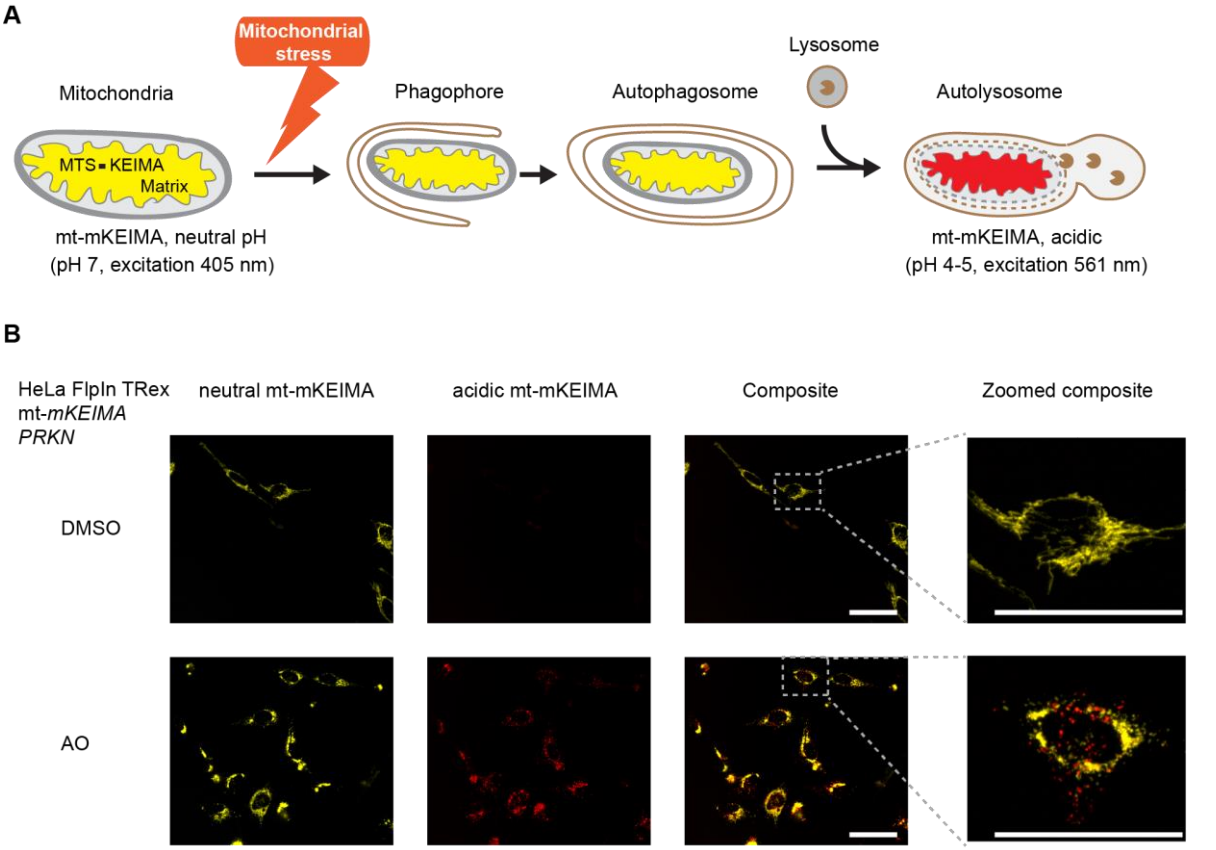

Figure 10: **Mitochondrial mKEIMA fluorescence reports pH-changes of the mitochondrial environment.** (A) Illustration of mt-mKEIMA mitophagy flux approach. mKEIMA shifts its excitation maximum in the low-pH environment of autolysosomes from 405 nm to 561 nm. By fusion to a mitochondrial targeting sequence (MTS), it allows to monitor mitophagic flux and was measured in this study by live cell imaging or flow cytometric analysis. (B) HeLa FlpIn TRex cell line with mt-*mKEIMA* overexpression and inducible *PRKN* (protein name PARKIN) were used. Mitochondria showed morphology changes, fragmentation and increase of 561 nm excited fluorescence upon 6h 10 µM antimycin A1 and oligomycin (AO) treatment. Live cell microscopy was performed with CQ-1, Yokogawa, 40x, 5x digital zoom for zoomed image. Scale bar represents 50 µm.

A clear separation of the mt-mKEIMA populations in fluorescence flow cytometric measurement was observed between AO-treated and control samples after a 6 h treatment. The flow cytometric results were shown as pseudo color dot plots, showing each cell and its fluorescence for acidic and neutral mKEIMA (Figure 11A); and as histogram plot representing the ratio of the two channels (Figure 11B). By co-treatment with bafilomycin A1 (BafA1), a lysosomal inhibitor targeting the acidification and fusion of autophagosomes with lysosomes (Mauvezin & Neufeld, 2015), the autophagy induced

population was partially rescued (Figure 11A-C). This showed that the 561/405 mKEIMA ratio indeed corresponds to autolysosomal localization and acidification of mitochondria. To highlight the differences gates were used comprising mitophagy positive cells and excluding most of the control cells.

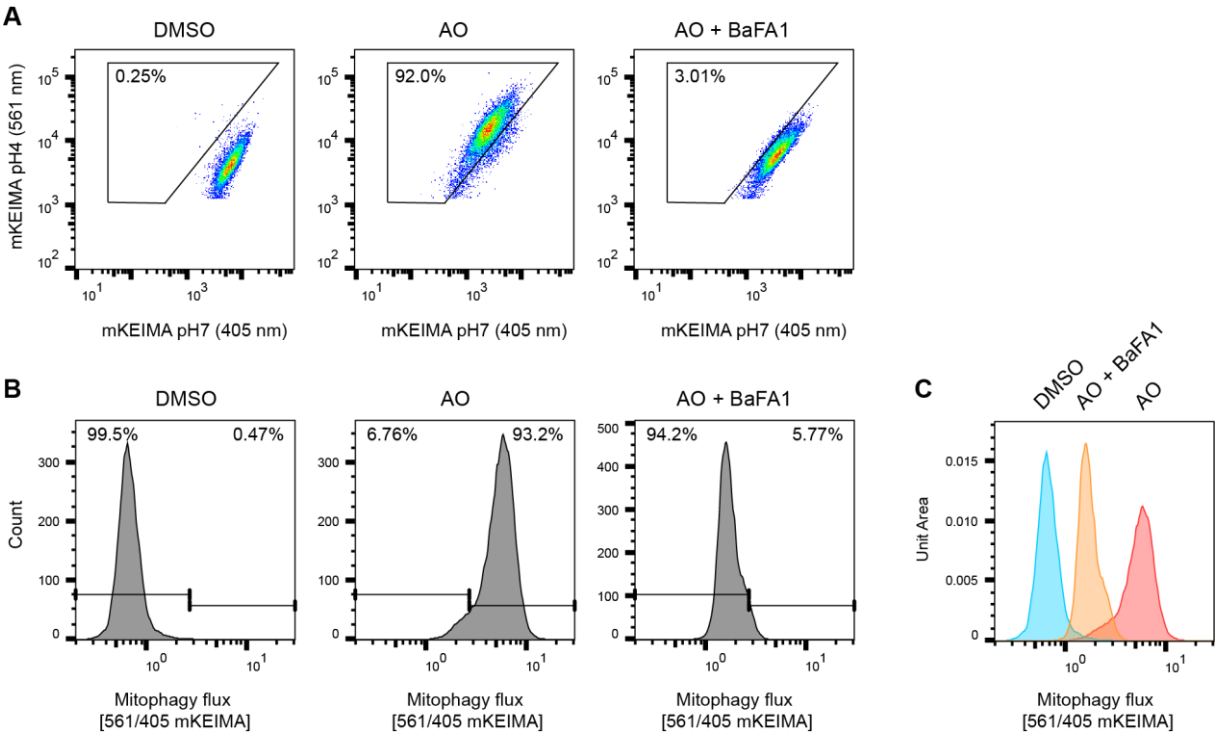

Figure 11: **Mitochondrial mKEIMA assay sensitively detected mitophagic flux and can be inhibited by known autophagy inhibitor bafilomycin A1**. (A) Pseudocolor representation of low pH 4 mt-mKEIMA vs. neutral pH 7 excited mt-mKEIMA fluorescence. A minimum of 5000 cells were measured per replicate and treatment. Co-treatment of 10 µM antimycin and oligomycin (AO) for 6 h was compared to DMSO and AO with 200 nM Bafilomycin A1 (BafA1). (B, C) Histogram plot of (A) shows ratios of acidic to neutral mt-mKEIMA representing mitophagic flux from low, basal (left) to high mitophagy (right). (B) gives the individual frequencies and (C) allows a qualitative comparison of the individual treatments relative to each other. All experiments were done in triplicates and one representative replicate is shown.

4.1.2 Optimization of screening conditions

To investigate what genetic knockouts (KO) and depletion of pathways drive mitophagy, I performed an unbiased genome-wide CRISPR/Cas9 mt-mKEIMA screen. To optimize the assay conditions for a genome-wide screen and to validate that I was measuring canonical PINK1/PARKIN-mitophagy, the *PINK1* gene was targeted with 3 guide RNAs and compared to an empty vector control (Figure 12A). In pseudo color dot plots WT cells treated with 1 µM AO overnight showed 98% mitophagy-positive, while the mixed *PINK1* KO population showed a reduction to about 24% mitophagy-positive cells. These remaining mitophagy-positive cells still responded to lysosomal inhibition via BafA1 and likely did not develop a *PINK1* KO (Figure12B). In this regard, the mitophagy reduction by 74% exceeded my prior expectations, as statistically, it was expected to reach a frame shift in about 67% of cells, which would result in formation of an early Stop codon. Therefore, these described results confirmed that my screening set up works for crucial mitophagy gene depletions.

After carefully evaluating the experimental conditions, I aimed to identifying additional pathways capable of inducing mitophagy that may explain mitochondrial membrane potential breakdown-independent mitophagy.

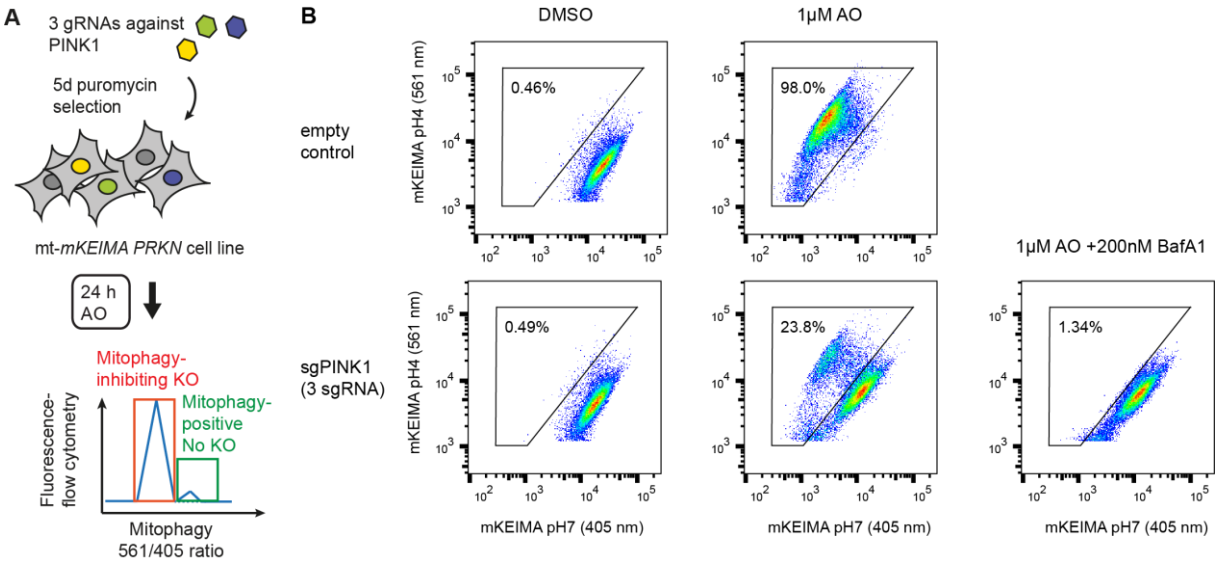

Figure 12: **Test-CRISPR-screen targeting essential mitophagy gene *PINK1* shows clear separation between AO-activated and by *PINK1* KO mitophagy-inhibited cells.** (A) Experimental scheme illustrating CRISPR/Cas9 test experiment. HeLa FlpIn cells expressing the mitophagy reporter mt-*mKEIMA* and *PRKN* were infected with lentiviral particles containing gRNAs against *PINK1*. After two days to express the resistance gene, cells were selected for 5 days with 2 µg/ml puromycin. Cells were treated over night with 1 µM AO and analyzed via flow cytometry measuring (described in Figure 11). (B) Pseudo color representation for empty control or sg*PINK1* treated cells upon DMSO, AO or AO with BafA1 co-treatment after 24 h. A minimum of 5,000 cells were measured per replicate and treatment.

4.1.3 Genome-wide Mitophagy CRISPR/Cas9 screen

The final genome-wide mitophagy CRISPR/Cas9 screen comprised 19,114 targeted human genes, with 4 gRNAs per gene and 1000 control gRNAs. In total, 77,441 different lentiviral particles were generated in a pooled manner. The experimental workflow is depicted in Figure 13 and shows the individual steps to receive finally functional data to pathways critical for mitophagy. Depending on the population sorted in mt-mKEIMA-based fluorescence-activated cell sorting (FACS) (mitophagy-induced by gene depletion or gene depletions that inhibit mitophagy upon mitochondrial stress), the mitophagy screen can be used to understand the mitophagic pathway in more detail (Figure 13).

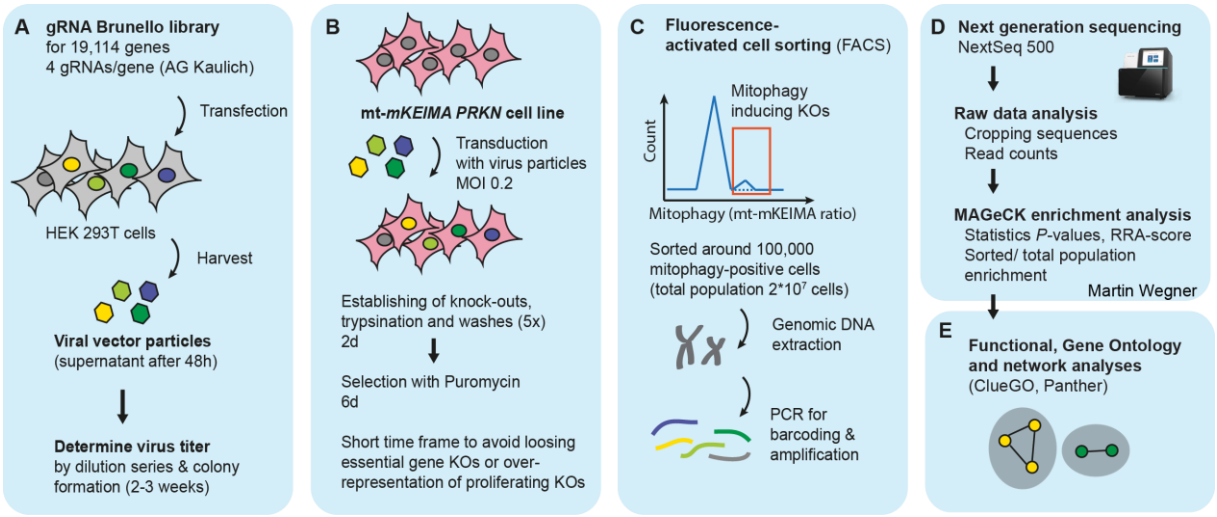

Figure 13: **Experimental design of the mitophagy CRISPR/Cas9 screen.** The workflow can be divided in five parts: (A) generation of lentiviral particles from pLenti gRNA Brunello plasmid library, (B) transduction, establishing of gene deletions and selection of cells containing one gRNA, (C) FACS (e.g. here shown for mitophagy-inducing KOs), DNA extraction, amplification and barcoding of the samples by PCR, (D) quantification of gRNA per sample by next generation sequencing and data processing, (E) functional analysis of the data and identification of biological relevance. The Brunello plasmid library was provided by Manuel Kaulich (Goethe Universität Frankfurt). Martin Wegner (Kaulich group, Goethe Universität Frankfurt) supported during sample barcoding and performed the next generation sequencing, raw data analysis and MAGeCK enrichment analysis.

As my focus was on stresses that induce mitophagy, I first studied the population of genes which trigger mitophagy upon depletion. In this data set (Figure 14), I identified 68 targeted genes in sorted cells that were significantly enriched with three gRNAs per gene and over 1000-fold when compared to the unsorted population (Figure 14 A and B, see Supplementary table 1). Strikingly, components of the PAM complex and mitochondrial protein import/ protein targeting to mitochondria in general were prominent within this group and its GO-terms/ Reactome pathway significantly increased (Figure 14C and D).

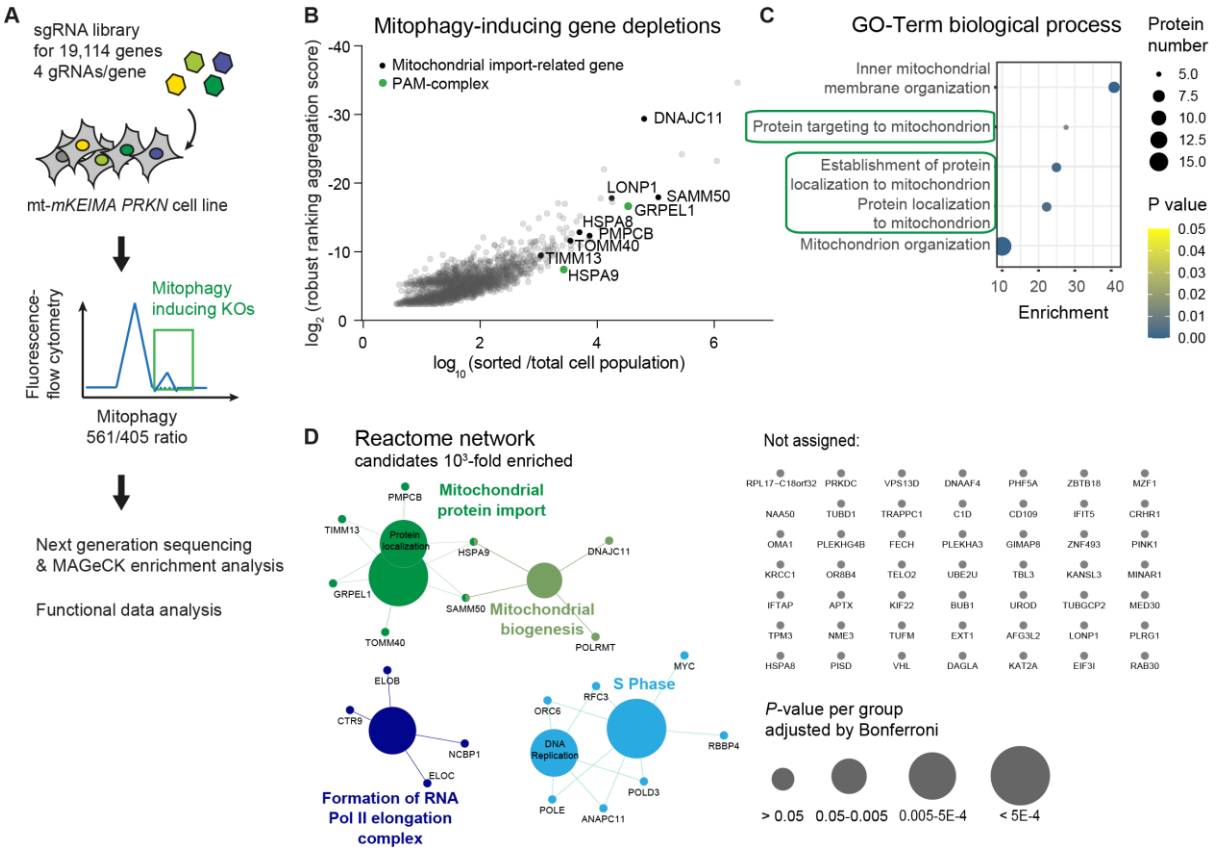

Figure 14: **Genome-wide CRISPR/Cas9 screen identifies protein import gene depletion as driver for mitophagy.** (A) Brief experimental scheme of a genome-wide CRISPR/Cas9 screen to identify genes that induce mitophagy when knocked-out. HeLa FlpIn cells expressing the mitophagy reporter mt-*mKEIMA* and *PRKN* were infected with a lentiviral particle library cultured for eight days in selection medium. Cells exhibiting induced mitophagy were sorted and analyzed by next generation sequencing. (B) Scatter plot presenting enrichment of targeted genes and determined robust ranking aggregation value of this gene in positive selection (sorted versus total population). (C) GO term analysis of biological processes enriched in the 1000-fold elevated significant candidates from B. (D) Reactome network analysis using Cytoscape and ClueGO-CluePedia as C.

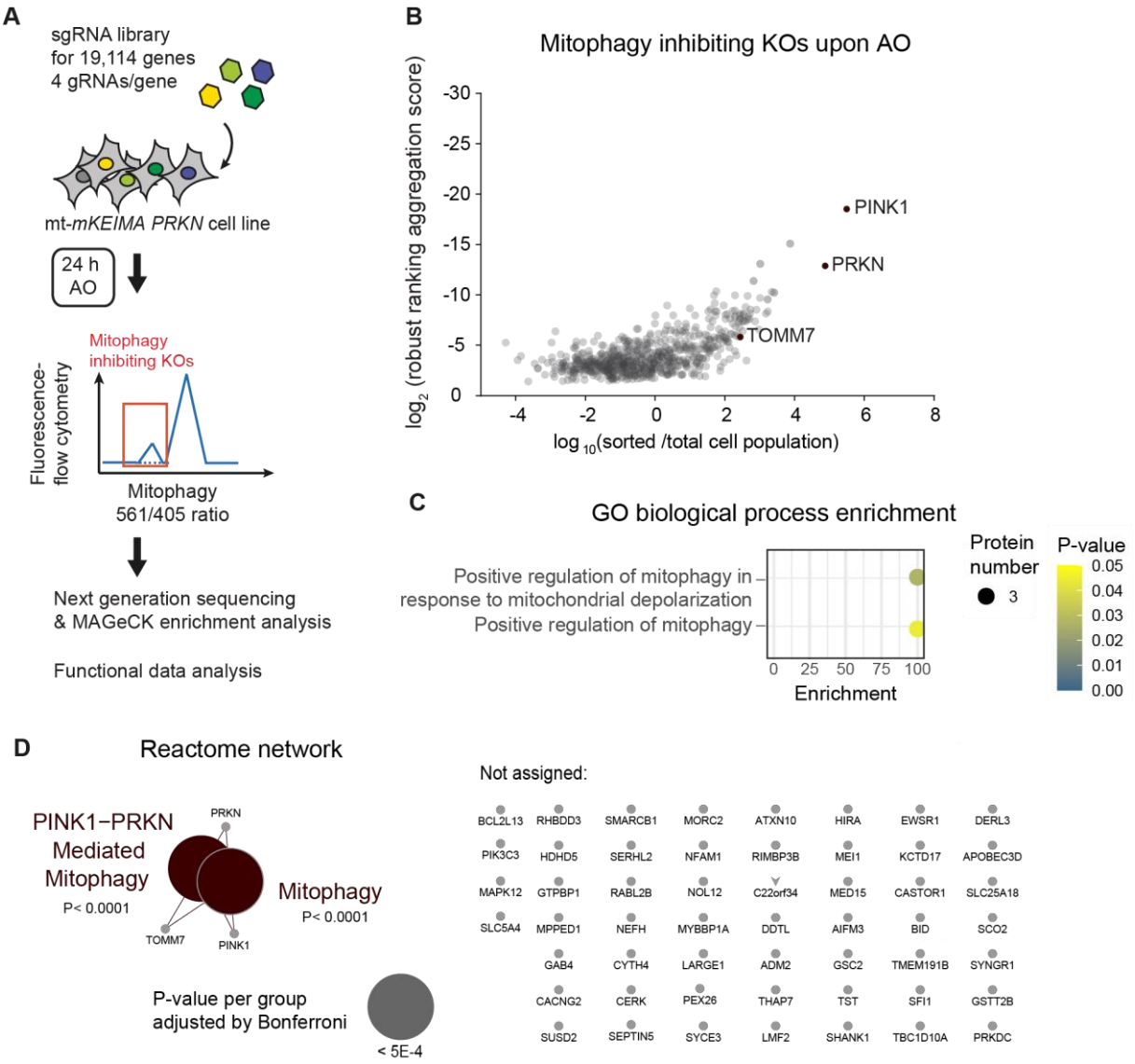

Figure 15: **Mitophagy CRISPR/Cas9 screen identified novel PINK1-mitophagy-essential genes.** (A) Brief experimental scheme of a genome-wide CRISPR/Cas9 screen to identify genes deletions inhibiting PINK1/PARKIN- mediated mitophagy. HeLa FlpIn cells expressing the mitophagy reporter mt-*mKEIMA* and *PRKN* were infected with a lentiviral particle library and treated after seven days of selection. Cells exhibiting no mitophagy upon 1 µM AO treatment overnight were sorted and analyzed by next generation sequencing. (B) Scatter plot presenting enrichment of targeted genes and determined robust ranking aggregation value of this gene in positive selection (sorted versus total population). (C) GO term analysis of biological processes 100-fold significantly enriched candidates from B from three replicates. (D) Reactome network analysis using Cytoscape and ClueGO-CluePedia for candidates as in C.

Next, I also measured which gene depletions prevent mitophagy upon AO-treatment and during the

here applied screening conditions (Figure 15A). *PINK1* and *PRKN* (here: *PARK2*) knockouts enriched as top candidates. *TOMM7*, coding for a component of the TOM complex which stabilizes PINK1 on the OMM upon mitochondrial stress, was also increased (Figure 15B). These findings demonstrated that the screening strategy robustly reproduced published results (Figure 15C) (Hasson et al., 2013; Potting et al., 2018). Besides deletions of *PIKC3C*, no other genes of the core autophagy machinery were significantly enriched upon AO-treated sorting conditions (Figure 15 D).

4.1.4 Validation of mitochondrial protein import and quality control gene KOs as inducers of PINK/PARKIN-dependent mitophagy

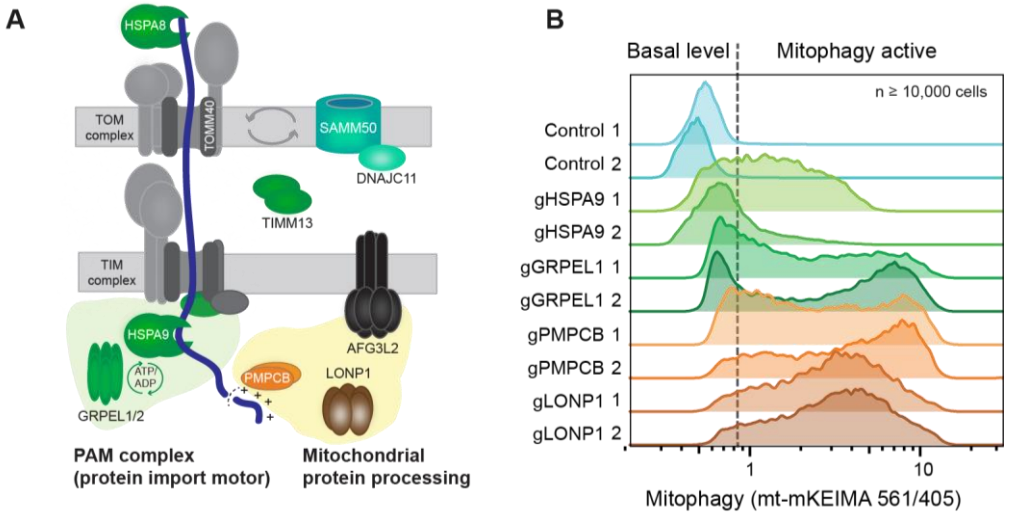

Figure 16: **Loss of PAM and mitochondrial protein processing peptidases induced mitophagy**. (A) Depiction of the mitochondrial import machinery and mitochondrial protein processing. Genes identified in Figure 14B as mitophagy inducers were labeled by protein names. (B) Two PAM components and two mitochondrial protein processing genes were validated via individual gene KOs (2 independent gRNAs) and mitophagy flux assays. All analyzed KOs induced mitophagy after 8 days or 6 days for g*HSPA9*, compared to empty vector controls. Data is shown as histogram plot representation for ≥10,000 fluorescent cells per sample. Basal and induced level of mitophagy is depicted via dotted line between the two conditions.

Showing a strong effect in the mitophagy CRISPR screen, I focused on protein import related and protein quality genes to validate candidates which induced mitophagy when depleted. I carried out single gene KOs with two guide RNAs (gRNAs) per gene for: PAM components (*HSPA9* and *GRPEL1*) and the mitochondrial processing peptidases *PMPCB* and *LONP1* (Figure 16A). These gene depletions were tested individually for their effect on mitophagy flux (Figure 16B). *PMPCB*, *LONP1* and PAM complex component deletions induced mitophagy, being consistent with the genome-wide screen.

To verify the role of the PAM complex in mitophagy in an organism, I collaborated with Ludovico Alves (Pohl/Eimer group, Goethe Universität Frankfurt) who monitored mitochondrial degradation upon RNAi-mediated loss of PAM complex components in *Caenorhabditis elegans.* To follow mitophagy *in vivo*, mitochondrial matrix protein NAD-dependent protein deacylase (Sir2.2), as a marker for mitochondria and its co-localization with autophagosomal Protein LGG-1 (orthologue to human GABARAP) was determined via microscopy and co-localization image analyses (Figure 17A) (Costes et al., 2004; Wirth et al., 2013; Chen et al., 2017). PAM component (human orthologues: *GRPEL1/2*, *PAM16*, *TIMM44* and *DNAJC19*) depletions induced mitophagy significantly in adult worms (Figure 17B-E), showing that mitophagy activation upon loss of PAM complex is conserved from human to *C. elegans*. *HSPA9* orthologue *hsp-6* depletion was lethal in *C. elegans* and therefore not included in this experiment.

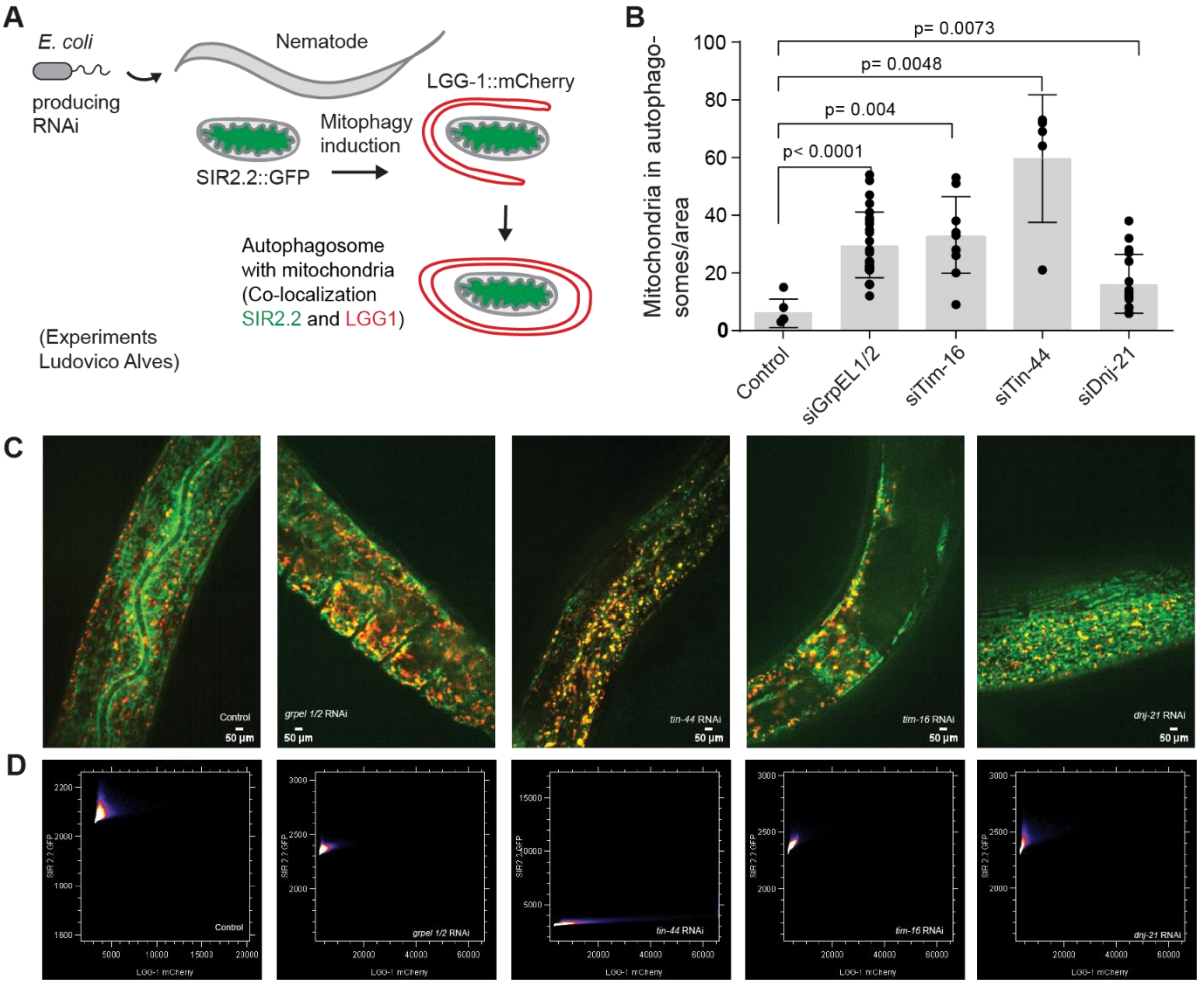

Figure 17: **Loss of PAM components induced mitophagy in *C.elegans*.** (A) Experimental scheme to assess mitophagy in *C. elegans* using the autophagosomal marker LGG-1::mCherry (red) and mitochondrial matrix marker SIR2.2::GFP (green). Co-localization of the markers showed existence of mito-autophagosomes, which correlates with mitophagy, as previously shown with comparable markers (Palikaras et al., 2019). RNAi depletion was reached by feeding *Escherichia coli* producing double stranded inhibitory RNA to adult worms, accordingly to Timmons et al., 2001. (B) RNAi knock-down of components of the PAM complex in *C. elegans*. Shown are ratios of autophagosomes containing mitochondria, representing mitophagic flux, after knock-down of individual PAM components in worms. Histograms indicate median values ±s.d. (n ≥ 5 biological replicates, p-values were calculated by two-sided unpaired t-test). (C) Representative pictures shown and measured for a minimum of five biological replicates. (D) Two-channel matching and co-localization scoring by Pearson's correlation confirmed visual observation from (C). Scatter plot represents pixel information and was scored accordingly to the method described in Costes et al., 2004. These experiments were performed by Ludovico Alves.

4.2 CHARACTERIZATION OF IMPORT DEFECT- / PROTEIN MISFOLDING-DRIVEN MITOPHAGY

To further characterize the observed phenotypes and to understand the underlying mechanism, I investigated in this chapter PINK1 accumulation, PINK1 dependency, protein import into mitochondria, mitochondrial membrane potential and the tendency of mitochondrial proteins to form an insoluble protein fraction upon misfolding stress inside the matrix.

4.2.1 Establishing a clonal *PINK1* KO cell line to study PINK1-dependency

First, to determine whether the observed mitophagy activation by PAM component depletion depends on the PINK1-PARKIN pathway, I depleted *PINK1* with the CRISPR/Cas9 system using a single guide RNA. The cell population was then individualized and single cell clones expanded. *PINK1* depletion was examined via quantitative near-infrared immunoblotting versus wild type (WT) cells and compared to a *PINK1* WT overexpression cell line. As PINK1 only reaches observable protein levels during mitochondrial stress conditions, the cells were either treated with AO or PINK1 degradation was attenuated by proteasomal inhibition with MG-132 (Figure 18A). During both treatments no significant PINK1 accumulation was detectable for KO cells, while WT cells showed present bands. Upon AO treatment, full length (FL) PINK1 increased 2.5-fold, upon MG-132 about 1.5-fold for PARL-processed PINK1 (Δ) (Figure 18A-C). Moreover, the *PINK1* KO blocked the reduction of the mitochondrial proteins TOMM20 and TOMM40 during AO treatment (Figure 18A and D). In line with this observation, the *PINK1* KO blocked mitophagy in the mt-mKEIMA mitophagy flux assay (Figure 18E and F). Here, *PINK1* KO reduced the amount of mitophagy-positive cells upon AO and CCCP treatment by approximately 90%.

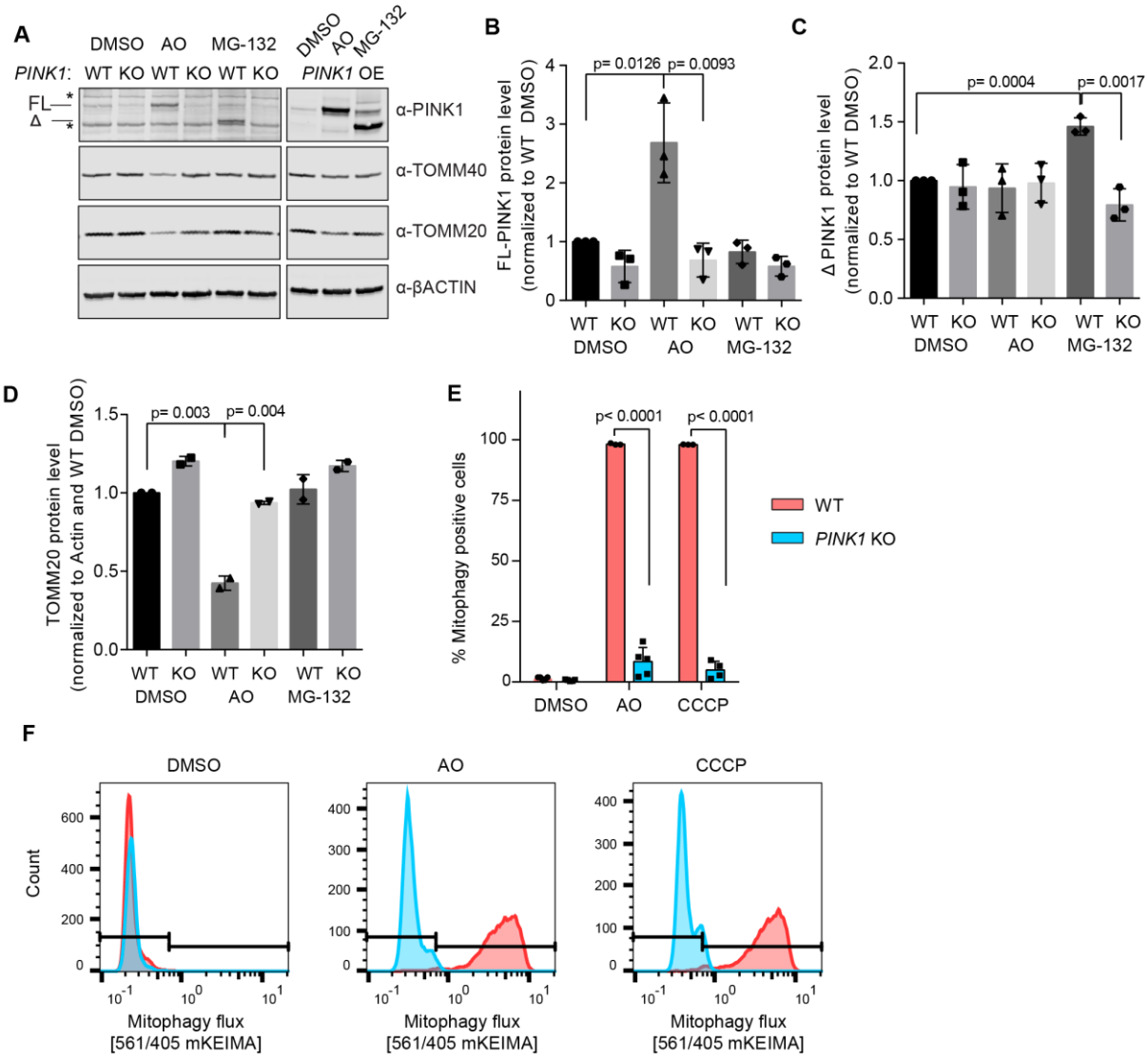

Figure 18: **Monoclonal *PINK1* depleted cell line allows to follow PINK1/PARKIN-dependent mitophagy.** (A) Immunoblotting of whole cell lysates treated for 6h with 10 µM AO or MG-132 of HeLa FlpIn mt-*mKEIMA PRKN* cells with (WT) or without *PINK1* KO. Representative blot shown. PINK1 full length (FL) and PARL-digested PINK1 (Δ) are labeled. Asterisks mark unspecific bands. *PINK1* overexpression (OE) cell line was loaded on same gel to highlight the two most abundant forms upon AO or MG-132 treatment. The *PINK1* OE image is shown with reduced brightness and contrast settings. (B, C) PINK1 quantification of full length and PARL-digested PINK1, lower molecular weight band, for n=3 with mean value s.d. indicated. Replicates were handled in parallel. (D) Quantification of TOMM20 level from immunoblotting A. Data shown for n=2 with mean value ± s.d.. (E, F) mt-*mKEIMA* transduced WT and *PINK1* KO HeLa FlpIn cells, both with inducible *PRKN*, were tested for mitophagy flux upon 1 µM AO or 10 µM CCCP overnight. Data represented as mean value ±s.d. with n≥3 replicates. (F) One representative replicate from E showing the distribution of WT and PINK1 mt-mKEIMA cells during treatment.

With this mt-*mKEIMA PINK1* KO cell line in hand, I confirmed that depletion of the PAM component *HSPA9* induced PINK1-mitophagy. WT cells showed significant mitophagy flux, while *PINK1* KO cells almost none, demonstrating that *HSPA9* depletion induced PINK1-dependent mitophagy (Figure 19A). This observation was further confirmed by a significant PINK1 accumulation in *PINK1* WT cells during *HSPA9* RNAi (Figure 19B). Instead of a CRISPR KO, RNAi for 4 days was used to avoid cell death due to the lethality of a *HSPA9* KO (Hart et al., 2015).

Next, to understand the molecular effects leading to PINK1 accumulation, I tested mitochondrial matrix-targeted import by MTS-EGFP co-localization with Mitotracker Deep Red FM in life cell imaging (Figure 19C). A decrease of mitochondrial protein uptake was thereby reflected by extra-mitochondrial GFP staining. *HSPA9* depletion led to an increase of extra-mitochondrial fluorescence and thus to a significant reduction of matrix-targeted import (Figure 19D). As this observation could be a direct effect of mitochondrial protein import inhibition or an indirect by mitochondrial membrane depolarization, I also measured the membrane potential utilizing TMRE fluorescence and flow cytometry. The membrane potential during *HSPA9* knock-down stayed intact (Figure 19E). Summarizing these findings: I observed that *HSPA9* depletion inhibited the mitochondrial protein import, however without inducing a loss of membrane potential. This indicated that *HSPA9* depletion had a direct effect on matrix-targeted protein import. Simultaneously, to the reduced protein import, PINK1 accumulated and PINK1-dependent mitophagy was activated (Figure 19F).

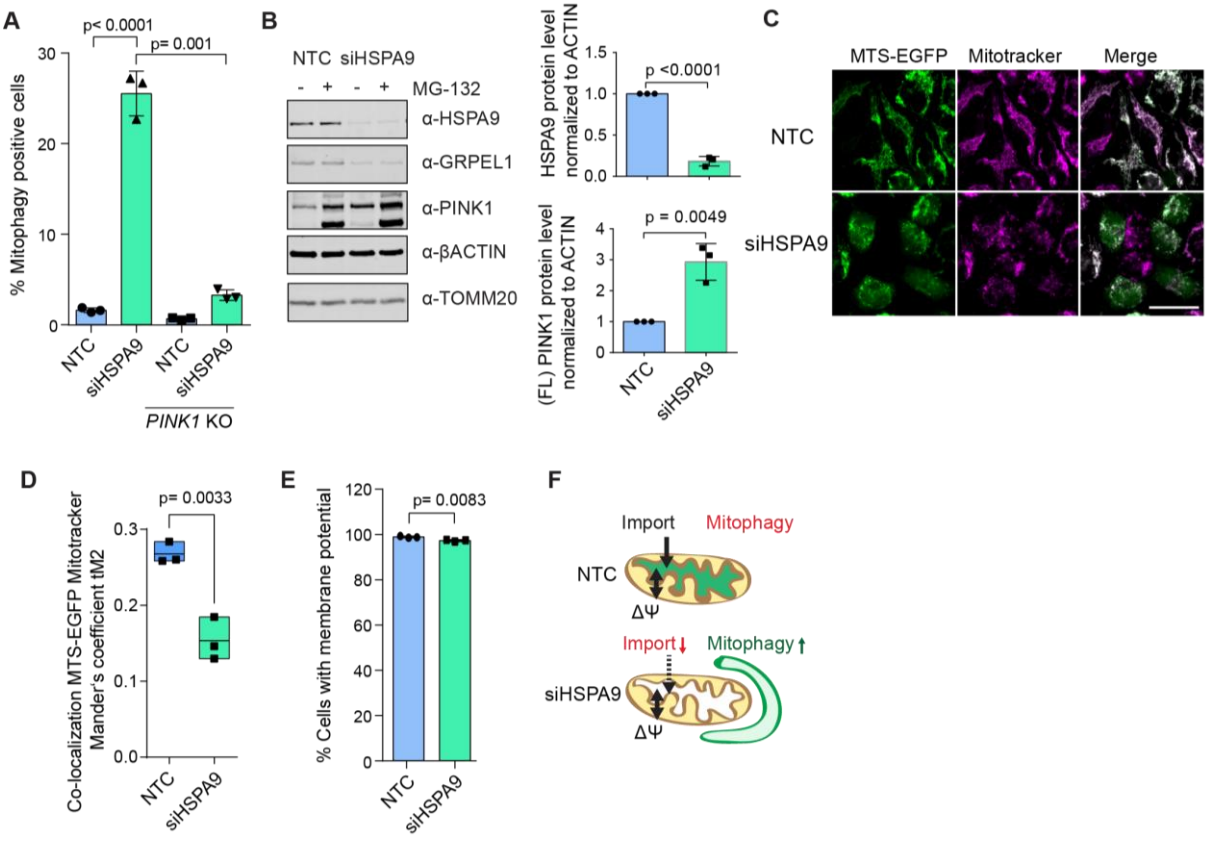

Figure 19: ***HSPA9* depletion reduced mitochondrial protein import and activated mitophagy without membrane depolarization.** (A) Analysis of mitophagy flux by mt-*mKEIMA* in WT or *PINK1* KO cells after knock-down of *HSPA9* for 4 days. Data represented as mean value ±s.d. (n= 3). (B) *HSPA9* depletion and full length (FL) PINK1 accumulation was confirmed on protein level via immunoblotting. Quantification for 3 parallel experiments was shown as mean value ±s.d.. (C) HeLa FlpIn TRex cells with inducible *MTS-EGFP* and *PRKN* expression were treated with *HSPA9* siRNA for 96 h. Dox was added 15 h before microscopy (to induce *MTS-EGFP* and *PRKN*). Mitochondrial localization of EGFP was analyzed via staining with Mitotracker Deep Red FM and live cell imaging. Scale bar 25 µm (in all images). (D) Co-localization image analysis for n= 3 biological replicates with 100 EGFP-positive cells per replicate, shown as mean ±minimum-maximum value. (E) Flow cytometry analysis to determine mitochondrial membrane potential changes in cells transfected with non-targeting control or *HSPA9* RNAi. A minimum of 5,000 fluorescent cells per biological replicate were measured and categorized by gating. (F) Schematic overview depicting the effects of *HSPA9* knock-down on mitochondrial import, on membrane potential and on mitophagy induction (from A-E). For all experiments, the two-sided unpaired t-test method was performed to determine statistical significance.

To rule out that HSPA9's function in protein folding was driving mitophagy during *HSPA9* depletion, rather than its involvement in protein import, I also investigated the effect of *PAM16* depletion on protein import and mitophagy induction. PAM16 is only known for its function in protein import (Frazier et al., 2004). Using MTS-EGFP-based co-localization data, a significant reduction of

mitochondrial MTS-EGFP was observed, this indicated that less protein import to the mitochondrial matrix was occurring when *PAM16* was depleted (Figure 20A, B). The reduction of protein import during *PAM16* depletion was accompanied by induction of mitophagic flux and stabilization of PINK1 on mitochondria (Figure 20C, D). This indicates that the absence of PAM protein import motor function leads to PINK1 mitophagy.

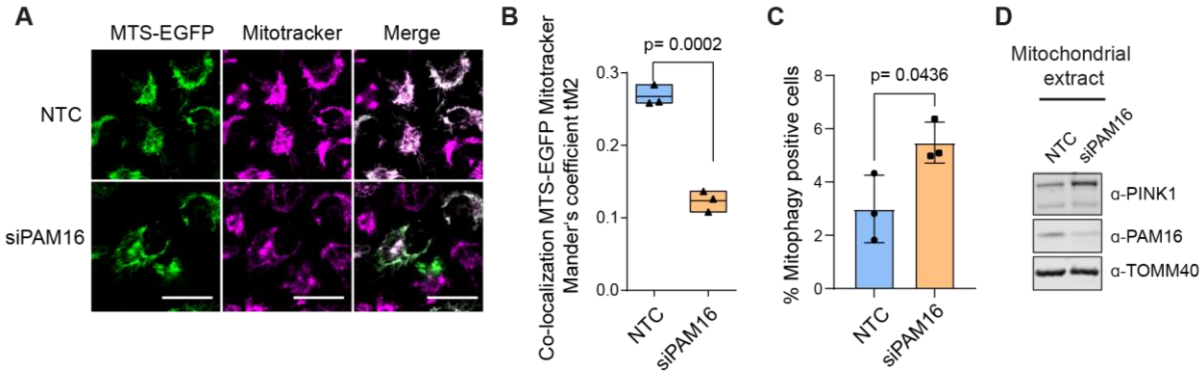

Figure 20**: PAM complex component *PAM16* depletion inhibits protein import and induces PINK1 mitophagy**. (A) HeLa FlpIn TRex cells with inducible *MTS-EGFP* and *PRKN* expression were treated with PAM16 siRNA for 96 h. Dox was added 15 h before microscopy (to induce *MTS-EGFP* and *PRKN*). Mitochondrial localization of EGFP was analyzed via staining with Mitotracker Deep Red FM and live cell imaging. Scale bar 25 µm (in all images). (B) Co-localization image analysis for n= 3 biological replicates with 100 EGFP-positive cells per replicate, shown as mean ±minimum-maximum value. (C) HeLa FlpIn TRex mt-*mKEIMA* cells with inducible *PRKN* expression were treated with *PAM16* siRNA for 96 h. Dox was added 15 h before flow cytometric measurements. Cells showing increased 561 nm/405 nm mt-mKEIMA ratios when compared to main population in NTC-treated cells were considered mitophagy-positive. Mean ±s.d. for n=3. (D) Representative immunoblot of mitochondrial extracts from 96 h *PAM16* RNAi treated HeLa FlpIn TRex *PINK1* IRES *PRKN* cells. Dox was added 15 h before harvest. Statistical significance was determined by two-sided unpaired t-test method.

As previously stated in literature, there are several mitochondrial stressors leading to mitophagy without the induction of membrane potential break down (Allen et al., 2013). To investigate if these inhibitors would show a similar phenotype as *HSPA9* RNAi, reduced protein uptake into mitochondria, accompanied by stress-induced mitophagy, I developed a proteomic approach that can monitor and quantify mitochondrial protein import rates, also for short treatments, such as several hours. The method is discussed in detail in chapter 4.3. and recently published (Schäfer, Bozkurt, Michaelis et al., 2022).

Deferiprone (DFP, an iron-chelator), and oligomycin were used. DFP leads to BNIP3-dependent mitophagy, however the exact trigger for mitophagy induction remained elusive (Allen et al., 2013). Oligomycin inhibits the ATP-synthase complex, induces mitophagy, even though it does not depolarize the mitochondrial membrane potential, but rather increases it (Duchen & Biscoe, 1992). In pulsed SILAC protein import proteomics, I found that both compounds decreased the protein import into mitochondria (Figure 21A). The mitophagic flux was elevated, showing mitophagy activation, as expected, while the mitochondrial membrane potential was not affected by the treatments (Figure 21B and C). These experiments, RNAi of *HSPA9*, DFP and oligomycin treatment, showed reduced mitochondrial protein import and induction of depolarization-independent mitophagy during three independent conditions (Figure 19, Figure 21D). This demonstrated that the prevailing model for stress-induced mitophagy induction, which required mitochondrial membrane potential collapse, is not the only mechanism for mitophagy activation.

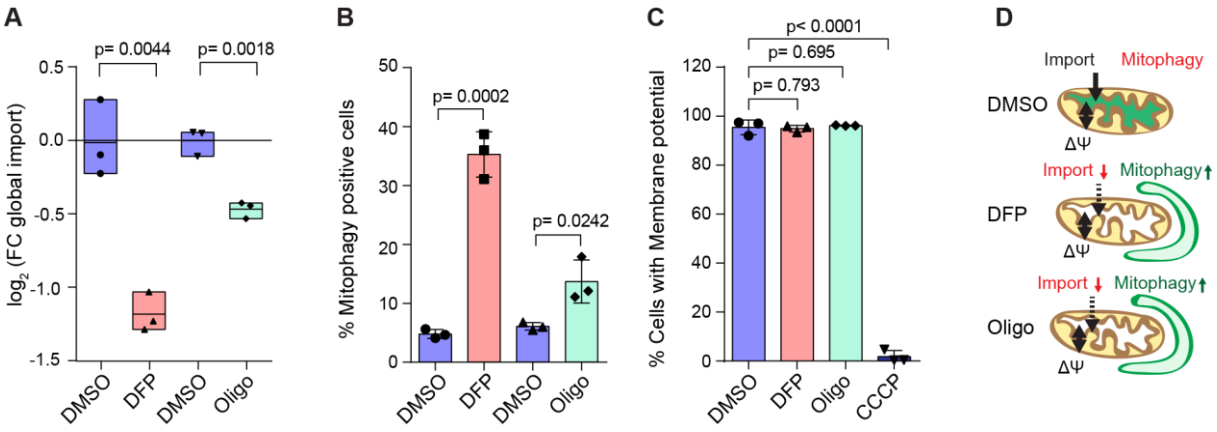

Figure 21: **Mitochondrial protein import reduction is accompanied by mitophagy without the necessity for mitochondrial membrane depolarization.** (A) Monitoring mitochondrial protein import by pulsed SILAC-proteomics showed a global import reduction during treatment with 10 µM oligomycin (Oligo) or 1 mM deferiprone (DFP) when compared to DMSO. Shown are minimum-maximum values and the mean value as central line for n= 3 (Method described in Chapter 4.3). (B) Assessment of mitophagy flux and (C) membrane potential in cells treated with DMSO, Oligo or DFP. 2h CCCP was included in membrane potential measurement as depolarized control. Shown are mean value ±s.d. for n= 3. (D) Schematic illustration of Oligo and DFP effects on mitophagy, on protein import

and on membrane potential. For all experiments, the two-sided unpaired t-test method was performed to determine statistical significance.

4.2.2 Mitochondrial protein folding stress diminished protein import and induced mitophagy in polarized and depolarized mitochondria.

Induction of mitophagy, independent of the loss of membrane potential, was also reported upon accumulation of misfolded mitochondrial proteins, but the mechanism behind it is not known (Jin & Youle, 2013). Based on my previous results, I hypothesized that protein misfolding in the matrix might affect mitochondrial protein import, ultimately inducing mitophagy. To test my hypothesis, I applied either an acute protein folding stress by the mitochondrial HSP90 inhibitor Gamitrinib-triphenylphosphonium (GTPP) (B. H. Kang et al., 2010) for 6 h, or an prolonged folding defect by depletion of *LONP1* utilizing RNAi. Treatment with GTPP significantly decreased mitochondrial protein import and induced PINK1-dependent mitophagy, as assessed by flow cytometry measurement of mt-mKEIMA and immunoblots for PINK1 stabilization (Figure 22A-C). However, upon GTPP treatment, mitophagic degradation was accompanied by a breakdown of the membrane potential (Figure 22D). To further assess the requirement of a loss in membrane potential upon protein folding stress, we next examined *LONP1* depletion for less acute stress.

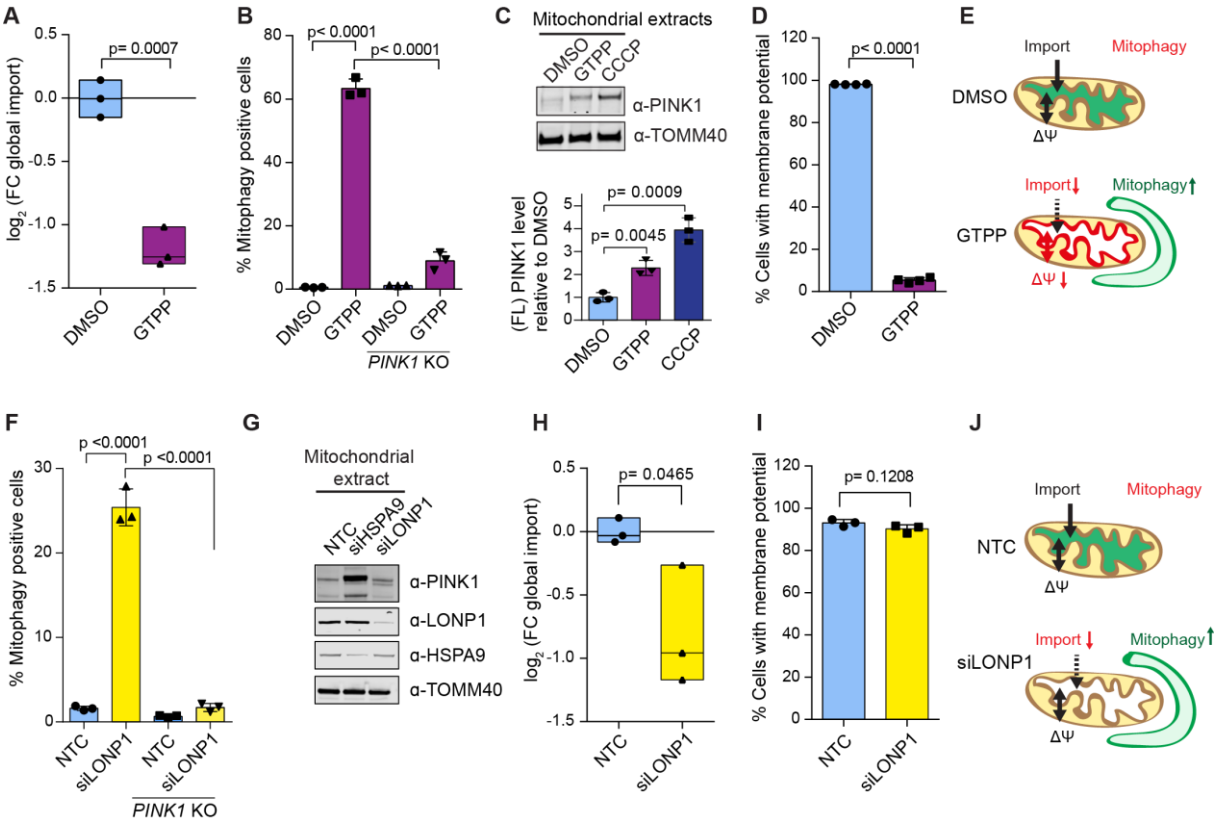

Figure 22: **Mitochondrial protein folding stress diminished protein import and induced PINK1-dependent mitophagy in polarized mitochondria.** (A) Pulsed-SILAC mitochondrial protein import assay measured a global import reduction in cells treated with 10 µM GTPP or DMSO for 6 h. SILAC pulse was performed for the last 2 h of the treatment and only proteins included in MitoCarta 2.0 were used for quantification. Shown are minimum-maximum values, median as central line (n= 3). Süleyman Bozkurt (Münch group, Goethe Universität Frankfurt) prepared the mass spectrometry samples for A. (B) Mitophagic flux was induced in mt-mKEIMA assay in WT cells and inhibited in clonal *PINK1* KO cells (n= 3). (C) Immunoblotting of crude mitochondrial extracts from 6h 10 µM GTPP or CCCP treated cells showed PINK1 stabilization. All replicates were run on the same SDS-gel and are represented as mean value ± s.d. for n=3. (D) Mitochondrial membrane potential was assessed by TMRE staining for n= 4 replicates. (E) Schematic illustration of reduced mitochondrial import and membrane potential while mitophagy was induced by GTPP. (F) RNAi of *LONP1* for 4 days induced mitophagic flux in mt-mKEIMA assay for WT cells but not in clonal *PINK1* KO cells (n= 3). (G) Representative immunoblot mitochondrial extracts from 4d *LONP1* RNAi treated HeLa FlpIn TRex *PRKN* cells. Data shown as mean value ±s.d. for n=3. (H) Pulsed-SILAC import assay of *LONP1* depleted cells (for 4 days) showed global import reduction. Shown are minimum-maximum values, median as central line (n= 3). (I) Mitochondrial membrane potential was assessed by TMRE staining for *LONP1* RNAi (n= 3). (J) Schematic illustration of reduced mitochondrial import, stable membrane potential and mitophagy induction by *LONP1* RNAi. TMRE and mt-mKEIMA data is shown as mean value +s.d. of n≥3 biological replicates with ≥ 5,000

fluorescent cells per replicate. For all experiments a two-sided unpaired t-test was performed to determine statistical significance.

In accordance with the observed effects upon *LONP1* CRISPR deletion, 4 days of *LONP1* depletion via RNAi also activated mitophagy (Figure 14 und 16). By comparing *PINK1* WT to the KO cell line, I found that the observed mitophagy phenotype was PINK1-dependent (Figure 22F and G). Furthermore, the *LONP1* depletion was accompanied by a significant reduction in mitochondrial protein import (Figure 22H). Strikingly, the membrane potential during *LONP1* depletion, in contrast to GTPP, stayed intact (Figure 22I). These results of *LONP1* RNAi show that loss of membrane potential is not a necessity for protein misfolding-induced mitophagy (Figure 22J).

In order to control for PINK1-independent mitophagy, I searched my mitochondrial proteome data sets for known PINK1-independent mitophagy receptors. Neither protein misfolding stress, via si*LONP1* or GTPP, nor mild oxidative stress via oligomycin led to the enrichment of the mitophagy receptors BNIP3, BNIP3L (NIX) or BCL2L13 on mitochondria (Figure 23). In contrast, iron depletion by DFP and IMS redox-relay-dependent import inhibition by MitoBlock-6 (Data from Schäfer, Bozkurt, Michaelis et al 2022) both resulted in significant BNIP3 and for DFP also BNIP3L enrichment on mitochondria (Figure 23). This further supports the observations made before, that mitochondrial proteostasis perturbations trigger PINK1-mitophagy and not alternative mitophagy pathways.

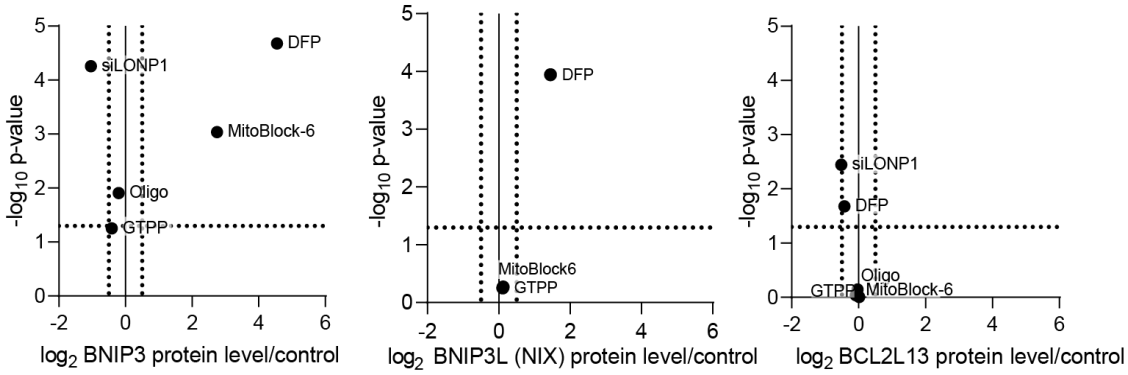

Figure 23: **Protein folding stress does not lead to the enrichment of PINK1-independent mitophagy receptors in mitochondrial extracts**. Mitochondrial proteome analyses of HeLa FlpIn TRex *PRKN* cells treated with DFP (24 h), oligomycin (oligo, 24 h), GTPP (6 h), MitoBlock-6 (6 h) or *LONP1* siRNA

(si*LONP1*, 96 h). Three PINK1-independent mitophagy receptors were plotted for their accumulation on mitochondria upon the respective treatment. BNIP3L was not identified in mitochondrial extracts of all treatments. Horizontal dotted lines indicate p-value=0.05, vertical log_2 fold change=±0.5. Significance was tested by two-sided unpaired t-test. MitoBlock-6 data set taken from Schäfer, Bozkurt, Michaelis et al 2022.

4.2.3 PAM complex enriches in insoluble protein fraction upon protein folding stress

To determine how mitochondrial protein misfolding connects to protein import defects and ultimately induces mitophagy, I next aimed to identify the mitochondrial proteins affected by folding stress. Mitochondrial misfolding was induced by mtHSP90 inhibition (GTPP) or knock-down of *LONP1*. Next, mitochondria were extracted and insoluble mitochondrial proteins purified by mild detergent lysis. This insoluble protein fraction was analyzed via multiplexed quantitative proteomics (Figure 24A). The PAM complex was enriched in the protein insoluble fraction by both treatments when compared to control treatments (Figure 24B). This behavior of the detected PAM components indicated that they are either sensitive to misfolding and aggregating themselves, or that they bind to misfolded or unfolded proteins. In particular, TIMM44, the recruiting platform for the complex and adaptor to the TIM translocon (Ting et al., 2017) and the HSPA9 nucleotide exchange factor, GRPEL1 and 2 were significantly enriched in the insoluble protein fraction (Figure24C-E). This finding was in accordance with a recently published study, in which the insoluble protein fractions induced by *LONP1* or *DNAJA3* depletion in 143B cells was measured by label-free mass spectrometry quantification (Shin et al., 2021). I reanalyzed their data sets and found GRPEL1/2, TIMM44 and HSPA9 significantly elevated in the insoluble protein fraction (Figure 24F). From these findings, I concluded that the soluble PAM complex has a general tendency to bind unfolded proteins or become insoluble itself, when the proteostasis is disturbed.

To also test if *HSPA9* depletion interferes with protein folding in mitochondria, I performed the insoluble protein proteomics on si*HSPA9* treated cells. However, no significant formation of an insoluble protein fraction in mitochondria was observed (Figure 24G, H). This shows that *HSPA9* RNAi

did not have a severe effect on protein folding in mitochondria or that the import inhibition at an early protein uptake stage interfered with the accumulation of insoluble proteins.

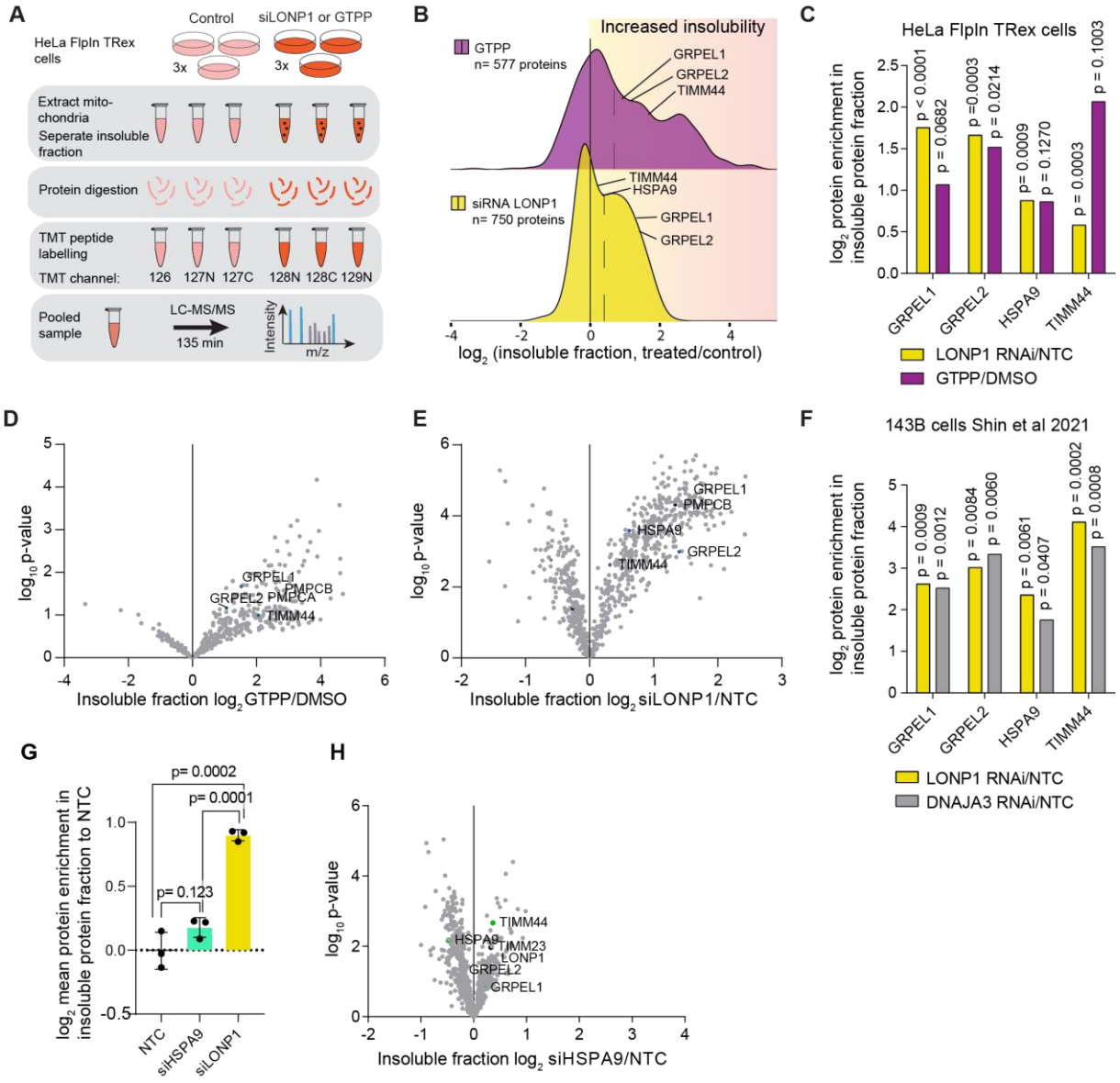

Figure 24: **PAM complex enriches in insoluble protein fraction upon protein folding stress.** (A) Experimental scheme for the analysis of insoluble mitochondrial proteins by tandem mass tag (TMT)-multiplexing, quantitative proteomics. (B) Density plot representation of the insoluble mitochondrial protein fraction upon mitochondrial proteostasis perturbation by *LONP1* RNAi (4 d) or GTPP (10 µM for 6 h). The dotted line indicates the median of all identified proteins. Fold change for averaged n=3 replicates used. Süleyman Bozkurt prepared the mass spectrometry samples for GTPP and DMSO under my supervision. (C-E) Volcano and bar plots showing enrichment of proteins in the insoluble protein fraction upon mitochondrial protein folding stress. (C, D) Statistical significance was determined using two-sided unpaired t-test and (E) the Holm-Sidak method, with α=0.05. (F) Bar graph representing PAM complex protein level in insoluble fraction during *LONP1* or *DNAJA3* depletion in 143B cells and quantified by label-free mass spectrometry. The data from Shin et al., 2021 is depicted with adjusted p-values, showing statistical significance for all shown PAM proteins. Mean

value ±s.d. for n=3 indicated. (G) Mean log_2 fold change for all mitochondrial proteins found in insoluble mitochondrial protein fractions were compared. Statistical significance was determined using two-sided unpaired t-test. Mean value with p-values for n=3 indicated. (H) volcano plot for insoluble proteins after 96h RNAi for *HSPA9* as E.

To validate the proteomic findings that PAM components became insoluble during GTPP treatment, I extracted mitochondria from treated cells and carried out immunoblotting. I compared all GTPP results to CCCP, which induced mitophagy by membrane depolarization and should not lead to the formation of an insoluble protein fraction. In the total mitochondrial extracts, the PAM component abundances changed, GRPEL1 and HSPA9 protein levels were reduced upon GTPP treatment, while TIMM44 levels were increased (Figure 25A, B). In the same mitochondrial lysates TIMM23 and TOMM40 levels showed equal loading. Upon these conditions PINK1 was stabilized on the mitochondria of GTPP or CCCP treated cells (Figure 25A). CCCP, even though it was also stabilizing PINK1, only affected PAM protein levels to a smaller extend and for TIMM44, in the opposite direction (Figure 25B).

When looking at the insoluble protein fraction, I identified major solubility changes of PAM components, while CCCP did not trigger any increased protein insolubility. GRPEL1 and particularly TIMM44 enriched significantly in the insoluble protein fraction upon GTPP treatment, whereas they remained unchanged upon CCCP treatment (Figure 25C). This finding shows, that the behavior of PAM components to accumulate in the insoluble protein fraction does not solely rely on membrane depolarization, but is rather driven by protein folding stress and potentially aggregation.

In the soluble protein fraction, TIMM44 and GRPEL1 were almost completely depleted by GTPP treatment. During control/ healthy conditions TIMM44 and GRPEL1 were soluble. Thus, it is likely that the active protein import motor function happens with soluble TIMM44 and GRPEL1. Hence, reduced protein levels of HSPA9, as well as GRPEL1, and the lack of soluble TIMM44 and GRPEL1 during GTPP treatment, indicate that the protein import motor was inactive upon GTPP-induced protein misfolding (Figure 25C and D). Notably, CCCP had a milder effect on PAM protein levels solubility, even though it completely removed the mitochondrial membrane potential (Figure 21C, Figure 25D and E). This shows that GTPP triggered a specific response on the PAM components TIMM44 and GRPEL1.

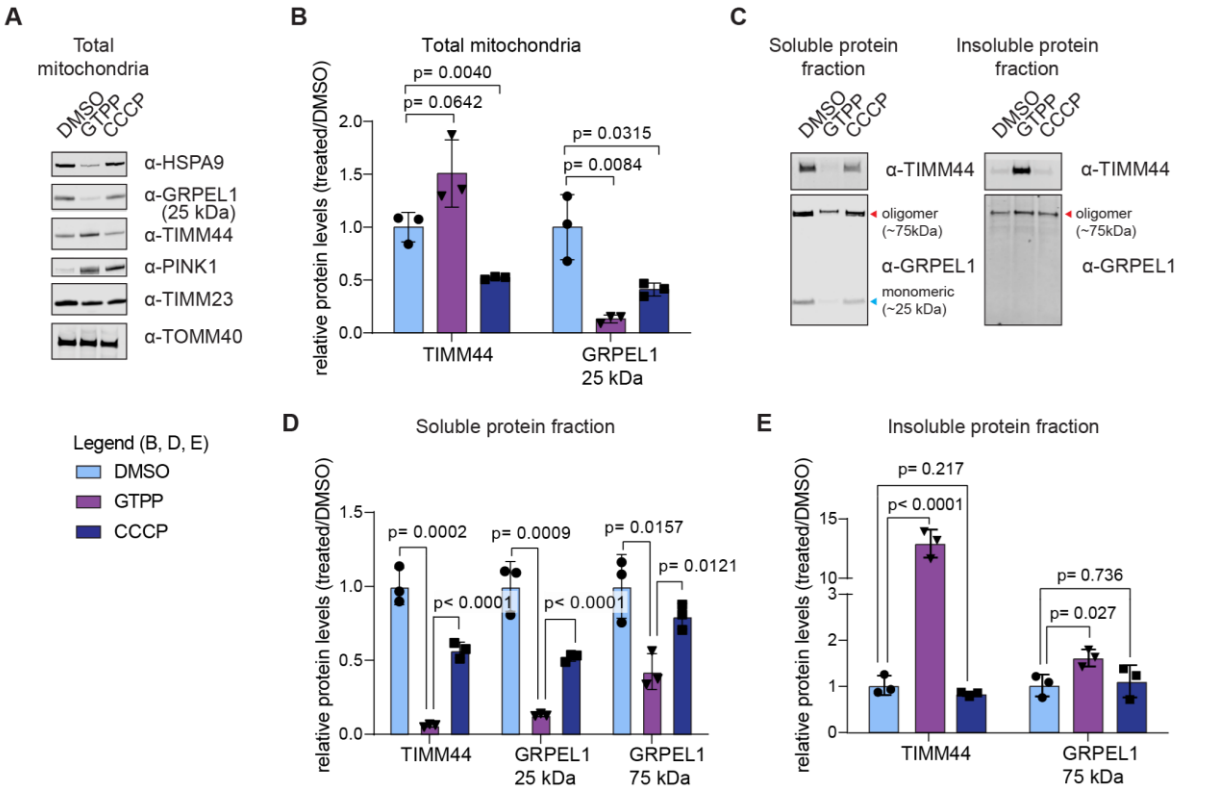

Figure 25: **PAM complex insolubility is driven by proteostasis disturbance not by mitochondrial depolarization.** HeLa FlpIn TRex cells expressing *PRKN* were treated with 10 µM GTPP or CCCP for 6h, mitochondria were extracted, total protein normalized by BCA and membranes solubilized with 1% digitonin. (A) Representative immunoblots of whole crude mitochondrial extracts. Blots show representative one experiment. (B) Quantification of crude mitochondrial extract represented for n=3 of parallel experiments. Mean value ±s.d. indicated. (C) Representative immunoblots of the soluble and insoluble protein fractions. Blots show each one representative experiment. Blots were processed in parallel. Quantification represented n=3 of parallel experiments. Mean value ±s.d. indicated. (D) Quantification of soluble protein fractions and (E) insoluble protein fractions represented n=3 of parallel experiments. Statistical significance was determined by two-sided unpaired t-test and mean values ±s.d. are indicated.

4.2.4 Composition of the insoluble protein fraction upon mitochondrial misfolding stress

In the aforementioned experiments, the insoluble protein fraction showed enrichment of the PAM complex and mitochondrial protein quality control proteins. To evaluate whether further specific proteins accumulate, I analyzed its content. First, I compared if the GTPP or *LONP1* RNAi data sets for

insoluble proteins showed overlapping proteins by Pearson analysis. They correlated with R = 0.76 and R^2 = 0.58 (Figure 26A). By hierarchical clustering utilizing 'heatmap function 2' from R studio, a clear cluster of commonly increased proteins in the insoluble protein fraction over all replicates and both treatments grouped together (Figure 26B). Cytoscape and ClueGO-CluePedia analysis revealed the most prominent Reactome pathways of this cluster. The network showed that in addition to PAM complex components and mitochondrial protein import, GTPP and *LONP1* depletion led to the accumulation in an insoluble fraction of proteins involved in mitochondrial translation, especially components of the mitochondrial ribosomes, proteins belonging to metabolism and mitochondrial processing, such as PMPCA/B (Figure 26C).

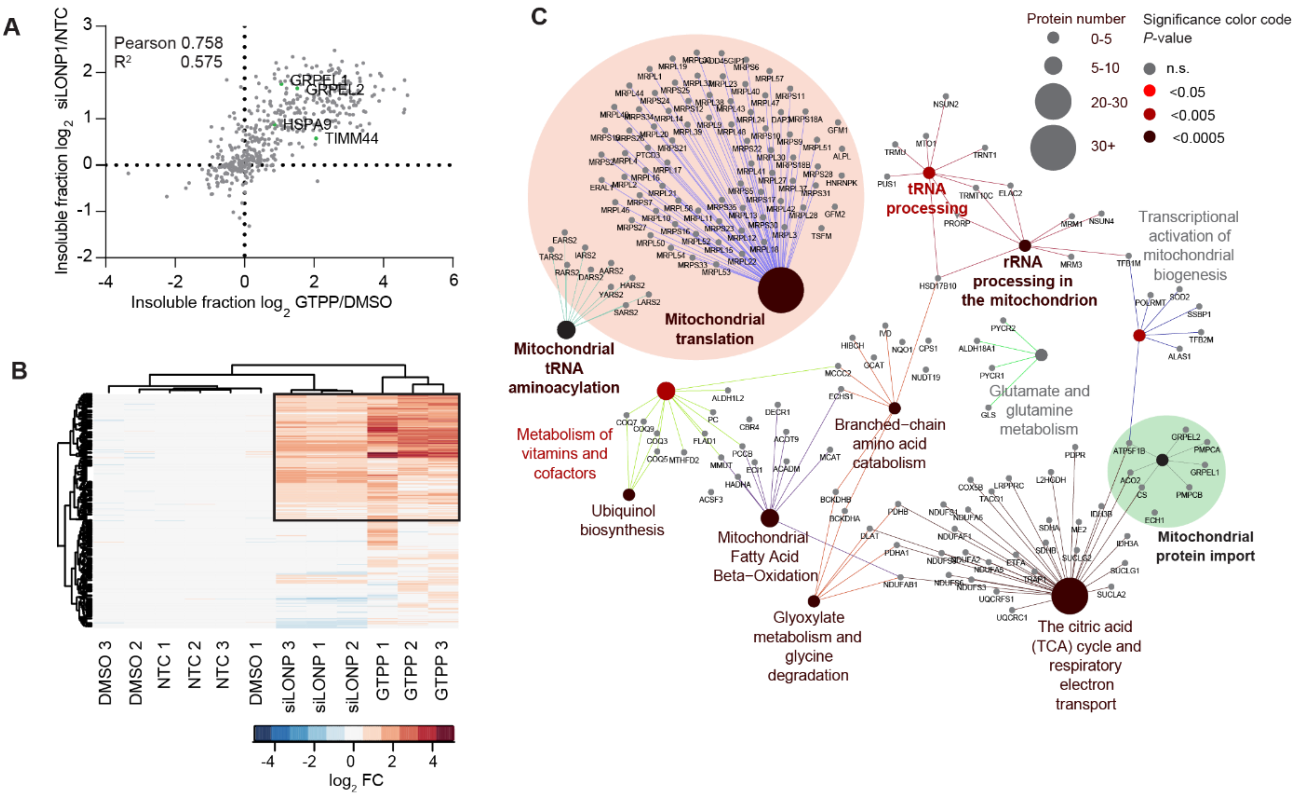

Figure 26: **PAM complex enriched in insoluble protein fraction upon protein folding stress.** (A) Pearson analysis GTPP and *LONP1* knock-down data set show correlation with r = 0.758. (B) Hierarchical clustering and heat map representation (R software, heatmap2.0, standard settings) shows cluster of commonly elevated proteins in the insoluble protein fractions from GTPP and si*LONP1*. (C) Proteins found in elevated cluster (B) are presented as ClueGO-CluePedia network and most prominent Reactome pathways are indicated. Similar GO terms were fused and translation-related and mitochondrial protein import highlighted by light red and green.

4.2.5 TIMM44 proximity labeling allowed to monitor PAM-TIM complex interaction

To obtain a better understanding which interaction changes took place upon PAM localization into the insoluble protein fraction upon proteotoxic stress, I monitored TIMM44 interactors by proximity proteomics. Expressing recombinant *TIMM44* with the biotin ligase *TurboID* enabled proximity labeling of proteins near to the bait. By streptavidin-immunoprecipitation (IP) and multiplexed proteomics close proteins and complexes were identified (Figure 27A) (Branon et al., 2018). Melinda Brunstein (Münch group, Goethe Universität Frankfurt) performed the IP and proteomics for me, while I did cell culturing, treatments, harvest, lysis and data analyses.

First, I tested *TIMM44-TurboID* by doxycycline-induced expression at basal conditions. A variety of different proteins showed significant interaction over non-induced conditions. HSPA9, GRPEL1 and PAM16 were identified as close interactors, which showed that the PAM complex forms also with the TIMM44-TurboID fusion protein (Figure 27B). The close proximity of TIMM44 to TIMM21 and TIMM50, which are part of the TIM translocon, indicate interaction of TIMM44 with the TIM complex. This confirmed that TIMM44-TurboID, as the endogenous protein localized during basal conditions to the TIM translocon and recruited HSPA9 and GRPEL1 (van der Laan et al., 2006; Mokranjac et al., 2009; Schulz et al., 2011). In addition, I found TIMM44 to bridge to other mitochondrial functions, such as the membrane integration of mitochondrially translated proteins via OXA1L, the respiratory chain complex I, including two mitochondrial encoded proteins (NADH-ubiquinone oxidoreductase chain 2 (MT-ND2), ATP synthase subunit a (MT-ATP6)), and mitochondrial ribosomal proteins (Figure 27B). This suggests further functions of TIMM44 in the integration of mitochondrially translated proteins in the IMM. The close proximity with the ATP/ADP-uniporter ANT-1 (gene symbols: *SLC25A4,5,6*), PARL, serine/threonine-protein phosphatase PGAM5 and prohibitin (PHB) and prohibitin 2 (PHB2), could indicate also functional interaction regarding mitophagy regulation (Greene et al., 2012; Wei et al., 2017; Hoshino et al., 2019; Yan et al., 2020).

4.2.6 PAM complex sequesters from TIM translocon during protein folding stress

Upon mitochondrial misfolding stress by GTPP treatment or upon *LONP1* depletion, TIMM44 lost its interactions with the TIM complex and PAM16 (Figure 27C) This likely explains why the PAM complex was not active as mitochondrial protein import motor during protein folding stress.

In the density plot representation, it becomes obvious that upon acute misfolding stress by GTPP, a loss of most interactions took place. During prolonged, possibly milder, folding stress via *LONP1* depletion, the interaction with the TIM translocon was lost, while the majority of other interactions stayed intact (Figure 27D). The mechanism of protein import regulation, however, remained the same for both treatments: Upon mitochondrial folding stress, the PAM complex sequestered from the inner membrane translocon into an insoluble protein fraction, as shown by proteomics and immunoblot (Figure 24, 25 and 27). This ultimately inhibited the matrix-targeted import, as the active protein import by HSPA9 binding and pulling of translocating proteins could not take place without HSPA9-recruitment to the TIM translocon via TIMM44, or without the HSPA9 co-chaperone GRPEL1, which facilitates ADP/ATP exchange of HSPA9 (Liberek et al., 1991; Choglay et al., 2001).

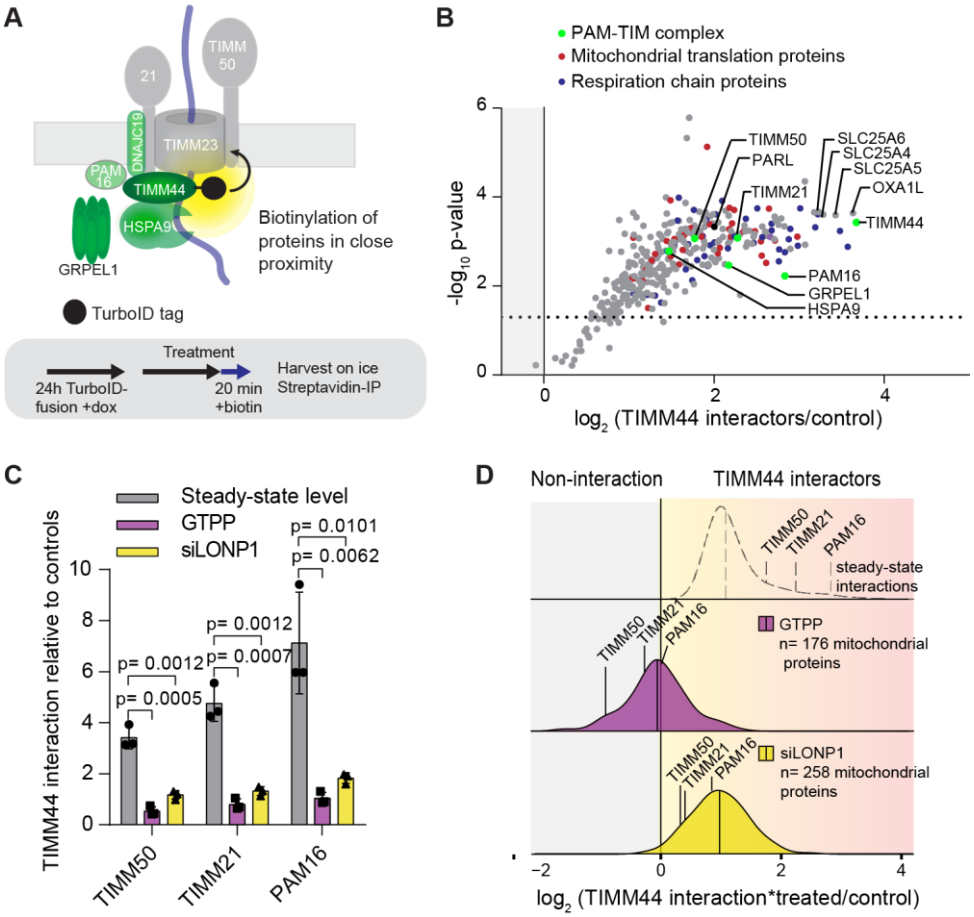

Figure 27: **PAM complex sequestered from TIM translocon upon protein folding stress.** (A) Illustration of TIMM44-TurboID proximity labelling. *Turbo-ID* construct expression was induced 24h prior to the treatment and biotin-labelling started in last 20 min of the experiment by addition of 500 mM biotin to the medium. (B) Volcano plot showing enrichment of proteins in close proximity of TIMM44-TurboID at steady state condition +/- doxycycline-induced *TIMM44-TurboID* expression (n=3). PAM components and highly enriched protein groups are highlighted. (C) Bar graph illustrating loss of TIMM44-TIM translocon interaction upon protein folding stress. Statistical significance was determined using a two-sided unpaired t-test (B, C) and the Holm-Sidak method for (C), with α=0.05 and no further assumptions about s.d. variance. (D) Density plot representation of TIMM44 interactions without or with treatments. Steady-state conditions are shown as dotted line, under treatment (10 µM GTPP/ DMSO 6h or *LONP1* RNAi /NTC 4 days) fold change values were multiplied with steady-state values from C indicating, if treated/control leads to the loss of interaction (non-interaction, grey) or shows interaction (yellow-red gradient).

By normalization of the interactome data upon GTPP and si*LONP1* to the TIMM44 protein levels, I was able to focus on the relative changes in the TIMM44 proximity proteome and compare it to the insoluble protein fraction proteomics. The data sets were clustered by hierarchal Euclidean analysis (Figure 28A). I received three prominent clusters: One large, commonly elevated cluster, shared between GTPP and si*LONP1*. This cluster contained many proteins that were already found in the insoluble protein fraction also shared for both treatments (Figure 28A, black). Two smaller clusters were grouped, one which was only enriched in TIMM44 proximity proteome (Figure 28A, blue) and one which was mainly elevated for the insoluble protein fraction (Figure 28A, yellow).

GO-term and Reactome analyses of the commonly elevated cluster revealed an enrichment of proteins that belong to a group of “unfolded protein binding” proteins, including GRPEL1 and HSPA9. This could explain the behavior of the endogenous, HSPA9 and GRPEL1, as they bind unfolded proteins which have the tendency to form an insoluble fraction. Other parts of the commonly elevated cluster were mitochondrial translation, TCA, as well as respiratory chain proteins. They made a considerable large part of this overlapping cluster and therefore can be considered to become insoluble upon proteostasis disturbance (Figure 28B).

The second, yellow cluster contained mainly the same pathways as the larger, black cluster. It includes also TIMM44, which seems to stay in contact with mitochondrial translation, TCA and respiratory electron transport proteins upon mitochondrial misfolding stress (Figure 28C).

Proteins found in the blue cluster were not part of the insoluble protein fraction. However, TIMM44 also seemed to be in closer proximity. The mitophagy-related proteins PHB, PARL and AFG3L2 were found within the term “mitochondrial calcium ion transport”. Additionally, some cytosolic ribosomal proteins and proteins of the gluconeogenesis were identified here (Figure 28D).

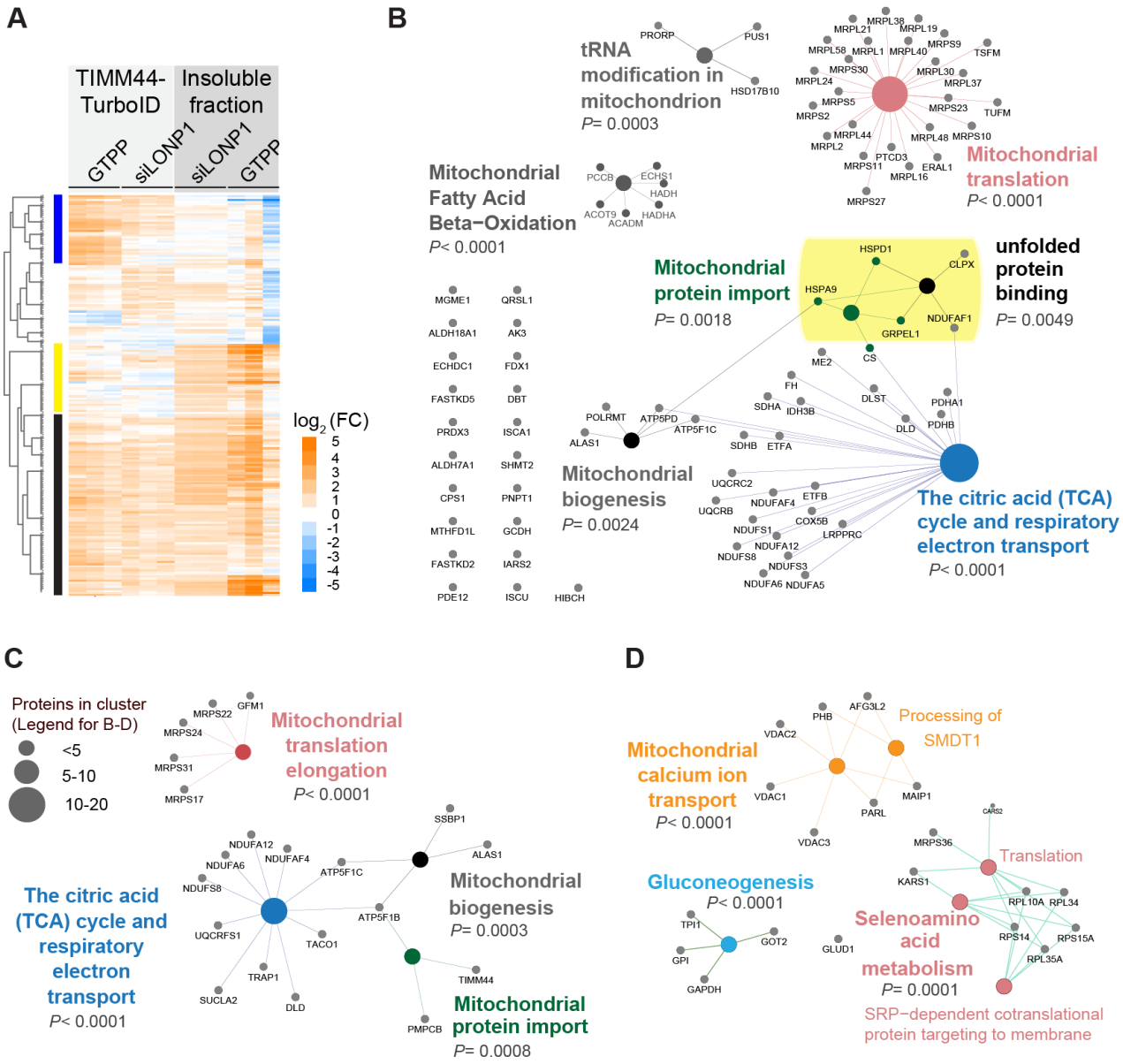

Figure 28: **Upon mitochondrial proteome perturbation, the PAM complex sequestered from the TIM translocon and enriched in the insoluble fraction.** (A) Hierarchal Euclidean, average clustering (Perseus software: 6 row clusters, 14 iterations) and heatmap representation. Clusters, containing commonly elevated (black), proteins increased in the insoluble protein fraction, but not consistently enriched in the TIMM44-TurboID data upon GTPP or si*LONP1* (yellow) and proteins showing increased interaction but no enrichment in the insoluble protein fraction (blue), were highlighted. (B) ClueGO-CluePedia protein network of commonly elevated clusters from (black) A. Prominent Reactome pathways and the GO-term for molecular function of unfolded protein binding were indicated. (C) ClueGO-CluePedia protein network of yellow cluster and (D) of blue cluster from A. Dot size for groups are described in the figure. All data sets were filtered for mitochondrial proteins using the MitoCarta2.0. *P*-values corrected with Bonferroni step down for GO-term group against reference genome were calculated and are indicated next to the main GO-term per group.

As a conclusion of the presented experiments, I propose the following model to explain how mitochondrial protein folding stress could induce PINK1-dependent mitophagy: (I) During normal conditions, most mitochondrial precursor proteins are synthesized extra-mitochondrially in an unfolded state and are imported into mitochondria post-translationally through membrane transporter complexes of the outer and inner mitochondrial membrane. In particular, these unfolded precursor proteins are channeled through the translocons and actively pulled into the matrix by the PAM protein import motor complex. There, they are processed and folded with the help of chaperones. Factors involved in this process, such as TIMM44, GRPEL1 and HSPA9 thereby have many interaction partners, as they assist with the import and folding of cytosol-derived mitochondrial inner membrane and matrix proteins. (II) Upon conditions of protein folding stress, like the inhibition of mtHSP90 by GTPP or the depletion of the protease and chaperone *LONP1*, unfolded proteins accumulate in the matrix. This causes PAM components to localize in the insoluble protein fraction, possibly due to their molecular function to bind to unfolded proteins. This change of PAM localization is accompanied by a significant reduction of soluble PAM complex and its detachment from the inner membrane translocon, resulting in the inhibition of mitochondrial protein import. (III) Direct interference with the protein import into mitochondria, e.g. *HSPA9* RNAi have a similar effect: the active matrix-targeted import is reduced. Without an active protein import motor, PINK1 is not partially transferred over the IMM and therefore not processed by PARL in the IMM. Consequently, PINK1 is stabilized and accumulates on the OMM, leading to its auto-phosphorylation and activation of mitophagy, without the need for membrane depolarization (Figure 29). Finally, mitochondria with accumulated, potentially toxic, misfolded proteins are removed from the cell which protects the cell of further damage.

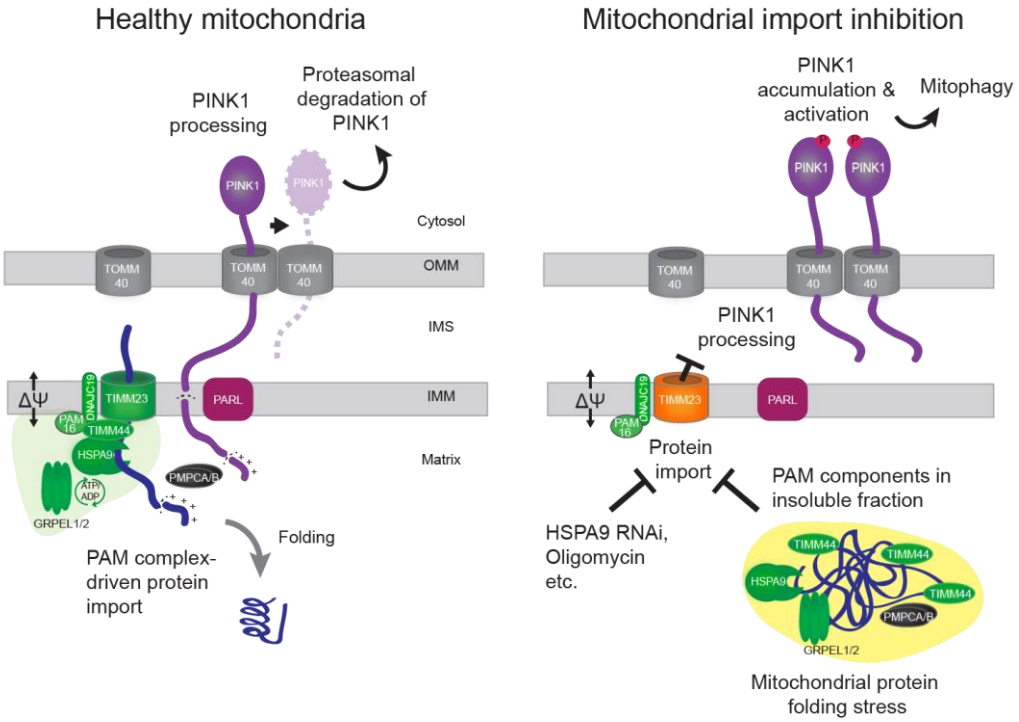

Figure 29: **Proposed model for protein import inhibition-induced mitophagy in polarized mitochondria**: (Left) Under basal/ healthy mitochondrial conditions, the PAM complex associates with the TIM translocon and allows protein import. PINK1 is partially imported, leading to its degradation and prevention of mitophagy. (Right) Reduced mitochondrial protein import (e.g. genetic or pharmacological perturbation) inhibits PINK1 processing by PARL, which leads to PINK1 stabilization and activation on the OMM to induce mitophagy. IMM depolarization is not required for this process. This mechanism of PINK1-induced mitophagy is also activated during mitochondrial protein misfolding stress, in which PAM components become insoluble, lose their interaction with the translocon, and protein import is reduced.

4.3 DEVELOPMENT OF A MEASUREMENT FOR GLOBAL MITOCHONDRIAL PROTEIN IMPORT

In this chapter, I present the "mitochondrial protein uptake proteomics approach", which I co-invented together with Christian Münch (who made the initial suggestion to deploy such an approach) and which I worked out and developed. It was later on refined by me, together with Süleyman Bozkurt,

Münch group Goethe Universität Frankfurt (providing in particular additional measuring of my experiments and validations that are not presented in this thesis) and Jasmin Schäfer, Münch group Goethe Universität Frankfurt (providing in particular data analysis, data visualization and mechanistic interpretation). I used this protein uptake approach in order to get a deep insight into translational regulation and uptake regulation of mitochondrial protein import during basal and upon stressed conditions.

4.3.1 Pulsed SILAC labelling with mitochondrial isolation allowing to monitor protein uptake into mitochondria (mePROD^{mt})

By Stable Isotope Labeling by Amino acids in Cell culture (SILAC), I specifically labeled newly synthesized proteins. As the labeling percentage after a 2 h pulse was low compared to the percentage of light amino acids from the regular RPMI medium, I combined the 2 h-labeled samples with a fully SILAC-labeled booster channel, as it was done previously for whole cell translatome analyses, also called multiplexed enhanced protein dynamics (mePROD) (Klann et al., 2020). This combination led to the detection of more heavy-labeled peptides and hence enabled to receive a sufficient dynamic range. By the extraction of mitochondria from Hela cells and removal of the cytosol in the sample, the mitochondrial protein uptake during the SILAC-pulse was measured (Figure 30A). We called this mitochondrial protein uptake method: mitochondrial proteome-targeting mePROD (mePROD^{mt}). To test the quality of the used mitochondrial extraction, the crude mitochondrial isolate was compared to a whole cell lysate, measured by label-free quantification (LFQ)-mass spectrometry by Süleyman Bozkurt. The quantified proteins showed a clear enrichment of mitochondrial proteins over ER, Golgi and especially cytosolic proteins, while nuclear proteins even though they were still prominent, were decreased compared to whole cell abundances (Figure 30B and C). This confirmed that the crude mitochondrial isolation protocol (Bozidis et al., 2007) was suitable to remove other cellular compartments if combined with an extra washing step. Next, we tested if the mixture of pulsed SILAC-labeled samples with a fully heavy SILAC-labeled mitochondrial extract was able to increase/ “boost”

the detection of heavy labeled mitochondrial peptides. The addition of heavy mitochondrial extracts thereby indeed doubled the identifications, while heavy-labeled whole cell extracts only led to a minor increase (Figure 30D). Consequently, the fully heavy labeled mitochondrial extract was from now on used as booster channel for the protein uptake approach.

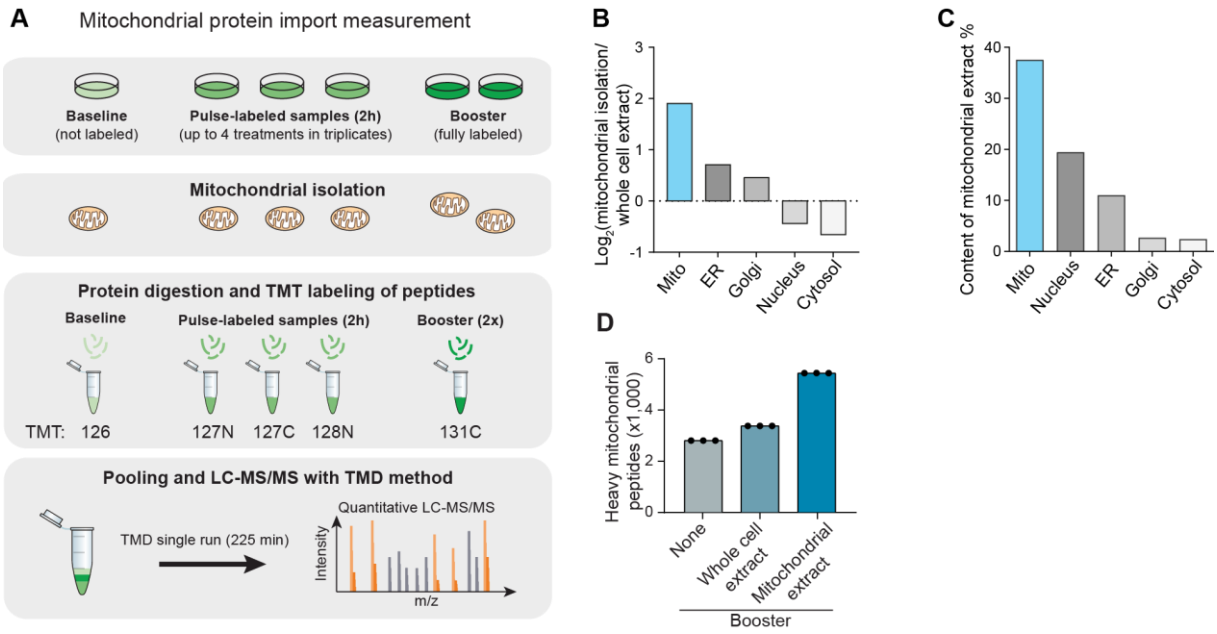

Figure 30: **Mitochondrial isolation and organelle-specific SILAC-boosting allows monitoring of mitochondrial translation and protein import.** (A) Experimental scheme of mitochondrial-selective pulsed-SILAC proteomics for uptake of mitochondrial proteins. A non-labeled baseline sample and samples of cells pulse-labeled for 2 h were subjected to mitochondrial isolation for measuring protein uptake. Equally, cells of a fully SILAC-labeled booster sample were subjected to whole cell extraction or to mitochondrial isolation in order to yield a whole cell or a mitochondrial booster sample. Baseline and pulse-labeled samples for protein uptake measurements were complemented with a whole cell or with a mitochondrial booster to improve the sensitivity for all or mitochondrial proteins. Proteins were digested, labeled with TMT11, pooled and measured by LC-MS/MS with targeted mass difference (TMD) (Klann & Münch, 2020). (B, C) Mitochondrial protein enrichment shown as bar plot. Here, label-free quantification was used for one mitochondrial extraction, which was compared to whole cell extract of HeLa cells. (D) Shown are numbers of heavy SILAC-labeled mitochondrial peptides, dependent on the addition of either no booster, or of booster signals derived from whole cell- or mitochondrial extracts. Three replicates are pooled after TMT-labeling in one multiplex.

4.3.2 The mitochondrial import assay shows global and specific mitochondrial uptake inhibition during mitochondrial depolarization

To verify that the mePROD^{mt} method indeed shows mitochondrial protein uptake differences, I depolarized the mitochondria with CCCP- or AO-treatment, which both blocked matrix-targeted mitochondrial protein import (Figure 31A, B). As a result, heavy-labeled mitochondrial protein levels significantly decreased upon both treatments compared to the control, while the total mitochondrial protein levels remained largely unchanged in 2 h labeling during the treatments (Figure 31A-F). By taking the median of all quantified heavy mitochondrial proteins per replicate, the global protein uptake reduction can be assessed. AO-treatment significantly reduced the mitochondrial protein uptake down to about 14% and CCCP down to 30% of global heavy labeling compared to DMSO (Figure 31G). As the mePROD^{mt} method measured all the proteins individually, it was also possible to filter for sub-organelle populations or to look at specific proteins. For proteins that showed no heavy-peptides in the treated samples, but were quantified in the controls, no fold change was determined. However, due to the tandem mass tag (TMT)-multiplexing, it can be concluded that these proteins were not imported at a detectable level during CCCP (Figure 31C) or AO treatment (Figure 31D), as the MS1 peak was collected together for all treatments and only afterwards quantified for each TMT-channel. If there were any peptides for these proteins, they should also be identified upon treatment. In addition to the protein uptake detection by heavy peptides, I also received a mitochondrial proteome from total (light and heavy) peptide quantification within the same mePROD^{mt} measurement (Figure 31E, F). Here, the observed changes upon CCCP or AO between treatment and control were 5 to 10-fold smaller than for the SILAC import data. Nevertheless, this mitochondrial proteome contains data about proteins being synthesized before the SILAC pulse. For example, upon CCCP treatment, a significant decrease of OPA1 protein levels was detected, which is likely the result of specific OPA1 degradation upon depolarization. This observation is consistent with what was described before (Ishihara et al., 2006), showing that these mePROD^{mt} experiments create multiple useful data sets simultaneously. For the AO treatment, the overall effects were very similar to those of CCCP-treated cells. A Venn diagram analysis of the

mitochondrial protein import inhibition also showed a clear overlap of affected mitochondrial proteins for both treatments, but at the same time indicates that there were still clear differences in the groups of affected proteins (Figure 31H).

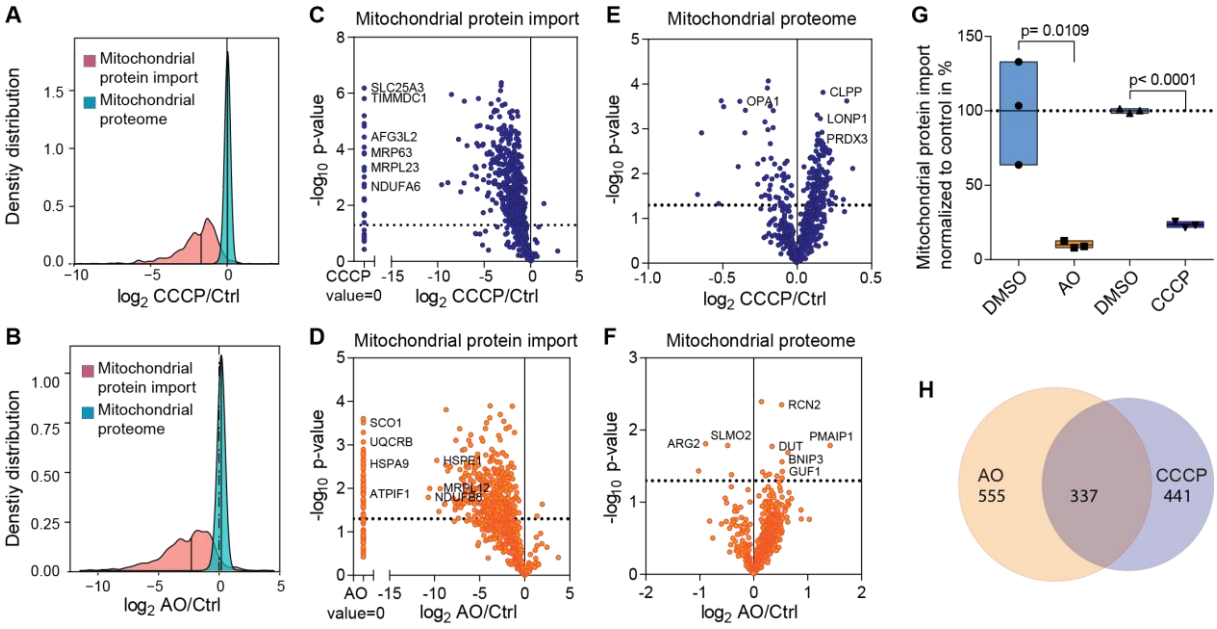

Figure 31: **Protein uptake proteomics by mePROD^{mt} allows to follow broad import inhibition of endogenous proteins.** (A, B) Density distribution of mitochondrial protein import quantified by heavy labeled peptides and compared with a mitochondrial extract proteome. Average of n=3, log_2 2h 10µM CCCP/DMSO (A) and AO/ DMSO (B) are shown. Protein with no value for CCCP, AO or DMSO were excluded. (C, D) mePROD^{mt} and (E, F) mitochondrial proteome from A and B, visualized as volcano plots, indicate protein specific changes. Several proteins showed no value upon 2h CCCP or AO, plotted on the left-hand side on individual x-axis. Dotted lines indicate statistical significance (*P*-value < 0.05) which was determined using a two-sided unpaired t-test. (G) Box min-max plot showing the global protein uptake rate into mitochondria. Each dot represents the average of all identified heavy mitochondrial proteins per replicate. (H) Venn diagram showing the overlapping proteins being significantly changed in mePROD^{mt} during AO or CCCP treatment.

4.3.3 MTS-EGFP localization upon treatment confirmed that mitochondrial depolarization inhibits matrix-targeted protein import

To validate that the observations via the pulsed-SILAC protein uptake proteomics were indeed reflecting protein import in an MS-independent way, I expressed matrix-targeted *MTS-EGFP* in cells which were treated with CCCP and followed its localization via microscopy. As a result, co-localization of Mitotracker Red FM with mitochondrial EGFP could almost exclusively be detected in the control (DMSO), while CCCP treated cells showed extra-mitochondrial GFP-fluorescence. I quantified these observations by manual categorization into no, low, predominant and complete co-localization of green and magenta fluorescence (Figure 32).

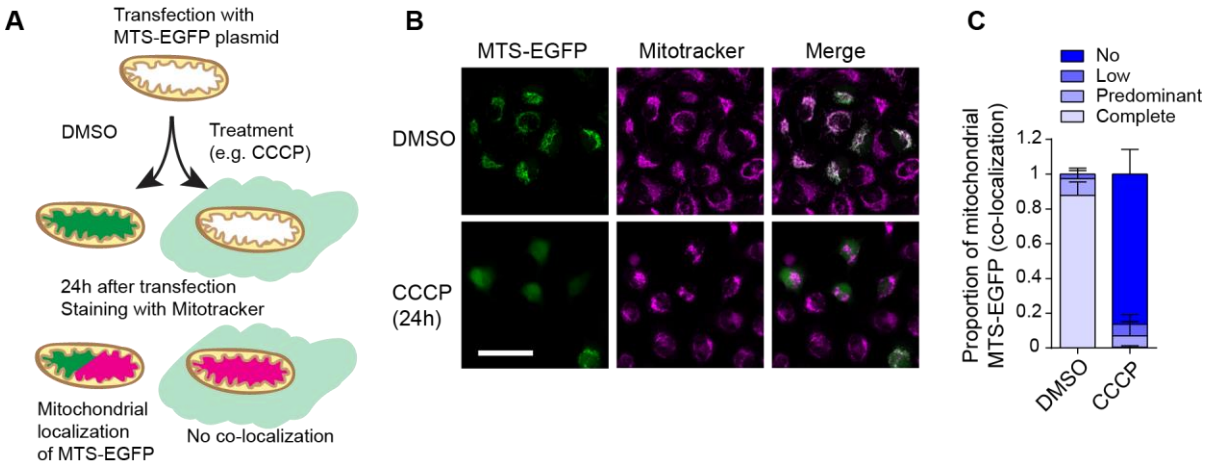

Figure 32: **MTS-EGFP confirmed mitochondrial protein import inhibition via CCCP treatment.** (A) Illustration of mitochondrial targeting sequence (MTS)-EGFP experimental work-flow with CCCP treatment. (B) Representative microscopic images of *MTS-EGFP* expressing cells, treated with 10 µM CCCP for 24h and stained with Mitotracker Red FM for 30 min. 40x live cell imaging was performed, scale bar represents 50 µm. (C) Quantification of cells showing no, low, predominant or complete mitochondrial co-localization of MTS-EGFP with Mitotracker Red FM. Co-localization was determined by eye via ImageJ merging. Mean +s.d. (n= 3 biological replicates, 100 EGFP-positive cell per replicate).

4.3.4 HaloTag pulsed Biotin-labeling validated quantification of import defects, observed by pulsed SILAC protein uptake assay

The MTS-EGFP localization assay with transient expression worked well for treatments of at least 24 hours. For shorter treatments, it however did not provide reliable results as it had to be transfected within the treatment, which additionally stressed the cells and had to reach detectable protein amounts by being expressed from the recently transfected plasmid. Thus, this MTS-EGFP assay was not capable to validate acute (2 to 6 h) CCCP or AO treatments. As consequence, a pulsed approach was necessary which only detects newly synthesized and imported proteins. For this purpose, I utilized the HaloTag technology from Promega and established a novel workflow (Figure 33A). In this experiment, a HaloTag-fusion protein (e.g. GRPEL1 or HSPD1) was stably expressed in HeLa cells. The HaloTag-fusion protein thus reached a constant level before the treatment was applied. The HaloTag-fusion protein then was saturated with empty HaloTag ligand, which were bound covalently to the tag, blocking the interaction site with biotin-coupled HaloTag ligand. Free empty HaloTag ligand was washed off and the treatment with CCCP started. During the last hour of treatment, HaloTag ligand coupled to biotin was added, which labeled all HaloTag-tagged proteins synthesized during the treatment. After the treatment, cells were harvested and mitochondria extracted (Figure 33A). By analyzing the biotinylated HaloTag-fusion in mitochondria using Streptavidin coupled to near infrared fluorophore and by comparing it to the total HaloTag-fusion protein via anti-HaloTag immunostaining, the protein uptake was followed. The six hour CCCP treatment led to significant lower protein uptake, confirming the observed results from pulsed SILAC mePROD^{mt} measurements (Figure 33B and C).

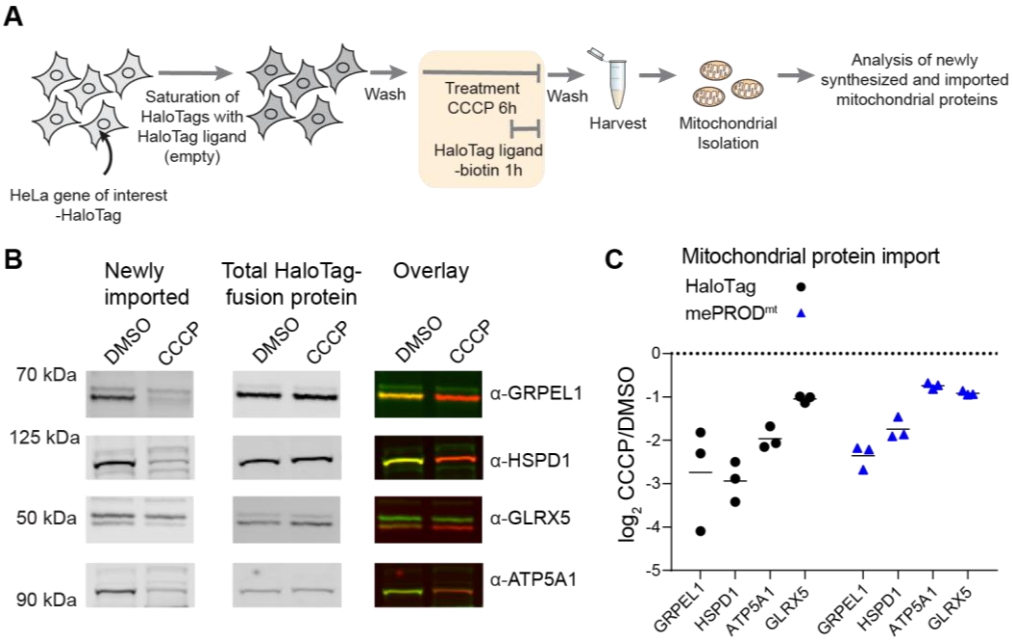

Figure 33: **HaloTag-pulsed fluorescence and biotin labeling validated pulsed-SILAC mePROD^{mt} quantifications.** (A) Workflow for recombinant HaloTag-fusion uptake assay. (B) Immunoblots detecting biotinylated HaloTag via Streptavidin-800 nm and total HaloTag-fusion protein via anti-HaloTag antibody plus anti-Mouse-IRdye680 nm are shown. Experiments were performed n=3. (C) Quantification of HaloTag-labeling log_2 CCCP/DMSO fold changes being compared to mePROD^{mt}. mePROD^{mt} was quantified via pulsed SILAC heavy labeled proteins.

4.3.5 Hierarchical clustering of multiple mePROD^{mt} data sets allowed to identify commonly affected pathways upon mitochondrial depolarization stress

The quantitative pulsed-SILAC import assay for mitochondrial proteins allowed to follow global trends and to identify commonly affected pathways over multiple data sets. Hierarchal Euclidean average clustering and heat map representation revealed that 2h AO and 2h CCCP data sets grouped together (Figure 34A). The mitochondrial protein uptake inhibition showed low variation throughout both data sets and in most replicates. Using Reactome network analysis, done via ClueGO of the two mainly decreased clusters (log_2 fold change < -0.5 and significance of *P*-value below 0.05), I found that metabolic pathways and mitochondrial translation were particularly affected (Figure 34B). Thus, in addition to global quantification of mitochondrial protein import and specific quantification of

individual protein uptake, the mePROD^{mt} method allowed us to examine pathways and find similarities between different treatments.

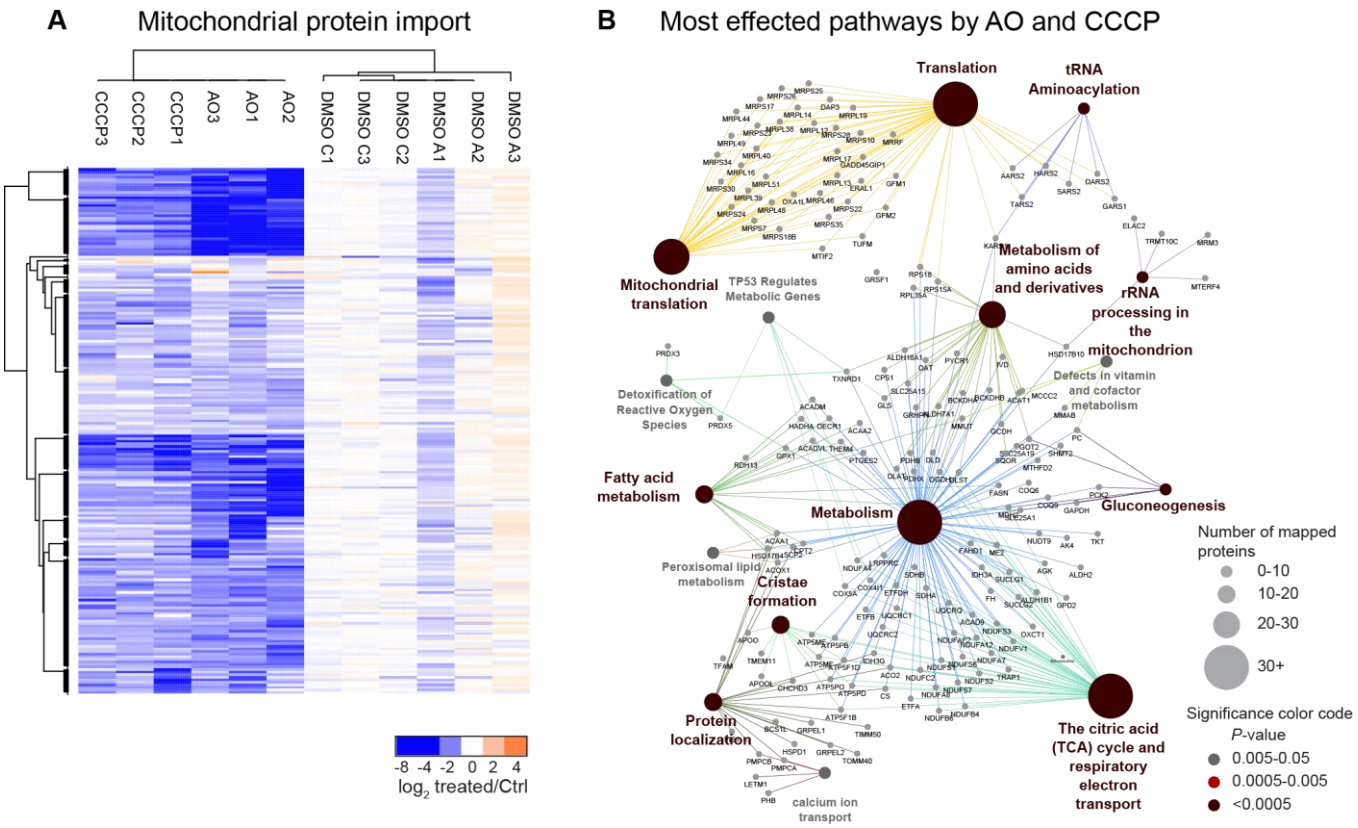

Figure 34: **mePROD^{mt} followed by hierarchical clustering shows shared pathways commonly effected by CCCP and AO treatment.** (A) Hierarchal Euclidean average clustering grouped the mitochondrial protein import data of 2h 10 µM AO or CCCP treated cells. Control samples treated with DMSO are shown for CCCP experiment as DMSO C1-3 and for AO as DMSO A1-3. The heatmap representation was generated and the cluster was performed in Perseus with 15 row clusters and iterations. Data was filtered for proteins with values in all replicates. (B) Reactome pathway network of proteins with decreased mitochondrial uptake after treatment with CCCP or AO by $\log_2$ treated/control < -0.5, *P*-value < 0.05, and which could be found in all replicates of both treatments. The network was prepared with the Cytoscape plug-in ClueGO and shows only significantly enriched pathways. Group dot size is described in the figure. *P*-values corrected with Bonferroni step down.

4.3.6 Whole cell translation analysis, conducted simultaneously with mePROD^{mt}, presents a broad image of newly synthesized proteins and their transportation

For a global overview of the effects of mitochondrial stressors onto cells, I measured changes on the cytosolic translation using a whole cell pulsed-SILAC mePROD, in addition to protein uptake proteomics measured by mePROD^{mt} (Figure 35A). As for this previously described mePROD method (Klann et al., 2020) only a fraction of the cell material was needed, I used 10% of it for whole cell lysates and 90% for mitochondrial extraction and mePROD^{mt}. Thereby, by addition of different fully heavy-SILAC labeled booster channels, the identification of heavy peptides and proteins in the whole cell translatome or in particular the identification of mitochondrial proteins can be selectively increased (Figure 35B, C). This approach also enabled the translation detection of 6 of the 13 mitochondrial-encoded genes (Figure 35D). With the combined measurement of mitochondrially boosted mePROD and the mitochondrial protein uptake approach mePROD^{mt}, Jasmin Schäfer, Süleyman Bozkurt and I were able to distinguish between direct, import-driven, or indirect effects that resulted from cytosolic translation.

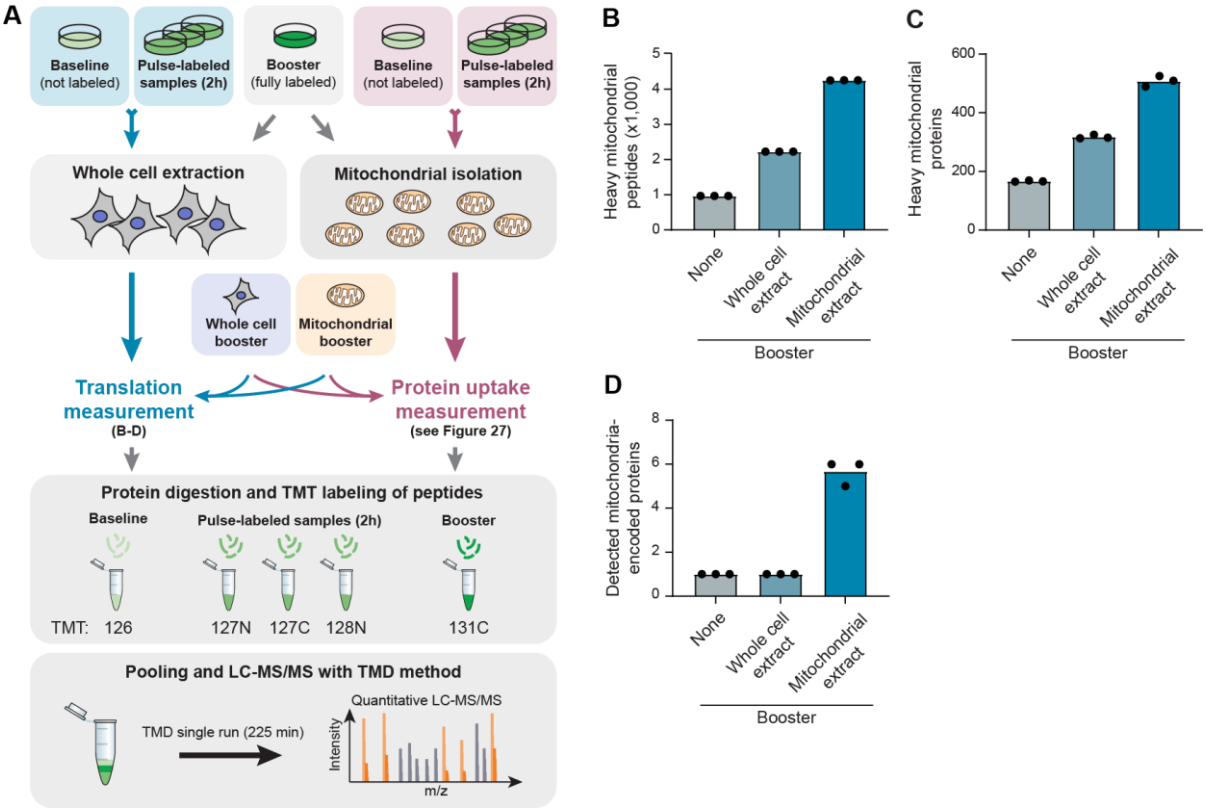

Figure 35: **Compartment selective signal enhancing of translation measurements allows to measure mitochondrial and whole cell translation.** (A) Workflow of whole cell translation using mePROD proteomics (left, blue) and mitochondria-selective protein import proteomics by mePROD^{mt} (right, magenta). A baseline sample from cells cultured without SILAC and samples of cells pulse-labeled for 2 hours were subjected to whole cell extraction (left) for translation measurement or mitochondrial extraction (right) for mePROD^{mt}. Likewise, a sample from fully SILAC-labeled cells was subjected to mitochondrial extraction or whole cell lysis, in order to receive a mitochondrial or whole cell booster. All samples were individually digested and labeled with one TMT11 channel. By pooling the TMT-labeled samples with a booster channel selectively whole cell or mitochondrial translation detection was enhanced. The samples were analyzed by LC-MS/MS with TMD (Klann & Münch, 2020). (B-D) Numbers of SILAC-labeled mitochondrial peptides (B), proteins (C), or mitochondrially-encoded proteins (D) are shown, dependent on which booster channel was added. Three replicates were pooled in one TMT multiplex. MS sample preparation was done by Süleyman Bozkurt, and are also shown in Schäfer, Bozkurt, Michaelis et al., 2022.

4.3.7 Whole cell translation was decreased by mitochondrial depolarization via CCCP

CCCP reduced the mitochondrial matrix-targeted protein import (Figure 31). In addition, it also significantly decreased whole cell translation (Figure 36A). To test if this was a consequence of an ISR activation, I co-treated cells with ISRIB (*integrated stress response inhibitor*) and CCCP. ISRIB reversed the effects of eIF2α phosphorylation, which decreases cytosolic translation (Figure 36B, C). Co-treatment with CCCP and ISRIB, indeed revealed partial rescue of the translation, demonstrating that either the mitochondrial depolarization – and with it, mislocalized mitochondrial proteins in the cytosol – or the increased reactive oxygen levels activated the ISR. In this regard, Jasmin Schäfer further analyzed which proteins were decreased upon CCCP, but not upon CCCP plus ISRIB. Thereby, she showed that 368 proteins were decreased upon both treatments, while the translation of 41 proteins were only decreased in CCCP treated cells, but recovered by ISRIB. The uptake into mitochondria of these 41 proteins was thus translationally regulated (Figure 36D, E).

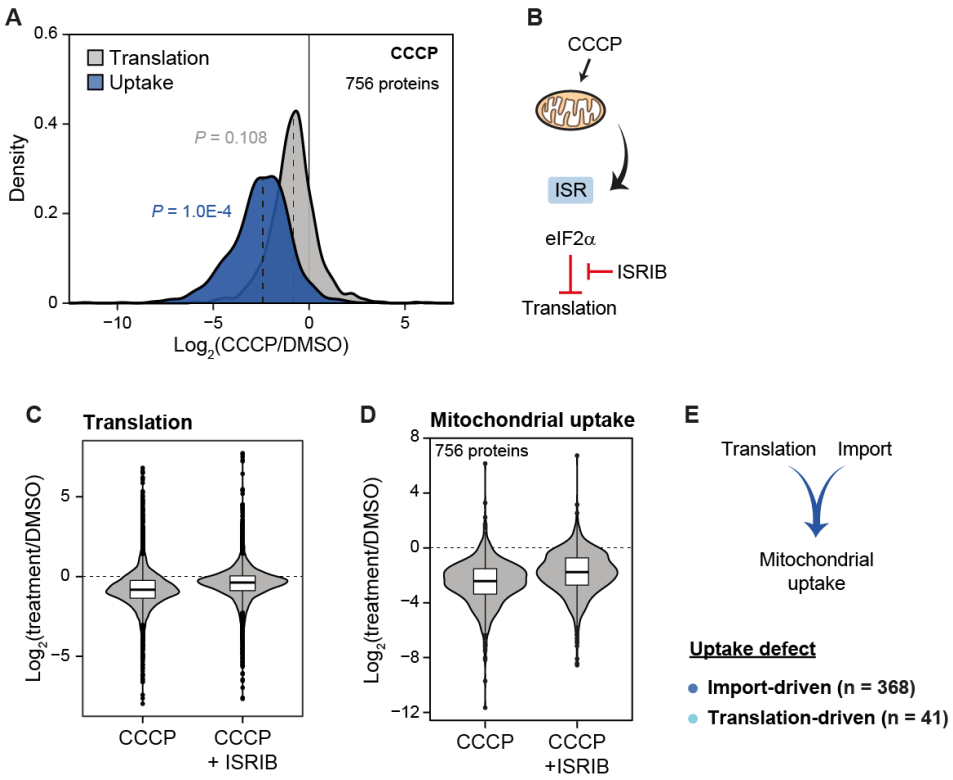

Figure 36: **CCCP modulates mitochondrial protein import by translation- and import-driven regulation.** (A) Fold changes of translation and mitochondrial import of mitochondrial proteins upon CCCP treatment are compared to DMSO-treated control cells for n = 3, shown as density plot. Dashed

lines indicate median values of the distributions. *P*, *P value* (two-sided, unpaired t-test of median values CCCP against DMSO). (B) Illustration CCCP effects on the integrated stress response (ISR) and eIF2α. The ISR inhibits translation during stress; this process is partially reversible by ISRIB co-treatment. (C, D) Violin distribution plots of CCCP-induced translation (C) and mitochondrial protein uptake inhibition (D), with and without ISRIB co-treatment are compared to DMSO control. Data shows average $\log_2$ fold change for three replicates. Center line, median; box limits, upper and lower quartiles; whiskers, 1.5x interquartile range; points, outliers. (E) Translation and protein import effects determine the mitochondrial protein uptake rate. The experimental design and procedure was performed by me, data analysis and visualization was done by Jasmin Schäfer (Schäfer, Bozkurt, Michaelis et al., 2022).

4.3.8 Outer mitochondrial membrane and inter-membrane space protein uptake is regulated by the translation rate

To gain a better understanding of the protein populations which were showing import- or translation-driven uptake defects, Jasmin Schäfer analyzed their sub-mitochondrial localization from experiments that I had performed. All four sub-compartments contained proteins with import- or translation-driven uptake defects upon mitochondrial depolarization by CCCP; still though, the sub-compartments showed clear differences (Figure 37A). The OMM and IMS-uptake defects were largely recovered by ISRIB co-treatment, while the IMM and matrix related defects were mainly import-driven and showed only marginal changes upon translation rescue. Hence, in order to visualize what pathways were affected, Reactome pathway-based network analyses of import- and translation-driven targets was performed (Figure 37B, C). Thereby, it was shown that proteins exhibiting translation-driven uptake defects were part of multiple mitochondrial metabolic pathways. However, only the GO terms peroxisomal protein import and metabolism of nucleotides showed significant enrichment. In comparison, the general term metabolism was found in both networks, whereby in the import-driven data set, extensive links for multiple metabolic pathways were found, with the citric acid and respiratory electron transport and complex I biogenesis being significantly enriched. Within these groups also mitochondrially encoded proteins co-grouped with nuclear encoded ones (Figure 37C). In

accordance, all identified mitochondria-encoded proteins, which are crucial components of respiratory complexes, showed import-driven reduction (Figure 37D) (Schäfer, Bozkurt, Michaelis et al. 2022).

Hence, as a further result of this data set, multiple proteins of the mitochondrial import machinery had CCCP-induced uptake defects. The OMM-located TOM complex components showed translationally-regulated import defects (Figure 37E), which was in accordance with overall finding that OMM proteins were enriched in the translation-driven import defects upon CCCP (Figure 37A). Also, the inner membrane-resident TIM complex and matrix-based PAM complex were differently regulated and exhibited import-driven uptake defects (Figure 37F). These results suggest that the mitochondrial protein import machinery abundance represents another layer of import rate regulation, besides the membrane potential loss observed during CCCP treatment.

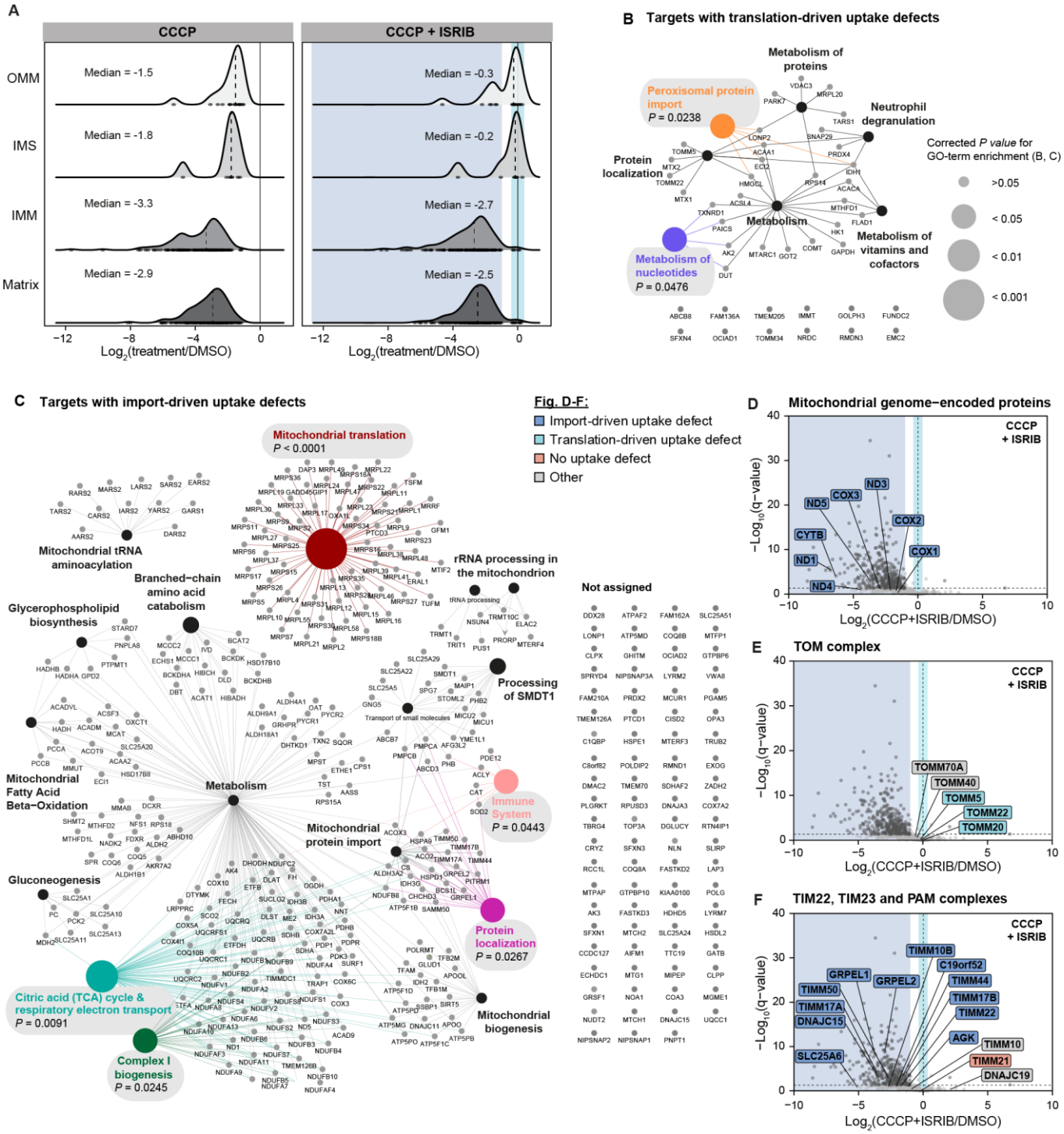

Figure 37: **Outer mitochondrial membrane and inter-membrane space protein uptake is regulated by the translation rate.** (A) Fold changes of mitochondrial protein import separated by sub-mitochondrial compartments for cells treated with CCCP (left) or CCCP + ISRIB (right) compared to DMSO. Data shown as density plots for n=3. Dots shown at the bottom of each plot indicate the number and location of data points. The dashed lines represent the median values per sub-mitochondrial population. CCCP + ISRIB data is labeled blue for import-driven protein uptake defects

and cyan for translation-driven protein import defects. (B-C) Network analysis of Reactome pathways of targets with translation-driven (B) or import-driven uptake defects (C) upon CCCP treatment. Networks prepared utilizing the Cytoscape plug-in ClueGO. Significantly enriched pathways are colored and contain grey boxes with Bonferroni step down-corrected *P*-values. (C-F) Volcano representation of mitochondrial protein import for cells co-treated with CCCP and ISRIB. Fold changes of treatment compared to DMSO are shown against adjusted *P*-values. Data points of the mitochondrial large ribosomal subunit (C), mitochondria-encoded proteins (D), respiratory complex I (E), TOM complex (F) or TIMM22, TIM23 and PAM complexes are labeled. Significant data points are shown in dark grey (fold change [log_2] ≤ -1 or ≥ 1, and adjusted $P \leq 0.05$). Areas of targets with import- or translation-driven uptake defects were highlighted in blue and cyan, respectively. Experiments were performed by me and Jasmin Schäfer generated density and volcano plots. Data also published in Schäfer, Bozkurt, Michaelis et al. 2022.

5 Discussion

Since 2010, when Jin and collegues showed that PINK1 accumulates on depolarized mitochondria upon CCCP treatment the model arose that lack of PINK1 import into mitochondria inhibits its processing via proteases and thus stabilizes the mitophagy sensor on mitochondria. At that time, it was thought that only mitochondrial depolarization can induce this type of mitophagy. Since then, multiple studies found evidence that the membrane potential loss is not necessary to induce mitophagy, just one very effective way to activate mitophagy (Jin & Youle, 2013; Burman et al., 2017; Fiesel et al., 2017). In this study, I further investigated mitophagy without the need for depolarization and show that in all studied conditions, with or without membrane depolarization, a decrease of mitochondrial protein import is the common factor. We established a novel pulsed-SILAC protein import assay and performed commonly used MTS-EGFP approaches to investigate the mitochondrial protein uptake inhibition. By measuring mitophagy flux, PINK1 stabilization, mitochondrial membrane potential, additionally to protein import and mitochondrial proteomics, I received an overview over mitochondrial function and which mitophagy pathway was activated. For example, I directly interfered with protein import by knocking out or RNAi silencing of protein import motor components or studied the effects of a defective mitochondrial protein quality control machinery on mitochondrial protein import and mitophagy. By comprehensive techniques as a genome-wide mitophagy CRISPR screen, mitochondrial and whole cell proteomic approaches, we further characterized the underlying mechanisms and discuss it here in context of recent literature.

5.1 MITOPHAGY CRISPR-SCREEN REVEALED LETHAL KNOCKOUTS OF PROTEIN IMPORT AS MITOPHAGY DRIVERS

My focus was firstly to identify novel factors which induce mitophagy. The genome-wide CRISPR screen distinguish mitophagy-positive populations from mitophagy-negative cells. As HeLa cells need recombinant *PRKN* (protein PARKIN) expression to show efficient PINK1-PARKIN-mitophagy, a HeLa FlpIn TRex cell line expressing mt-*mKEIMA* with inducible *PRKN* was used, which allowed to control the

main stress-induced mitophagy pathway. This screening set up exceeded the enrichment and differentiation of populations from other recent mitophagy screens (Potting et al., 2018; Hoshino et al., 2019), and this possibly led to the identification of so far unidentified mitophagy-inducing and mitophagy-essential knockouts.

During mitochondria depolarizing conditions, sorting for mitophagy-essential genes *PINK1*, *PRKN* and *TOMM7* gRNAs enriched significantly, confirming previously results and the generally excepted mitophagy model, that PINK1 is stabilized on damaged mitochondria by support of TOMM7 and the downstream process is enhanced via the E3 ligase PARKIN (D. Narendra et al., 2008; Jin et al., 2010; Hasson et al., 2013; Hoshino et al., 2019). Furthermore, these findings validate the overall experimental design to be suitable to study gene knockouts affecting mitophagy. As we chose a shorter selection time than other mitophagy studies with measurements after 8 days after gRNA library addition, several lethal gene knockouts were still present in the data set. This becomes clear when comparing a lethality/ fitness screen data set performed with the same gRNA library (Brunello) as used here (Hart et al., 2015) (e.g. Figure 14). By analysis of the mitophagy-incapable gene knockouts, several so far unknown PINK1/PARKIN-mitophagy-essential genes were identified, showing that this data set can be a valuable resource for the mitophagy research field.

The main focus, however, was to study mitophagy-inducing gene knockouts. In this population, I detected many proteins involved in mitochondrial protein uptake and mitochondrial protein quality control. For some identified gene depletions previous findings confirm my observations of increased mitophagy flux, for example *SAMM50* and *HSPA9* knockouts (Burbulla et al., 2014; Jian et al., 2018). For DNAJC11, as it is part of the SAM-MICOS complex (Xie et al., 2007), it was not surprising that a knockout activates mitophagy, as it likely perturbed the same complexes as a *SAMM50* knockout does; however, to my knowledge, I am the first to report this.

Two other highly enriched candidates, which induced mitophagy when depleted, were *UROD* or *TELO2*. There is no publication so far relating them with mitophagy, thus I can only make a carefully considered guess about possible mechanisms. In case of UROD, as it is an essential enzyme of the heme

biosynthesis and inhibition of another heme biosynthesis protein was described to induce mitochondrial dysfunction, membrane depolarization and increases mitochondrial ROS (Shetty et al., 2020). Hence, it is probable that a lack of heme affects the respiratory chain, results over time in mitochondrial membrane depolarization and by that induces PINK1-dependent mitophagy. TELO2 is part of the mTORC1/2 complex and important for its stability (Rockel & Kapoor, 2016). Therefore, a loss of TELO2 could drive the mitophagic flux by generally increased autophagy. These few chosen examples show that the data set of mitophagy-inducing knockouts contains further possible mitophagy regulating genes.

I have focused on the most enriched pathways, while there are many interesting individual candidates. This CRISPR screen was performed in a cancer cell line (HeLa FlpIn TRex *PRKN*) with induced *PRKN* expression. For the purpose of finding gene knockouts which induce PINK1-PARKIN mitophagy this was a sensitive and sufficient experiment, but some regulations in non-cancerous cells and cells with low *PRKN* expression might be different. Further studies should take this into account and perform similar experiments on non-cancerous cells, e.g. cells of high metabolic activity or neurons (McWilliams et al., 2018). These cells especially depend on mitochondrial function and could give further insights.

5.2 LACK OF PROTEIN IMPORT MOTOR FUNCTION RESPONSIBLE FOR MITOPHAGY INDUCTION

My data set for mitophagy-inducing knockouts showed import-related gene depletions mostly enriched (Figure 14). Of the protein import motor PAM, I identified HSPA9 and its co-chaperone GRPEL1 significantly enriched. However, TIMM44, which is essential for PAM complex recruitment and PAM16 were not detected in the CRISPR screen to induce mitophagy when depleted. This finding could have meant that HSPA9's function in protein folding as a chaperone, together with its nucleotide exchange factor GRPEL1, was important to prevent mitophagy or its function in the PAM complex. To investigate these possibilities, I looked at the factors individually. PAM16 has only a function in protein import motor and sits close to the translocon. It seems to function in timing how long HSPA9 is bound

to imported precursors by regulating HSPA9's ATPase activity. Thus, *PAM16* depletion would affect the import efficiency. While PAM16 was described to be essential for protein import motor function in yeast (Frazier et al., 2004), I saw reduced MTS-EGFP uptake, but milder than with *HSPA9* RNAi. At the same time, *PAM16* depletion resulted in significant mitophagy induction which was accompanied by PINK1 accumulation in mitochondrial extracts (Figure 20). Thus, this showed that also this PAM component, in addition to *HSPA9* and *GRPEL1*, was possible to activate mitophagy, when depleted. Next, I looked at *HSPA9* RNAi and if it also induced an insoluble protein fraction, as observed for *LONP1* RNAi. However, *HSPA9* depletion did not lead to a significant increase in insoluble proteins compared to non-targeting control or *LONP1* (Figure 24). Possibly, the lack of protein import during *HSPA9* knock-down prevented the accumulation of misfolded/unfolded proteins. This data is furthermore supported by Shin et al., who shows on immunoblot that their maker proteins for the insoluble protein fraction did not accumulate upon *HSPA9* siRNA, while they did during e.g. *DNAJA3* depletion (Shin et al. 2021, Supplementary Figure S2). Taken together, the data demonstrates that indeed the inactivity of PAM protein import motor function drives mitophagy and not the lack of folding capacity by itself.

5.3 TIMM44 REGULATES IMPORT AND MITOPHAGY

TIMM44 is known to be an essential part of the PAM complex (Miyata et al., 2017) and in our experiments we also found it to inhibit MTS-EGFP protein uptake into mitochondria (Supplementary figure 1). Thus, I assumed that there might be secondary effects preventing mitophagy induction upon TIMM44 loss, explaining why I did not identify it in the mitophagy CRISPR screen. Hoshino et al. in 2019 showed that TIMM44 seem to be essential for mitophagy induction via interaction with ADP/ATP-translocases (ANT-1, synonym SLC25A4, 5, 6). They could not explain how TIMM44 was involved in the mitophagy mechanism, but *TIMM44* depletion prevented PINK1 accumulation upon CCCP treatment, while a rescue by *TIMM44* re-expression was possible. This showed that TIMM44 has a function in regulating PINK1-dependent mitophagy. In TIMM44 proximity experiments, I also detected ANT-1 with all components (SLC25A4, 5, 6) as one of the main interactors, which supports the hypothesis that

TIMM44 could have a signaling function via ANT-1 (Figure 27). Furthermore, I also saw the PINK1-protease PARL, as well as the proposed mitophagy receptor prohibitin (PHB and PHB2) (Wei et al., 2017; Yan et al., 2020) in close proximity to TIMM44; this interaction stayed even stable during protein misfolding stress (Figure 27, 28). These interactions make various mitophagy regulation steps possible, as PARL processing could be affected or PHB's mitophagy receptor function by TIMM44. To understand the observed effects, an in depth interaction study of different mutations at/or lacking the interaction sites would be necessary.

Besides, these stress-related interactions, TIMM44 was found to be in close proximity to OXA1L, which is required for the insertion of integral membrane proteins into the IMM from the matrix (Hell et al., 2001; Jia et al., 2007). In addition, many mitochondrial ribosomal proteins, translation-linked proteins, the respiratory chain complex and two mitochondrially-encoded proteins were detected (Figure 27). This associates TIMM44 with mitochondrial translation and the integration of the 13 mitochondrially-encoded proteins into the IMM-located respiratory chain. TIMM44 could have an undiscovered function between mitochondrial protein import at the TIM complex and the synchronization with the mitochondrial translation. Such a synchronization was described in yeast (Couvillion et al., 2016), but TIMM44 has so far not been linked to this mechanism. During protein misfolding stress, a clear loss of interaction between TIMM44 and OXA1L was observable, while many mitochondrial ribosome and TCA/respiratory chain proteins became insoluble and stayed in proximity to TIMM44 (Figure 28). Thus, TIMM44 could mediate protein import and possibly coordinate it with the mitochondrial translation machinery. A further study to the integration of mitochondrial encoded proteins into the IMM and the possible role of TIMM44 would be necessary to substantiate this hypothesis, e.g. by TIMM44 mutations in possibly interacting domains and measuring its effect on respiratory chain complex protein level in the IMM.

5.4 PROTEIN FOLDING STRESS INDUCES MITOPHAGY WITHOUT DEPOLARIZATION OF MITOCHONDRIA

As the CRISPR screen showed mitochondrial protein processing/protein quality control as another pathway to be critical for mitophagy prevention, I validated gene knockouts individually of LONP1 protease and PMPCB, the catalytic subunit of the mitochondrial precursor peptidase MPP. Indeed, as reported before, accumulation of LONP1- or MPP-substrates resulted in mitochondrial degradation via the lysosome (Greene et al., 2012; Zurita Rendón et al., 2018). To understand how proteostasis perturbation in the matrix can trigger mitophagy, I induced mitophagy by prolonged "mild" stress via *LONP1* or *HSPA9* RNAi or by acute inhibition of mtHSP90. This led to PINK1 accumulation on mitochondria and poly-phospho-ubiquitination of mitochondria (Fiesel et al., 2017), while the mitochondrial membrane potential stayed intact. This was not in accordance to the prevailing theory that PINK1-dependent mitophagy induction requires mitochondrial depolarization (D. P. Narendra et al., 2010). However, Jin and Youle already published in 2013 that the expression of a deletion mutant of rat ornithine carbamoyl transferase (*ΔOTC*) triggered the formation of a mild detergent insoluble protein fraction in human cells, which resulted in PINK1 accumulation on mitochondria without a significant reduction in membrane potential. Nevertheless, a model describing how PINK1 could be stabilized was missing. Thus, to propose a model, explaining this open question, I generated more information about the accumulation of misfolded proteins in the mitochondrial matrix and analyzed the content of protein folding stress-induced insoluble protein fractions. The PAM components HSPA9, GRPEL1/2 and TIMM44 were enriched in the insoluble protein fraction upon *LONP1* RNAi and GTPP. As the PAM is directly involved in mitochondrial protein import, this led to the first speculations about its involvement with PINK1 stabilization. Comparing my findings with a recent proteomic study on protein folding in mitochondria showed that PAM components consistently localize to the insoluble protein fraction upon protein folding stress (Figure 24, 25) (Shin et al., 2021). Shin et al. performed RNAi against *LONP1* and *DNAJA3* on 143B cells and measured via label-free quantification MS protein levels, while we used HeLa FlpIn TRex cells and TMT quantification, *LONP1* RNAi and compared it to acute inhibition of mtHSP90. These results demonstrate that GRPEL1/2, HSPA9 and TIMM44 of the

PAM complex have a general tendency to become insoluble or bind to the insoluble fraction upon proteostasis perturbation and this is not limited to the conditions studied here.

For the yeast orthologue TIM44, it was shown that it contains a large unstructured N-terminal region, which is thought to interact with the membrane, the TIM translocon, the pre-sequence of newly translocated proteins, HSPA9 and PAM16 (Ting et al., 2017). Its N-terminus was described to be intrinsically disordered or unfolded without interaction partners. This unstructured domain, based on the sequence, is conserved in human TIMM44. Likely this N-terminal domain makes TIMM44 especially aggregation-prone, which could explain the significant accumulation in the insoluble protein fraction compared to other mitochondrial proteins.

HSPA9 and GRPEL1/2 on the other hand are chaperones/ co-chaperones. Thus, they have the tendency to bind unfolded proteins. These different mechanisms seem also to be reflected in protein level upon protein folding stress. By looking at the mitochondrial extracts upon GTPP or si*LONP1* (Figure 22 or MS data of Figure 20), a decrease of HSPA9 and GRPEL1 protein level was observable. This suggested that HSPA9 and its co-chaperone became degraded during misfolding stress. As the reduction of protein levels was not observable during CCCP treatment, which blocks protein uptake almost entirely, transcriptional and translational regulation were excluded, as newly synthesized proteins could not reach the matrix anymore. TIMM44 total protein levels were, however, not decreased and rather increased, indicating that TIMM44 is differently regulated upon GTPP. Possibly, TIMM44 itself misfolds and aggregates, which protects it from degradation, while HSPA9/ GRPEL1/2 cover the aggregate. This makes HSPA9 and GRPEL1/2 accessible to mitochondrial proteases, which were also found enriched in/at the insoluble protein fraction.

The TIMM44 proximity experiment showed the loss of interaction between TIMM44 and the TIM translocon upon protein misfolding stress (Figure 27), while TIMM44 increased its interactions with the insoluble protein fraction. These findings show the transition of soluble TIMM44, which is active in the PAM protein import motor to being part of the insoluble protein fraction and inactive. As the import motor cannot function without TIMM44, these observations also explains why the protein

import to the mitochondrial matrix is inhibited during protein folding stress. During these experimental conditions, PINK1 is stabilized as it cannot be processed by PARL when it is not transferred through the IMM. Here, irrespective of the method of inhibition (RNAi of *HSPA9*, *LONP1* or mitochondrial depolarization by e.g. AO or CCCP), PINK1 accumulates and that accumulation leads to its *trans*-autophosphorylation and activation of mitophagy. Thus, I concluded that PAM removal from the import pore is a possible explanation for PINK1 stabilization and mitophagy induction. This finding is especially relevant, as it is the first theory on how membrane potential break down-independent PINK1/PARKIN-mitophagy can be activated.

5.5 MITOCHONDRIAL UNFOLDED PROTEIN RESPONSE REGULATION BY PROTEIN IMPORT INHIBITION

As I show in this study that mitochondrial protein import is decreased upon disturbance of the mitochondrial protein homeostasis, one should also consider which other pathways are subsequently activated. The UPR^{mt} is a protective nuclear transcriptional response that is activated upon the accumulation of unfolded or misfolded proteins in mitochondria. First it was reported in cell culture for cells, depleted of mtDNA by long-term ethidium bromide treatment (Martinus et al., 1996) or by cells overexpressing *ΔOTC*, a deletion mutant protein, which is incapable to properly fold inside the matrix (Q. Zhao et al., 2002). As a consequence, UPR^{mt}-target genes like mitochondrial chaperonins, chaperones, and proteases are expressed (Aldridge et al., 2007), which presumably increases the mitochondrial protein folding capacity and stabilizes stressed mitochondria. It was shown before that the treatments used in this study, e.g. GTPP or *LONP1* depletion, increase UPR^{mt}-target gene transcription (Münch & Harper, 2016; Zurita Rendón et al., 2018).

Interestingly, my study shows that protein uptake into mitochondria is reduced upon these conditions, thus increased expression of UPR^{mt}-target genes seems to be paradox: Elevated mitochondrial chaperone and protease precursors in the cytosol would maybe not be able to be imported into the mitochondrial matrix. Consequently, if general translation would continue and translation of UPR^{mt}

mRNAs would be increased, it could potentially lead to further stress in the cytosol, where newly synthesized proteins have to be held in an unfolded, import-competent state bound to cytosolic chaperones. However, during stresses used in this study, such as GTPP, the cell co-activates together with the UPR^{mt}, the ISR; a stress response that is characterized by the inhibition of global translation via the phosphorylation of eIF2α. Translation initiation depends on the loading of eIF2 with guanosine-5'-triphosphate (GTP) by the translation initiation factor eIF-2B subunit epsilon (eIF2B). However, phosphorylated eIF2α prevents this process resulting in inhibition of cap-dependent translation (Hinnebusch et al., 2016). eIF2α phosphorylation then results in reduced global translation during the stress. Stress response genes, however, often are cap-independent so that e.g. *CHOP* and *ATF4*, which are needed for UPR^{mt}-target gene expression, are translated (Vattem & Wek, 2004; Palam et al., 2011; Andreev et al., 2015). Data for HSPD1/E1 protein level, however are inconclusive. While in previous publication their protein level were observed to be increased (Münch & Harper, 2016), in our whole cell or mitochondrial proteome data, they did not show increased protein levels (Supplementary table 2). This indicates that, even though *HSPD1/E1* were transcribed upon GTPP, they are either not translated or not actively imported. Maybe the mRNA or mitochondrial precursors in the cytosol are prepared to be translated/imported when the acute stress has passed, which would lead to the formation of stress granules or processing bodies (Riggs et al., 2020). (II) The other hypothesis is based on the fact that during physiological stress only some mitochondria are affected, while the mitochondrial fission machinery fragments damaged mitochondria and segregates healthy from dysfunctional ones (Burman et al., 2017). Therefore, protein import into healthy mitochondria might be possible. In regard to this study, we know that upon conditions triggering the UPR^{mt}, e.g. GTPP treatment, RNAi of *LONP1* or overexpression of *ΔOTC*, also mitophagy is activated (Q. Zhao et al., 2002; Jin & Youle, 2013; Münch & Harper, 2016; Fiesel et al., 2017). Thus, damaged mitochondrial fragments could be removed via mitophagy at the same time with UPR^{mt} proteins being imported, as it was shown for mtDNA heteroplastic cells (Suen et al., 2010). However, differentiation between healthy and damaged mitochondria cannot be studied with treatments used in this study, as GTPP or RNAi treatment affect all mitochondria of a cell simultaneously. These treatments were useful to highlight

the acute signaling and allow to measure low abundant protein changes as PINK1 stabilization on mitochondria. However, to solve the cross-talk between removal of damaged mitochondria versus its repair via UPR^{mt}, a live cell microscopy-based approach might be necessary. In *C. elegans*, UPR^{mt} was followed by fluorescently-labeled *hsp-6,* but for mammalian systems, no reporter cell line was so far successfully developed for any of UPR^{mt} -induced genes. When a cellular system to monitor UPR^{mt} would be established, it could be combined with fluorescently-labelled PINK1 to prove the interplay and demonstrate if the two stress responses happen simultaneously on different mitochondria or only in different cells. The first hypothesis, the reversibly halt of mitochondrial protein import, could also be tested with GTPP washout and recovery experiments. Theoretically, also both hypotheses could be true, the mitochondrial protein import is reduced during the stress, while it still occurs at some mitochondria and increases as soon as the stress attenuates. These experiments could provide the missing link between the two fields of transcriptional mitochondrial stress responses and mitophagy.

5.6 MITOCHONDRIAL APOPTOSIS INDUCTION VERSUS MITOPHAGY

The pathways discussed in the paragraph above focused on pro-survival responses. However, increased mitochondrial stress can also result in programmed cell death, apoptosis. There are two types: extrinsically and intrinsically induced apoptosis. During cellular damage causing cell death, the intrinsic pathway is relevant. In brief: When cells or mitochondria are exposed to severe stress, this stress can activate BH3-only proteins (e.g. Bcl2-associated agonist of cell death (BAD)). BH3-only proteins propagate apoptotic signals, activating apoptosis regulator BAX/ Bcl-2 homologous antagonist/killer (BAK1) and by suppressing the anti-apoptotic BCL-2 proteins at the mitochondria (Shamas-Din et al., 2011). BAX and BAK1 oligomerize, forming high-molecular weight pores that permeabilize the OMM (Westphal et al., 2013). These pores allow the release of cytochrome c to the cytosol. Cytosolic cytochrome c forms an apoptosome together with apoptotic protease-activating factor 1 (APAF-1), recruiting and activating initiator caspase-9 (P. Li et al., 1997; Srinivasula et al., 1998). Caspase-9 itself activates the executioner caspases-3 and -7, this leads to wide spread proteolysis of

cellular content, reprogramming of the cell and resulting in the controlled cell death of the effected cell (Kumar, 2007).

Besides their previously discussed protective impact by activating mitophagy, it is known that PINK1 and PARKIN have anti-apoptotic functions (Wanderoy et al., 2020). PARKIN ubiquitylates BAX among others, which prevents its oligomerization and thus the permeabilization of the OMM (Cakir et al., 2017). PINK1 phosphorylates most prominently Bcl-2-like protein 1 (BCL2L1 aka BCL-x_L), which prevents its pro-apoptotic processing (Arena et al., 2013). These regulatory steps raise the threshold for apoptosis and give the cell time to solve mitochondrial stress via mitophagy.

Another crosstalk between mitophagy and apoptosis is mediated by the mitophagy receptor BCL2-L13, which is a BCL-2 family protein and ATG32 homologue that is recruited to damaged mitochondria and seems to function as a PARKIN-independent mitophagy receptor (Murakawa et al., 2015). In my CRISPR screen I have found that BCL2-L13 knockout cells show less mitophagy upon AO treatment (Figure 15) supporting the data that it functions as potential mitophagy receptor. Additionally to the mitophagy-driving function, BCL2-L13 inhibits apoptosis as previously shown (Fujiwara et al., 2019). Thus my data supports that crosstalk between mitophagy and apoptosis also takes place at the stage of mitophagy receptors.

Interestingly, the CRISPR data set also showed a pro-apoptotic protein as mitophagy driver – BH3-interacting domain death agonist BID. BID is known to be activated via caspase-8 during the extrinsic apoptosis cascade. Here, it was enriched within the group of mitophagy-essential genes during AO-induced mitophagy (Figure 15). To my knowledge, this link between extrinsic apoptosis signaling and mitophagy has not been made and suggests mitophagy inhibition upon loss of BID-dependent apoptosis. It will be interesting for the future to further investigate apoptosis- and mitophagy-dependent regulation, especially in the context of disease development. In case of mitophagy-deficient neurons e.g. the likelihood for cell death and thus neurodegeneration is increased (Martinez-Vicente, 2017).

5.7 CROSSTALK BETWEEN REACTIVE OXYGEN SPECIES SIGNALING AND MITOPHAGY

One trigger of apoptosis is the accumulation of DNA damage, which can be caused by reactive oxygen species (ROS) (Van Houten et al., 2006; Redza-Dutordoir & Averill-Bates, 2016). Elevated ROS levels have been observed, e.g. when mitochondria were damaged or depolarized (Demine et al., 2019). However, it seems that ROS is not only a side product, but also necessary for mitophagy induction after uncoupling of the membrane potential (Xiao et al., 2017). Gao and colleagues showed in 2020 that ROS in the IMS plays an important role in PINK1 stabilization, at least for depolarization-induced mitophagy, e.g. upon CCCP treatment (Gao et al., 2020). Their finding showed that the IMS protein CHCHD4 interacts with PINK1 during depolarization and in the presence of ROS. As CHCHD4 together with GFER catalyze the formation of disulfide-bridges in the IMS (Al-Habib & Ashcroft, 2021), it is likely that PINK1's cysteines are crosslinked (C166 and potentially C92, C96 or C125) (Gao et al., 2020). These disulfide-bridges would lead to a secondary structure, which could prevent PINK1 from retro-translocation to the cytosol.

During protein folding stress or *HSPA9* RNAi, as in this study, it is likely that ROS is also released into the IMS, which could contribute to PINK1 stabilization. For *LONP1* RNAi and GTPP, it was described that cellular or mitochondrial ROS levels increase (Yoo et al., 2015; Y. G. Lee et al., 2021). This would support ROS-dependent interaction of CHCHD4 with PINK1 and add another layer of PINK1-dependent mitophagy activation. It would be interesting to follow this downstream effect, which could further extend the here proposed protein folding stress-/protein import inhibition-induced PINK1-dependent mitophagy model. As PARL cleaves PINK1 between residue A103 and F104, a disulfide bridge between C166 and C92 or C96 would only be possible when PINK1 processing by PARL is inhibited. This would be an elegant way, how non-processed PINK1 could be further stabilized on the OMM by mitochondrial import inhibition and ROS release into the IMS. This hypothesis could be tested by the expression of recombinant cysteine-mutated PINK1 in a *PINK1* KO cell line, while inducing mitophagy.

5.8 PULSED-SILAC PROTEIN UPTAKE PROTEOMICS USEFUL TOOL TO MEASURE AND QUANTIFIY MITOCHONDRIAL PROTEIN IMPORT

The earlier discussed stress responses can be measured in various ways, e.g. by fluorescence reporter cell lines, specified dyes or immunoblotting for specific marker proteins; a different method to follow stress responses is to investigate the cellular proteome or translatome, via mePROD (Klann et al., 2020). In chapter 4.3, I introduced another method, which is based on pulsed-SILAC and TMT-multiplexing, mePROD^{mt}. This technique allows to monitor protein uptake of newly synthesized proteins via its degree of heavy SILAC labelling and being present in or tightly bound to mitochondria. I used this approach to measure global import inhibition upon mitochondrial folding stress (Figure 30).

Previous methods were largely based on individual proteins tagged with a fluorescent protein to estimate its protein import upon a certain condition. Thus, a reporter cell line with an artificial recombinant protein was needed, which could only give you information about the import of one specific protein. We used this method based on ATP synthase subunit 9 mitochondrial targeting sequence and EGFP to e.g. show for CCCP that it indeed inhibits mitochondrial matrix targeted protein import. However, it can only partially reveal protein uptake defects. As my colleagues, Jasmin Schäfer, Süleyman Bozkurt, Kevin Klann and I have shown, there are exclusively import-regulated proteins, which largely react upon depolarization of the inner mitochondrial membrane potential. But there are also translational-regulated proteins, which can still be integrated into mitochondria even when there is no import through the inner membrane. These proteins seem to be regulated via their transcription and translation. Thus, with a recombinant fusion protein, there are two disadvantages: They are often not expressed with their own promoter and untranslated regions on the mRNA, thus they lose possible regulation at that level and they might be over expressed, which can lead to artifacts itself. Furthermore, the fusion protein always brings the possibility of changed degradation and different interactions. MePROD^{mt} on the other hand uses heavy amino acids, which are chemically very similar to common amino acids, to label and follow imported proteins. Therefore, no labeling artifacts are expected. Additionally, the boosting of SILAC-labeling allows to follow protein uptake into

mitochondria even for short labeling durations, as low as 15 min SILAC labeling time (Schäfer, Bozkurt, Michaelis et al 2022), which is far below the effects that can be seen by transient transfection or inducible fluorescent protein systems, as tetracycline induced *MTS-EGFP* expression. For transient transfection during a treatment, at least overnight expression of the construct was needed to receive high quality images to determine the protein's location (Figure 32). Even though the inducible protein expression is faster in that regard and better controlled, also here several hours are needed to synthesize enough fluorescently labeled fusion protein. The pulsed SILAC protein import approach therefore has a better dynamic range representing protein import changes especially upon acute treatments.

One other previously used method is based on radio-labeling of one specific protein of interest (e.g. Yano et al., 2014). To follow protein import in this approach: mitochondria were extracted, the protein of interest synthesized *in vitro* by cell-free protein synthesis with radio-actively labeled amino acids, both components mixed together and incubated. Protein import was then measured by the accumulation of radioactivity in the mitochondrion. As for SILAC-labeled proteins, the protein sequence should be unchanged by radio-active amino acids. However, the proteins are expressed outside the cell, thus the cellular regulation of the protein import from the cytosol or by translation regulation is not present. Furthermore, there is no cross-talk between organelles which could signal what usually in a cell would happen, especially upon stress responses.

In summary, these two examples show that there was a need for a more comprehensive, unbiased, mitochondrial protein import method. The presented pulsed-SILAC mitochondrial protein uptake assay is a novel global assay, as it measures hundreds of proteins at once without altering the cellular environment. It is a quantitative method, as it provides intensities for the SILAC-labeling of individual proteins and by using the summed intensities, also for whole mitochondrial trends.

To demonstrate that mePROD^{mt} indeed shows mitochondrial protein uptake, we utilized the protonophore CCCP. CCCP has been extensively described in the literature to remove the inner mitochondrial membrane potential and by that leading to a global mitochondrial import inhibition (J.

Martin et al., 1991). As expected, we found a broad decline in mitochondrial protein uptake in our mePROD^{mt} experiments. This likely contributes to a decrease of mitochondrial protein abundance that was reported before (Quirós et al., 2017). Interestingly, the detected mitochondrial uptake proteome was not uniformly affected by the depolarization. Proteins involved in mitochondrial translation and respiratory electron transport were among the most severely effect by CCCP. This is in accordance with studies reporting reduced levels of proteins of the respiratory chain and mitochondrial ribosomes upon mitochondrial stress (Zhu et al., 2012; Quirós et al., 2017; Franco-Iborra et al., 2018). We also detected several mitochondrial proteins with unchanged uptake rates during depolarization. These proteins would be interesting candidates to be further investigated, as the question remains how these proteins are taken up or if they tightly associate as pre-cursors to the mitochondria.

For validation of mePROD^{mt}-measured CCCP effects, I have combined the pulsed HaloTag-labeling for several mitochondrial proteins with mitochondrial extraction. This allowed to overcome detection issues of inducible constructs, which first need to be expressed in detectable amounts, while here the expression is continues, old protein becomes saturated with colorless HaloTag-ligand and only during the treatment newly synthesized protein is labeled. By the combination with mitochondrial extraction only newly synthesized and into mitochondria imported proteins are measured. Thus, the beauty of this novel HaloTag approach is to follow individual newly synthesized proteins in live cells, also for short treatment times. The labeling with HaloTag ligand biotin ultimately validated the mitochondrial uptake defects upon CCCP for HSPD1, ATP5A1, GLRX5 and GRPEL1. The protein uptake defect by CCCP was estimated and a decrease of loss of protein import similar to mePROD^{mt} was measured. In summary, the mePROD^{mt} method gives quantitative, unbiased data on steady-state protein uptake into mitochondria and shows changes of protein uptake for individual proteins, as well as the mitochondrial proteome. This technique is more powerful than methods used before and can even capture acute changes in protein import. We established another pulsed-labeling method, based on HaloTag labeling and are also the first to my knowledge, who combined organelle-extraction with pulsed-HaloTag measurements to look at protein import.

5.9 OMM AND IMS PROTEINS ARE TRANSLATIONALLY REGULATED RATHER THAN IMPORT-REGULATED, AS SHOWN BY TRANSLATOME ANALYSES

A further layer of information was generated by not only using mitochondrial extracts, but also by quantifying pulsed-SILAC whole cell lysates of the same samples. This data set represents whole-cell translation and is called mePROD (Klann et al., 2020). With these two proteomic data sets (mePROD and mePROD^{mt}) in hand, protein import inhibition and translational regulation were monitored in parallel. For example, the mePROD data set from the CCCP experiment showed whole cell translation attenuation upon CCCP treatment. By the addition of the ISR inhibitor ISRIB this translation attenuation was largely recovered (Figure 36). However, this only partially restored mitochondrial protein uptake during treatment with CCCP plus ISRIB. Here, we could identify especially OMM and IMS proteins being recovered, while IMM and matrix proteins were still largely decreased during CCCP plus ISRIB treatment (Figure 37). These results show the power of the two new methods: import- or solely translationally-regulated proteins can be distinguished giving a deeper understanding of the underlying mechanisms.

The limitation of mePROD^{mt} and mePROD is based on the fact that the cells have to be able to be cultured in SILAC medium with heavy amino acids. Large differences between access to the SILAC medium would result in higher variances between the SILAC-pulsed cells and might only allow longer treatment times to observe significant changes. For now, the comprehensive and non-invasive character of our mass spectrometry-based uptake approach makes it a promising tool to study mitochondrial protein uptake in cell culture, characterize the substrate spectrum of individual import pathways and investigate how different stresses alter the mitochondrial proteome. It would be exciting to try this technique also for or primary cells, patient samples or organoids, but the before mentioned limitations have to be considered.

5.10 PROTEIN IMPORT DEFECTS AND ITS LINK TO NEURODEGENERATION

The mitochondrial proteome and proper mitochondrial protein import are of crucial importance for cellular health. Deregulation of protein uptake into mitochondria therefore has severe consequences and has been found in various diseases, such as: cancer, Huntington's (HD) and Parkinson's disease (PD) (Y. Kang et al., 2018; Yablonska et al., 2019; Nicolas et al., 2019). For instance, the causative protein in HD, mutant huntingtin which contains long poly-glutamine stretches associates with the TIM23 complex. This mutant huntingtin-TIM interaction results in the inhibition of protein import in synaptic mitochondria, which is suggested to have early pathophysiologic consequences (Yablonska et al., 2019). A similar phenotype can also be observed for the PD-associated form of α-synuclein. These post-translationally modified species of α-synuclein bind to TOMM20 and inhibit mitochondrial protein import in nigrostriatal neurons (Di Maio et al., 2016). Likely, the loss of protein uptake into mitochondria is causative for deficient mitochondrial respiration, increased ROS production and loss of membrane potential (Di Maio et al., 2016). These observations already show the importance of mitochondrial protein uptake as crucial factors for neurodegenerative disease phenotypes. Thereby, the mePROD^{mt} approach could provide quantitative insight with cellular diseases models. Using mePROD^{mt} in a time-dependent manner, one could analyze which pathways are affected first after expression of such pathogenic protein species, what stress sensors are recruited and how this remodels the mitochondrial proteome.

In regard of stress responses in HD and PD models, it was observed that mitophagy becomes inhibited by the accumulation of misfolded proteins in the cytosol in close proximity to mitochondria (Shaltouki et al., 2018; Franco-Iborra et al., 2021). If this mitophagy inhibition is a direct effect or an indirect result has to be further investigated. A possible reason could be that the misfolded proteins (α-synuclein and mutant huntingtin) directly interact with the translocons of mitochondria. This interaction might interfere with the PINK1 stabilization or activity and thus prevent mitophagy downstream of protein import-inhibition mitophagy induction. Otherwise, the misfolded proteins could also recruit cytosolic chaperones and mitochondrial protein import receptors, as TOMM20 which are needed for efficient

import and by that intervene with correct PINK1 folding, stabilization or activity. PINK1 processing on mitochondria as shown in this study (Figure 22G) would be helpful to distinguish if PINK1 indeed is potentially active and in the right location.

Franco-Iborra and colleagues showed that PINK1-dependent mitophagy receptors (OPTN and CALCOCO2) are not recruited to mitochondria anymore in their HD model cell line (Franco-Iborra et al., 2021), supporting that HD causes PINK1-mitophagy defects. In PD it is even clearer that defects in mitophagy can drive the disease and lead to neural cell death, as loss-of-function mutations in PINK1 (synonym *PARK6*) or PARKIN (synonym *PARK2*) can induce early-onset PD (Valente et al., 2004). However, how PD develops and how α-synuclein (synonym *PARK1*) accumulates and interferes with mitophagy has to my knowledge not been clarified. But a recent study showed that intracellular administration of PARKIN can rescue both *in vitro* PD models and *in vivo* PD animal models (Chung et al., 2020); from previous findings about PARKIN it is known that it is only active on mitochondria when PINK1 is also stabilized, thus it is likely that α-synuclein attenuates mitophagy without blocking PINK1 completely. Thus, PARKIN upregulation could accelerate mitophagy and resolve proteotoxic stress by α-synuclein.

Interestingly, not only overexpression or intracellular delivery of PINK1 or PARKIN can enhance mitophagy, but also compounds e.g. urolithin A activate mitophagy, which seems to have beneficial effects in PD and other neurodegenerative disorders. In Alzheimer's for example, the clearance of amyloid-β as well as tau pathology was observed, combined with a decrease in cognitive deficits upon mitophagy activation (Du et al., 2017; Fang et al., 2019). The compound urolithin A has been tested in AD models and resulted in amelioration of disease phenotypes in both cellular and animal models (Ryu et al., 2016; Fang et al., 2019; Andreux et al., 2019; Esselun et al., 2021). However, the underlying mechanism of urolithin A is not completely clear (W. Zhao et al., 2018), as low concentrations induce mitochondrial biogenesis without mitochondrial membrane potential collapse, higher concentrations drive mitophagy while there was depolarization observed (Esselun et al., 2021). It is probable that both processes have beneficial effects for the cell. As this drug is a promising candidate for AD treatment, it

would be exciting to investigate and characterize its effects on PINK1-mitophagy further and test whether it induces the here described protein import inhibition-induced mechanism using our established methods. Thus, the techniques introduced in this work could also be useful to gain better knowledge of agents targeting neurodegenerative diseases and help in pre-clinical trials.

5.11 CONCLUDING REMARKS

The two studies combined in this thesis, focused both on mitochondrial homeostasis and identified mitochondrial protein import, as crucial for mitochondrial health and quality control. MePROD^{mt}, as a novel method to study protein uptake effects, allowed to distinguish between import- or translation driving uptake and giving researchers a better time resolution than mitochondrial and whole cell proteomics, which were often used before. The first mentioned study on mitophagy (chapter 4.1 and 4.2) identified many factors relevant for protein import into mitochondria and links it to the induction of PINK1-dependent mitophagy. As explained, the PAM-complex protein import motor reacts on proteostasis perturbations and reduces the matrix-targeted import by its sequestering from the translocon. We are the first to report this mechanism, and we believe that it creates another, more sensitive level of mitochondrial protein import control that leads to the induction of mitophagy when needed, and thus to the elimination of dysfunctional mitochondria even before membrane potential breakdown occurs. Possibly, this mechanism will also have an effect on other mitochondrial stress responses and their signaling, e.g. UPR^{mt}, which future studies will have to show. The development of the mePROD^{mt} method makes it possible to study treatments in a timely and comprehensive manner, while receiving protein-specific knowledge about their import into mitochondria. I mostly used this method as a tool to look at global import effects, however the data sets generated are a resource for commonly used compounds in the research field. The method itself will help to better quantify and understand proteostasis changes in mitochondria. This improvement in the quality of protein import data could be used, e.g. to improve mechanistic understanding of the mitochondrial import defects

observed in neurodegenerative diseases, but the developed workflow could also be extended to other organelles and thus further open questions.

6 References

Al-Habib H, & Ashcroft M. (2021). CHCHD4 (MIA40) and the mitochondrial disulfide relay system. *Biochemical Society Transactions*, *49*(1), 17.

Aldridge JE, Horibe T, & Hoogenraad NJ. (2007). Discovery of genes activated by the mitochondrial unfolded protein response (mtUPR) and cognate promoter elements. *PloS One*, *2*(9), e874.

Allen GFG, Toth R, James J, & Ganley IG. (2013). Loss of iron triggers PINK1/Parkin-independent mitophagy. *EMBO Reports*, *14*(12), 1127–1135.

Altmann R. (1894). *Die Elementarorganismen und ihre Beziehungen zu den Zellen*.

Anand R, Wai T, Baker MJ, Kladt N, Schauss AC, Rugarli E, & Langer T. (2014). The i-AAA protease YME1L and OMA1 cleave OPA1 to balance mitochondrial fusion and fission. *The Journal of Cell Biology*, *204*(6), 919–929.

Andreev DE, O'connor PB, Fahey C, Kenny EM, Terenin IM, Dmitriev SE, Cormican P, Morris DW, Shatsky IN, & Baranov P V. (2015). Translation of 5' leaders is pervasive in genes resistant to eIF2 repression. *ELife*, *4*(4).

Andreux PA, Blanco-Bose W, Ryu D, Burdet F, Ibberson M, Aebischer P, Auwerx J, Singh A, & Rinsch C. (2019). The mitophagy activator urolithin A is safe and induces a molecular signature of improved mitochondrial and cellular health in humans. *Nature Metabolism 2019 1:6*, *1*(6), 595–603.

Antón Z, Landajuela A, Hervás JH, Montes LR, Hernández-Tiedra S, Velasco G, Goñi FM, & Alonso A. (2016). Human Atg8-cardiolipin interactions in mitophagy: Specific properties of LC3B, GABARAPL2 and GABARAP. *Autophagy*, *12*(12), 2386–2403.

Araiso Y, Tsutsumi A, Qiu J, Imai K, Shiota T, Song J, Lindau C, Wenz L-S, Sakaue H, Yunoki K, Kawano S, Suzuki J, Wischnewski M, Schütze C, Ariyama H, Ando T, Becker T, … Endo T. (2019). Structure of the mitochondrial import gate reveals distinct preprotein paths. *Nature*, *575*(7782), 395–401.

Arena G, Gelmetti V, Torosantucci L, Vignone D, Lamorte G, De Rosa P, Cilia E, Jonas EA, & Valente EM. (2013). PINK1 protects against cell death induced by mitochondrial depolarization, by phosphorylating Bcl-xL and impairing its pro-apoptotic cleavage. *Cell Death and Differentiation*, *20*(7), 920–930.

Avendaño-Monsalve MC, Ponce-Rojas JC, & Funes S. (2020). From cytosol to mitochondria: the beginning of a protein journey. *Biological Chemistry*, *401*(6–7), 645–661.

Bakula D, & Scheibye-Knudsen M. (2020). MitophAging: Mitophagy in Aging and Disease. *Frontiers in Cell and Developmental Biology*, *8*.

Becker T, Song J, & Pfanner N. (2019). Versatility of Preprotein Transfer from the Cytosol to Mitochondria. *Trends in Cell Biology*, *29*(7), 534–548.

Benedetti C, Haynes CM, Yang Y, Harding HP, & Ron D. (2006). Ubiquitin-Like Protein 5 Positively Regulates Chaperone Gene Expression in the Mitochondrial Unfolded Protein Response. *Genetics*, *174*(1), 229–239.

Bernardini JP, Lazarou M, & Dewson G. (2017). Parkin and mitophagy in cancer. *Oncogene*, *36*(10), 1315–1327.

Bindea G, Galon J, & Mlecnik B. (2013). CluePedia Cytoscape plugin: pathway insights using integrated experimental and in silico data. *Bioinformatics (Oxford, England)*, *29*(5), 661–663.

Bindea G, Mlecnik B, Hackl H, Charoentong P, Tosolini M, Kirilovsky A, Fridman W-H, Pagès F, Trajanoski Z, & Galon J. (2009). ClueGO: a Cytoscape plug-in to decipher functionally grouped gene ontology and pathway annotation networks. *Bioinformatics (Oxford, England)*, *25*(8), 1091–1093.

Bingol B, Tea JS, Phu L, Reichelt M, Bakalarski CE, Song Q, Foreman O, Kirkpatrick DS, & Sheng M. (2014). The mitochondrial deubiquitinase USP30 opposes parkin-mediated mitophagy. *Nature*, *510*(7505), 370–375.

Bjørkøy G, Lamark T, Brech A, Outzen H, Perander M, Øvervatn A, Stenmark H, & Johansen T. (2005). p62/SQSTM1 forms protein aggregates degraded by autophagy and has a protective effect on huntingtin-induced cell death. *Journal of Cell Biology*, *171*(4), 603–614.

Blum TB, Hahn A, Meier T, Davies KM, & Kühlbrandt W. (2019). Dimers of mitochondrial ATP synthase induce membrane curvature and self-assemble into rows. *Proceedings of the National Academy of Sciences*, *116*(10), 4250–4255.

Bojkova D, Klann K, Koch B, Widera M, Krause D, Ciesek S, Cinatl J, & Münch C. (2020). Proteomics of SARS-CoV-2-infected host cells reveals therapy targets. *Nature 2020 583:7816*, *583*(7816), 469–472.

Bolte S, & Cordelières FP. (2006). A guided tour into subcellular colocalization analysis in light microscopy. *Journal of Microscopy*, *224*(3), 213–232.

Bonora M, Patergnani S, Rimessi A, de Marchi E, Suski JM, Bononi A, Giorgi C, Marchi S, Missiroli S, Poletti F, Wieckowski MR, & Pinton P. (2012). ATP synthesis and storage. *Purinergic Signalling*, *8*(3), 343.

Böttinger L, Oeljeklaus S, Guiard B, Rospert S, Warscheid B, & Becker T. (2015). Mitochondrial heat shock protein (Hsp) 70 and Hsp10 cooperate in the formation of Hsp60 complexes. *The Journal of Biological Chemistry*, *290*(18), 11611–11622.

Bozidis P, Williamson CD, & Colberg-Poley AM. (2007). Isolation of endoplasmic reticulum, mitochondria, and mitochondria-associated membrane fractions from transfected cells and from human cytomegalovirus-infected primary fibroblasts. *Current Protocols in Cell Biology*, *Chapter 3*(1), Unit 3.27.

Branon TC, Bosch JA, Sanchez AD, Udeshi ND, Svinkina T, Carr SA, Feldman JL, Perrimon N, & Ting AY. (2018). Efficient proximity labeling in living cells and organisms with TurboID. *Nature Biotechnology*, *36*(9), 880–898.

Brenner S. (1974). The genetics of Caenorhabditis elegans. *Genetics*, *77*(1), 71–94.

Bukau B, & Horwich AL. (1998). The Hsp70 and Hsp60 Chaperone Machines. *Cell*, *92*(3), 351–366.

Burbulla LF, Fitzgerald JC, Stegen K, Westermeier J, Thost A-KK, Kato H, Mokranjac D, Sauerwald J, Martins LM, Woitalla D, Rapaport D, Riess O, Proikas-Cezanne T, Rasse TM, & Krüger R. (2014). Mitochondrial proteolytic stress induced by loss of mortalin function is rescued by Parkin and PINK1. *Cell Death and Disease*, *5*(4), 1–19.

Burman JL, Pickles S, Wang C, Sekine S, Vargas JNS, Zhang Z, Youle AM, Nezich CL, Wu X, Hammer JA, & Youle RJ. (2017). Mitochondrial fission facilitates the selective mitophagy of protein aggregates. *Journal of Cell Biology*, *216*(10), 3231–3247.

Cakir Z, Funk K, Lauterwasser J, Todt F, Zerbes RM, Oelgeklaus A, Tanaka A, van der Laan M, & Edlich F. (2017). Parkin promotes proteasomal degradation of misregulated BAX. *Journal of Cell Science*, *130*(17), 2903–2913.

Calvo SE, Clauser KR, & Mootha VK. (2016). MitoCarta2.0: an updated inventory of mammalian mitochondrial proteins. *Nucleic Acids Research*, *44*(D1), D1251-7.

Chen Y, Scarcelli V, & Legouis R. (2017). Approaches for Studying Autophagy in Caenorhabditis elegans. *Cells*, *6*(3), 27.

Choglay AA, Chapple JP, Blatch GL, & Cheetham ME. (2001). Identification and characterization of a human mitochondrial homologue of the bacterial co-chaperone GrpE. *Gene*, *267*(1), 125–134.

Chu CT, Ji J, Dagda RK, Jiang JF, Tyurina YY, Kapralov AA, Tyurin VA, Yanamala N, Shrivastava IH, Mohammadyani D, Wang KZQ, Zhu J, Klein-Seetharaman J, Balasubramanian K, Amoscato AA, Borisenko G, Huang Z, … Kagan VE. (2013). Cardiolipin externalization to the outer mitochondrial membrane acts as an elimination signal for mitophagy in neuronal cells. *Nature Cell Biology*, *15*(10), 1197–1205.

Costes S V., Daelemans D, Cho EH, Dobbin Z, Pavlakis G, & Lockett S. (2004). Automatic and quantitative measurement of protein-protein colocalization in live cells. *Biophysical Journal*, *86*(6), 3993–4003.

Couvillion MT, Soto IC, Shipkovenska G, & Churchman LS. (2016). Synchronized mitochondrial and cytosolic translation programs. *Nature*, *533*(7604), 499–503.

Coyne LP, & Chen XJ. (2019). Consequences of inner mitochondrial membrane protein misfolding. *Mitochondrion*, *49*, 46–55.

Craig EA. (2018). Hsp70 at the membrane: driving protein translocation. *BMC Biology*, *16*(1), 11.

Crompton M, Virji S, & Ward JM. (1998). Cyclophilin-D binds strongly to complexes of the voltage-dependent anion channel and the adenine nucleotide translocase to form the permeability transition pore. *European Journal of Biochemistry*, *258*(2), 729–735.

Crowley LC, Christensen ME, & Waterhouse NJ. (2016). Measuring Mitochondrial Transmembrane Potential by TMRE Staining. *Cold Spring Harbor Protocols*, *2016*(12).

De Los Rios P, Ben-Zvi A, Slutsky O, Azem A, & Goloubinoff P. (2006). Hsp70 chaperones accelerate protein translocation and the unfolding of stable protein aggregates by entropic pulling. *Proceedings of the National Academy of Sciences of the United States of America*, *103*(16), 6166–6171.

Demine S, Renard P, & Arnould T. (2019). Mitochondrial Uncoupling: A Key Controller of Biological Processes in Physiology and Diseases. *Cells*, *8*(8).

Deshwal S, Fiedler KU, & Langer T. (2020). Mitochondrial Proteases: Multifaceted Regulators of Mitochondrial Plasticity. *Annual Review of Biochemistry*, *89*, 501–528.

Dey S, Baird TD, Zhou D, Palam LR, Spandau DF, & Wek RC. (2010). Both Transcriptional Regulation and Translational Control of ATF4 Are Central to the Integrated Stress Response. *The Journal of Biological Chemistry*, *285*(43), 33165.

Di Maio R, Barrett PJ, Hoffman EK, Barrett CW, Zharikov A, Borah A, Hu X, McCoy J, Chu CT, Burton EA, Hastings TG, & Greenamyre JT. (2016). α-Synuclein binds to TOM20 and inhibits mitochondrial protein import in Parkinson's disease. *Science Translational Medicine*, *8*(342), 342ra78.

Dikic I, & Elazar Z. (2018). Mechanism and medical implications of mammalian autophagy. *Nature Reviews Molecular Cell Biology*, *19*(6), 349–364.

Du F, Yu Q, Yan S, Hu G, Lue L-F, Walker DG, Wu L, Yan SF, Tieu K, & Yan SS. (2017). PINK1 signalling rescues amyloid pathology and mitochondrial dysfunction in Alzheimer's disease. *Brain : A Journal of Neurology*, *140*(12), 3233–3251.

Duchen MR, & Biscoe TJ. (1992). Relative mitochondrial membrane potential and [Ca2+]i in type I cells isolated from the rabbit carotid body. *The Journal of Physiology*, *450*(1), 33.

Dudek J. (2017). Role of Cardiolipin in Mitochondrial Signaling Pathways. *Frontiers in Cell and Developmental Biology*, *5*(SEP), 90.

Dutta P, Odedra D, & Pohl C. (2019). Planar asymmetries in the C. Elegans embryo emerge by differential retention of aPARs at cell-cell contacts. *Frontiers in Cell and Developmental Biology*, *7*(SEP), 209.

Esselun C, Theyssen E, & Eckert GP. (2021). Effects of Urolithin A on Mitochondrial Parameters in a Cellular Model of Early Alzheimer Disease. *International Journal of Molecular Sciences*, *22*(15).

Fang EF, Hou Y, Palikaras K, Adriaanse BA, Kerr JS, Yang B, Lautrup S, Hasan-Olive MM, Caponio D, Dan X, Rocktäschel P, Croteau DL, Akbari M, Greig NH, Fladby T, Nilsen H, Cader MZ, … Bohr VA. (2019). Mitophagy inhibits amyloid-β and tau pathology and reverses cognitive deficits in models of Alzheimer's disease. *Nature Neuroscience 2019 22:3*, *22*(3), 401–412.

Fessler E, Eckl E-MM, Schmitt S, Mancilla IA, Meyer-Bender MF, Hanf M, Philippou-Massier J, Krebs S, Zischka H, & Jae LT. (2020). A pathway coordinated by DELE1 relays mitochondrial stress to the cytosol. *Nature*, *579*(7799), 433–437.

Fiesel FC, James ED, Hudec R, Springer W, Fiesel FC, James ED, Hudec R, Springer W, Fiesel FC, James ED, & Springer RH and W. (2017). Mitochondrial targeted HSP90 inhibitor Gamitrinib-TPP (G-TPP) induces PINK1/Parkin-dependent mitophagy. *Oncotarget*, *8*(63), 106233–106248.

Finger Y, & Riemer J. (2020). Protein import by the mitochondrial disulfide relay in higher eukaryotes. *Biological Chemistry*, *401*(6–7), 749–763.

Fiorese CJ, Schulz AM, Lin YF, Rosin N, Pellegrino MW, & Haynes CM. (2016). The Transcription Factor ATF5 Mediates a Mammalian Mitochondrial UPR. *Current Biology*.

Fivenson EM, Lautrup S, Sun N, Scheibye-Knudsen M, Stevnsner T, Nilsen H, Bohr VA, & Fang EF. (2017). Mitophagy in neurodegeneration and aging. *Neurochemistry International*.

Franco-Iborra S, Plaza-Zabala A, Montpeyo M, Sebastian D, Vila M, & Martinez-Vicente M. (2021). Mutant HTT (huntingtin) impairs mitophagy in a cellular model of Huntington disease. *Autophagy*, *17*(3), 672–689.

Frazier AE, Dudek J, Guiard B, Voos W, Li Y, Lind M, Meisinger C, Geissler A, Sickmann A, Meyer HE, Bilanchone V, Cumsky MG, Truscott KN, Pfanner N, & Rehling P. (2004). *Pam16 has an essential role in the mitochondrial protein import motor*. *11*(3), 226–233.

Fu M, St-Pierre P, Shankar J, Wang PTC, Joshi B, & Nabi IR. (2013). Regulation of mitophagy by the Gp78 E3 ubiquitin ligase. *Molecular Biology of the Cell*, *24*(8), 1153–1162.

Fujiwara M, Tian L, Le PT, DeMambro VE, Becker KA, Rosen CJ, & Guntur AR. (2019). The mitophagy receptor Bcl-2-like protein 13 stimulates adipogenesis by regulating mitochondrial oxidative phosphorylation and apoptosis in mice. *The Journal of Biological Chemistry*, *294*(34), 12683–12694.

Galloway CA, Lee H, & Yoon Y. (2012). Mitochondrial morphology – Emerging role in bioenergetics. *Free Radical Biology & Medicine*, *53*(12), 2218–2228.

Gao F, Zhang Y, Hou X, Tao Z, Ren H, & Wang G. (2020). Dependence of PINK1 accumulation on mitochondrial redox system. *Aging Cell*, *19*(9), e13211.

Garriga M. (2019). Outstanding questions in mitophagy. *Journal of Molecular Biology*, *432*(1), 206–230.

Gómez-Rubio V. (2017). ggplot2 - Elegant Graphics for Data Analysis (2nd Edition). *Journal of Statistical Software*, *77*(Book Review 2).

Goswami AV, Chittoor B, & D'Silva P. (2010). Understanding the functional interplay between mammalian mitochondrial Hsp70 chaperone machine components. *Journal of Biological Chemistry*, *285*(25), 19472–19482.

Green DR, & Kroemer G. (2004). The pathophysiology of mitochondrial cell death. *Science (New York, N.Y.)*, *305*(5684), 626–629.

Greene AW, Grenier K, Aguileta MA, Muise S, Farazifard R, Haque ME, McBride HM, Park DS, & Fon EA. (2012). Mitochondrial processing peptidase regulates PINK1 processing, import and Parkin recruitment. *EMBO Reports*, *13*(4), 378–385.

Guo Xiaoyan, Aviles G, Liu Y, Tian R, Unger BA, Lin Y-HT, Wiita AP, Xu K, Correia MA, & Kampmann M. (2020). Mitochondrial stress is relayed to the cytosol by an OMA1-DELE1-HRI pathway. *Nature*, *579*(7799), 427–432.

Guo Xing, & Qi X. (2017). VCP cooperates with UBXD1 to degrade mitochondrial outer membrane protein MCL1 in model of Huntington's disease. *Biochimica et Biophysica Acta. Molecular Basis of Disease*, *1863*(2), 552–559.

Hamacher-Brady A, & Brady NR. (2015). Mitophagy programs: mechanisms and physiological implications of mitochondrial targeting by autophagy. *Cellular and Molecular Life Sciences 2015 73:4*, *73*(4), 775–795.

Hara Y, Yanatori I, Tanaka A, Kishi F, Lemasters JJ, Nishina S, Sasaki K, & Hino K. (2020). Iron loss triggers mitophagy through induction of mitochondrial ferritin. *EMBO Reports*, *21*(11), e50202.

Hart T, Chandrashekhar M, Aregger M, Steinhart Z, Brown KR, MacLeod G, Mis M, Zimmermann M, Fradet-Turcotte A, Sun S, Mero P, Dirks P, Sidhu S, Roth FP, Rissland OS, Durocher D, Angers S, & Moffat J. (2015). High-Resolution CRISPR Screens Reveal Fitness Genes and Genotype-Specific Cancer Liabilities. *Cell*, *163*(6), 1515–1526.

Hasson SA, Kane LA, Yamano K, Huang C-H, Sliter DA, Buehler E, Wang C, Heman-Ackah SM, Hessa T, Guha R, Martin SE, & Youle RJ. (2013). High-content genome-wide RNAi screens identify regulators of parkin upstream of mitophagy. *Nature*, *504*(7479), 291–295.

Haynes CM, Petrova K, Benedetti C, Yang Y, & Ron D. (2007). ClpP Mediates Activation of a Mitochondrial Unfolded Protein Response in C. elegans. *Developmental Cell*, *13*(4), 467–480.

Haynes CM, Yang Y, Blais SP, Neubert TA, & Ron D. (2010). The matrix peptide exporter HAF-1 signals a mitochondrial UPR by activating the transcription factor ZC376.7 in C. elegans. *Molecular Cell*, *37*(4), 529–540.

Hell K, Neupert W, & Stuart RA. (2001). Oxa1p acts as a general membrane insertion machinery for proteins encoded by mitochondrial DNA. *The EMBO Journal*, *20*(6), 1281.

Heo JM, Ordureau A, Paulo JA, Rinehart J, & Harper JW. (2015). The PINK1-PARKIN Mitochondrial Ubiquitylation Pathway Drives a Program of OPTN/NDP52 Recruitment and TBK1 Activation to Promote Mitophagy. *Molecular Cell*, *60*(1), 7–20.

Hinnebusch AG, Ivanov IP, & Sonenberg N. (2016). Translational control by 5'-untranslated regions of eukaryotic mRNAs. *Science*, *352*(6292), 1413–1416.

Höhr AIC, Straub SP, Warscheid B, Becker T, & Wiedemann N. (2015). Assembly of β-barrel proteins in the mitochondrial outer membrane. *Biochimica et Biophysica Acta (BBA) - Molecular Cell Research*, *1853*(1), 74–88.

Horwich AL, Fenton WA, Chapman E, & Farr GW. (2007). Two families of chaperonin: physiology and mechanism. *Annual Review of Cell and Developmental Biology*, *23*, 115–145.

Hoshino A, Wang W-J jia, Wada S, McDermott-Roe C, Evans CS, Gosis B, Morley MP, Rathi KS, Li J, Li K, Yang S, McManus MJ, Bowman C, Potluri P, Levin M, Damrauer S, Wallace DC, … Arany Z. (2019). The ADP/ATP translocase drives mitophagy independent of nucleotide exchange. *Nature*, *575*(7782), 375–379.

Hurst S, Baggett A, Csordas G, & Sheu S-S. (2019). SPG7 targets the m-AAA protease complex to process MCU for uniporter assembly, Ca2+ influx, and regulation of mitochondrial permeability transition pore opening. *The Journal of Biological Chemistry*, *294*(28), 10807–10818.

Igarashi R, Yamashita S ichi, Yamashita T, Inoue K, Fukuda T, Fukuchi T, & Kanki T. (2020). Gemcitabine induces Parkin-independent mitophagy through mitochondrial-resident E3 ligase MUL1-mediated stabilization of PINK1. *Scientific Reports*, *10*(1), 1–11.

Ishihara N, Fujita Y, Oka T, & Mihara K. (2006). Regulation of mitochondrial morphology through proteolytic cleavage of OPA1. *The EMBO Journal*, *25*(13), 2966.

Jackson KL, Lin W-L, Miriyala S, Dayton RD, Panchatcharam M, McCarthy KJ, Castanedes-Casey M, Dickson DW, & Klein RL. (2017). p62 Pathology Model in the Rat Substantia Nigra with Filamentous Inclusions and Progressive Neurodegeneration. *PLoS ONE*, *12*(1).

Jia L, Dienhart MK, & Stuart RA. (2007). Oxa1 Directly Interacts with Atp9 and Mediates Its Assembly into the Mitochondrial F1Fo-ATP Synthase Complex. *Molecular Biology of the Cell*, *18*(5), 1897.

Jian F, Chen D, Chen L, Yan C, Lu B, Zhu Y, Chen S, Shi A, Chan DC, & Song Z. (2018). Sam50 Regulates PINK1-Parkin-Mediated Mitophagy by Controlling PINK1 Stability and Mitochondrial Morphology. *Cell Reports*, *23*(10), 2989–3005.

Jin-Feng Zhao CERGFGASW and IGG, Rodger CE, Allen GFG, Weidlich S, & Ganley IG. (2020). HIF1α-dependent mitophagy facilitates cardiomyoblast differentiation. *Cell Stress*, *4*(5), 99.

Jin SM, Lazarou M, Wang C, Kane LA, Narendra DP, & Youle RJ. (2010). Mitochondrial membrane potential regulates PINK1 import and proteolytic destabilization by PARL. *The Journal of Cell Biology*, *191*(5), 933–942.

Jin SM, & Youle RJ. (2013). The accumulation of misfolded proteins in the mitochondrial matrix is sensed by PINK1 to induce PARK2/Parkin-mediated mitophagy of polarized mitochondria. *Autophagy*, *9*(11), 1750–1757.

Kamath RS, & Ahringer J. (2003). Genome-wide RNAi screening in Caenorhabditis elegans. *Methods (San Diego, Calif.)*, *30*(4), 313–321.

Kang BH, Siegelin MD, Plescia J, Raskett CM, Garlick DS, Dohi T, Lian JB, Stein GS, Languino LR, & Altieri DC. (2010). Preclinical characterization of mitochondria-targeted small molecule Hsp90 inhibitors, gamitrinibs, in advanced prostate cancer. *Clinical Cancer Research*, *16*(19), 4779–4788.

Kang Y, Fielden LF, & Stojanovski D. (2018). Mitochondrial protein transport in health and disease. *Seminars in Cell & Developmental Biology*, *76*, 142–153.

Karsli-Uzunbas G, Guo JY, Price S, Teng X, Laddha S V., Khor S, Kalaany NY, Jacks T, Chan CS, Rabinowitz JD, & White E. (2014). Autophagy is required for glucose homeostasis and lung tumor maintenance. *Cancer Discovery*, *4*(8), 914–927.

Kaspar S, Oertlin C, Szczepanowska K, Kukat A, Senft K, Lucas C, Brodesser S, Hatzoglou M, Larsson O, Topisirovic I, & Trifunovic A. (2021). Adaptation to mitochondrial stress requires CHOP-directed tuning of ISR. *Science Advances*, *7*(22), 971–997.

Katiyar A, Fujimoto M, Tan K, Kurashima A, Srivastava P, Okada M, Takii R, & Nakai A. (2020). HSF1 is required for induction of mitochondrial chaperones during the mitochondrial unfolded protein response. *FEBS Open Bio*, *10*(6), 1135–1148.

Kazlauskaite A, Martínez-Torres RJ, Wilkie S, Kumar A, Peltier J, Gonzalez A, Johnson C, Zhang J, Hope AG, Peggie M, Trost M, Aalten DM, Alessi DR, Prescott AR, Knebel A, Walden H, & Muqit MM. (2015). Binding to serine 65-phosphorylated ubiquitin primes Parkin for optimal PINK 1-dependent phosphorylation and activation . *EMBO Reports*, *16*(8), 939–954.

Kennedy EP, & Lehninger AL. (1949). Oxidation of fatty acids and tricarboxylic acid cycle intermediates by isolated rat liver mitochondria. *The Journal of Biological Chemistry*, *179*(2), 957–972.

Klann K, & Münch C. (2020). Instrument Logic Increases Identifications during Multiplexed Translatome Measurements. *Analytical Chemistry*, *92*(12), 8041–8045.

Klann K, Tascher G, & Münch C. (2020). Functional Translatome Proteomics Reveal Converging and Dose-Dependent Regulation by mTORC1 and eIF2α. *Molecular Cell*, *77*(4), 913-925.e4.

Komatsu M, Waguri S, Chiba T, Murata S, Iwata J, Tanida I, Ueno T, Koike M, Uchiyama Y, Kominami E, & Tanaka K. (2006). Loss of autophagy in the central nervous system causes neurodegeneration in mice. *Nature 2006 441:7095*, *441*(7095), 880–884.

König T, Tröder SE, Bakka K, Korwitz A, Richter-Dennerlein R, Lampe PA, Patron M, Mühlmeister M, Guerrero-Castillo S, Brandt U, Decker T, Lauria I, Paggio A, Rizzuto R, Rugarli EI, De Stefani D, & Langer T. (2016). The m-AAA Protease Associated with Neurodegeneration Limits MCU Activity in Mitochondria. *Molecular Cell*, *64*(1), 148–162.

Kraus F, Roy K, Pucadyil TJ, & Ryan MT. (2021, February 4). Function and regulation of the divisome for mitochondrial fission. *Nature*, Vol. 590, pp. 57–66.

Kulak NA, Pichler G, Paron I, Nagaraj N, & Mann M. (2014). Minimal, encapsulated proteomic-sample processing applied to copy-number estimation in eukaryotic cells. *Nature Methods*, *11*(3), 319–324.

Kumar S. (2007). Caspase function in programmed cell death. *Cell Death and Differentiation*, *14*(1), 32–43.

Kunová N, Ondrovièová G, Bauer JA, Bellová J, Ambro L, Martináková L, Kotrasová V, Kutejová E, & Pevala V. (2017). The role of Lon-mediated proteolysis in the dynamics of mitochondrial nucleic acid-protein complexes. *Scientific Reports*.

Langmead B, & Salzberg SL. (2012). Fast gapped-read alignment with Bowtie 2. *Nature Methods*, *9*(4), 357–359.

Lazarou M, Sliter DA, Kane LA, Sarraf SA, Wang C, Burman JL, Sideris DP, Fogel AI, & Youle RJ. (2015). The ubiquitin kinase PINK1 recruits autophagy receptors to induce mitophagy. *Nature*, *524*(7565), 309–314.

Lee J, Giordano S, & Zhang J. (2012). Autophagy, mitochondria and oxidative stress: cross-talk and redox signalling. *The Biochemical Journal*, *441*(2), 523–540.

Lee YG, Kim HW, Nam Y, Shin KJ, Lee YJ, Park DH, Rhee HW, Seo JK, & Chae YC. (2021). LONP1 and ClpP cooperatively regulate mitochondrial proteostasis for cancer cell survival. *Oncogenesis*, *10*(2), 1–14.

Lesanpezeshki L, Hewitt JE, Laranjeiro R, Antebi A, Driscoll M, Szewczyk NJ, Blawzdziewicz J, Lacerda CMR, & Vanapalli SA. (2019). Pluronic gel-based burrowing assay for rapid assessment of neuromuscular health in C. elegans. *Scientific Reports*, *9*(1), 15246.

Lesnik C, Cohen Y, Atir-Lande A, Schuldiner M, & Arava Y. (2014). OM14 is a mitochondrial receptor for cytosolic ribosomes that supports co-translational import into mitochondria. *Nature Communications 2014 5:1*, *5*(1), 1–11.

Levine B, & Kroemer G. (2019). Biological Functions of Autophagy Genes: A Disease Perspective. *Cell*, *176*(1–2), 11–42.

Li P, Nijhawan D, Budihardjo I, Srinivasula SM, Ahmad M, Alnemri ES, & Wang X. (1997). Cytochrome c and dATP-Dependent Formation of Apaf-1/Caspase-9 Complex Initiates an Apoptotic Protease Cascade. *Cell*, *91*(4), 479–489.

Li W, Xu H, Xiao T, Cong L, Love MI, Zhang F, Irizarry RA, Liu JS, Brown M, & Liu XS. (2014). MAGeCK enables robust identification of essential genes from genome-scale CRISPR/Cas9 knockout screens. *Genome Biology*, *15*(12), 554.

Liberek K, Marszalek J, Ang D, Georgopoulos C, & Zylicz M. (1991). Escherichia coli DnaJ and GrpE heat shock proteins jointly stimulate ATPase activity of DnaK. *Proceedings of the National Academy of Sciences of the United States of America*, *88*(7), 2874–2878.

Lodish H, Berk A, Zipursky SL, Matsudaira P, Baltimore D, & Darnell J. (2000). Electron Transport and Oxidative Phosphorylation. *Molecular Cell Biology*, (4th edition).

Lokireddy S, Wijesoma IW, Teng S, Bonala S, Gluckman PD, McFarlane C, Sharma M, & Kambadur R. (2012). The ubiquitin ligase Mul1 induces mitophagy in skeletal muscle in response to muscle-wasting stimuli. *Cell Metabolism*, *16*(5), 613–624.

Manders EMM, Verbeek FJ, & Aten JA. (1993). Measurement of co-localization of objects in dual-colour confocal images. *Journal of Microscopy*, *169*(3), 375–382.

Marchi S, Patergnani S, & Pinton P. (2014). The endoplasmic reticulum–mitochondria connection: One touch, multiple functions. *Biochimica et Biophysica Acta (BBA) - Bioenergetics*, *1837*(4), 461–469.

Marinković M, & Novak I. (2015). The Role of Autophagy Receptors in Mitophagy. *Autophagy: Cancer, Other Pathologies, Inflammation, Immunity, Infection, and Aging*, *6*, 243–256.

Martin J, Mahlke K, & Pfanners N. (1991). Role of an energized inner membrane in mitochondrial protein import. Delta psi drives the movement of presequences. *Journal of Biological Chemistry*, *266*(27), 18051–18057.

Martin M. (2011). Cutadapt removes adapter sequences from high-throughput sequencing reads. *EMBnet.Journal*, *17*(1), 10.

Martin W, & Mentel M. (2010). Origin of Mitochondria | Learn Science at Scitable. *Nature Education*, *3*(9), 58.

Martinez-Vicente M. (2017). Neuronal Mitophagy in Neurodegenerative Diseases. *Frontiers in Molecular Neuroscience*, *10*, 64.

Martinez-Vicente M, Talloczy Z, Wong E, Tang G, Koga H, Kaushik S, de Vries R, Arias E, Harris S, Sulzer D, & Cuervo AM. (2010). Cargo recognition failure is responsible for inefficient autophagy in Huntington's disease. *Nature Neuroscience 2010 13:5*, *13*(5), 567–576.

Martinus RD, Garth GP, Webster TL, Cartwright P, Naylor DJ, Høj PB, & Hoogenraad NJ. (1996). Selective induction of mitochondrial chaperones in response to loss of the mitochondrial genome. *European Journal of Biochemistry*, *240*(1), 98–103.

Matsushima Y, Goto Y, & Kaguni LS. (2010). Mitochondrial Lon protease regulates mitochondrial DNA copy number and transcription by selective degradation of mitochondrial transcription factor A (TFAM). *Proceedings of the National Academy of Sciences of the United States of America*, *107*(43), 18410–18415.

Mauvezin C, & Neufeld TP. (2015). Bafilomycin A1 disrupts autophagic flux by inhibiting both V-ATPase-dependent acidification and Ca-P60A/SERCA-dependent autophagosome-lysosome fusion. *Autophagy*, *11*(8), 1437–1438.

McWilliams TG, Prescott AR, Montava-Garriga L, Ball G, Singh F, Barini E, Muqit MMK, Brooks SP, & Ganley IG. (2018). Basal Mitophagy Occurs Independently of PINK1 in Mouse Tissues of High Metabolic Demand. *Cell Metabolism*, *27*(2), 439.

Meier F, Brunner A-D, Koch S, Koch H, Lubeck M, Krause M, Goedecke N, Decker J, Kosinski T, Park MA, Bache N, Hoerning O, Cox J, Räther O, & Mann M. (2018). Online Parallel Accumulation-Serial Fragmentation (PASEF) with a Novel Trapped Ion Mobility Mass Spectrometer. *Molecular & Cellular Proteomics : MCP*, *17*(12), 2534–2545.

Meyer N, Zielke S, Michaelis JB, Linder B, Warnsmann V, Rakel S, Osiewacz HD, Fulda S, Mittelbronn M, Münch C, Behrends C, & Kögel D. (2018). AT 101 induces early mitochondrial dysfunction and HMOX1 (heme oxygenase 1) to trigger mitophagic cell death in glioma cells. *Autophagy*, *14*(10), 1693–1709.

Miyata N, Tang Z, Conti MA, Johnson ME, Douglas CJ, Hasson SA, Damoiseaux R, Chang CEA, & Koehler CM. (2017). Adaptation of a Genetic Screen Reveals an Inhibitor for Mitochondrial Protein Import Component Tim44. *Journal of Biological Chemistry*, *292*(13), 5429–5442.

Mokranjac D, Sichting M, Popov-Celeketić D, Mapa K, Gevorkyan-Airapetov L, Zohary K, Hell K, Azem A, Neupert W, Popov-ČeleketíC D, Mapa K, Gevorkyan-Airapetov L, Zohary K, Hell K, Azem A, Neupert W, Popov-Celeketić D, … Neupert W. (2009). Role of tim50 in the transfer of precursor proteins from the outer to the inner membrane of mitochondria. *Molecular Biology of the Cell*, *20*(5), 1400–1407.

Mossmann D, Meisinger C, & Vögtle F-NN. (2012). Processing of mitochondrial presequences. *Biochimica et Biophysica Acta*, *1819*(9–10), 1098–1106.

Münch C, & Harper JW. (2016). Mitochondrial unfolded protein response controls matrix pre-RNA processing and translation. *Nature*, *534*(7609), 710–713.

Murakawa T, Yamaguchi O, Hashimoto A, Hikoso S, Takeda T, Oka T, Yasui H, Ueda H, Akazawa Y, Nakayama H, Taneike M, Misaka T, Omiya S, Shah AM, Yamamoto A, Nishida K, Ohsumi Y, … Otsu K. (2015). Bcl-2-like protein 13 is a mammalian Atg32 homologue that mediates mitophagy and mitochondrial fragmentation. *Nature Communications*, *6*, 7527.

Narendra D, Tanaka A, Suen D-FF, & Youle RJ. (2008). Parkin is recruited selectively to impaired mitochondria and promotes their autophagy. *Journal of Cell Biology*, *183*(5), 795–803.

Narendra DP, Jin SM, Tanaka A, Suen D-FF, Gautier CA, Shen J, Cookson MR, & Youle RJ. (2010). PINK1 is selectively stabilized on impaired mitochondria to activate Parkin. *PLoS Biology*, *8*(1), e1000298.

Nargund AM, Fiorese CJ, Pellegrino MW, Deng P, & Haynes CM. (2015). Mitochondrial and nuclear accumulation of the transcription factor ATFS-1 promotes OXPHOS recovery during the UPR(mt). *Molecular Cell*, *58*(1), 123–133.

Nargund AM, Pellegrino MW, Fiorese CJ, Baker BM, & Haynes CM. (2012). Mitochondrial import efficiency of ATFS-1 regulates mitochondrial UPR activation. *Science (New York, N.Y.)*, *337*(6094), 587–590.

Nicolas E, Tricarico R, Savage M, Golemis EA, & Hall MJ. (2019). Disease-Associated Genetic Variation in Human Mitochondrial Protein Import. *American Journal of Human Genetics*, *104*(5), 784–801.

Novoa I, Zhang Y, Zeng H, Jungreis R, Harding HP, & Ron D. (2003). Stress-induced gene expression requires programmed recovery from translational repression. *The EMBO Journal*, *22*(5), 1180.

Ohsumi Y. (2014). Historical landmarks of autophagy research. *Cell Research*, *24*(1), 9.

Ordureau A, Sarraf SA, Duda DM, Heo JM, Jedrychowski MP, Sviderskiy VO, Olszewski JL, Koerber JT, Xie T, Beausoleil SA, Wells JA, Gygi SP, Schulman BA, & Harper JW. (2014). Quantitative Proteomics Reveal a Feedforward Mechanism for Mitochondrial PARKIN Translocation and Ubiquitin Chain Synthesis. *Molecular Cell*, *56*(3), 360–375.

Orvedahl A, Sumpter R, Xiao G, Ng A, Zou Z, Tang Y, Narimatsu M, Gilpin C, Sun Q, Roth M, Forst C V., Wrana JL, Zhang YE, Luby-Phelps K, Xavier RJ, Xie Y, & Levine B. (2011). Image-based genome-wide siRNA screen identifies selective autophagy factors. *Nature*, *480*(7375), 113–117.

Ostermann J, Horwich AL, Neupert W, & Hartl FU. (1989). Protein folding in mitochondria requires complex formation with hsp60 and ATP hydrolysis. *Nature*, *341*(6238), 125–130.

Padman BS, Nguyen TN, Uoselis L, Skulsuppaisarn M, Nguyen LK, & Lazarou M. (2019). LC3/GABARAPs drive ubiquitin-independent recruitment of Optineurin and NDP52 to amplify mitophagy. *Nature Communications*, *10*(1), 408.

Palam LR, Baird TD, & Wek RC. (2011). Phosphorylation of eIF2 Facilitates Ribosomal Bypass of an Inhibitory Upstream ORF to Enhance CHOP Translation. *Journal of Biological Chemistry*, *286*(13), 10939–10949.

Palikaras K, Lionaki E, & Tavernarakis N. (2019). Mitophagy Dynamics in Caenorhabditis elegans. *Methods in Molecular Biology (Clifton, N.J.)*, *1880*, 655–668.

Pankiv S, Clausen TH, Lamark T, Brech A, Bruun J-A, Outzen H, Øvervatn A, Bjørkøy G, Johansen T, S P, TH C, T L, A B, JA B, H O, A Ø, G B, & T J. (2007). 62/SQSTM1 Binds Directly to Atg8/LC3 to Facilitate Degradation of Ubiquitinated Protein Aggregates by Autophagy. *The Journal of Biological Chemistry*, *282*(33), 24131–24145.

Paul BT, Manz DH, Torti FM, & Torti S V. (2017, January 2). Mitochondria and Iron: current questions. *Expert Review of Hematology*, Vol. 10, pp. 65–79. NIH Public Access.

Pereira J, & Lupas AN. (2018). The Origin of Mitochondria-Specific Outer Membrane β-Barrels from an Ancestral Bacterial Fragment. *Genome Biology and Evolution*, *10*(10), 2759–2765.

Perry SW, Norman JP, Barbieri J, Brown EB, & Gelbard HA. (2011). Mitochondrial membrane potential probes and the proton gradient: a practical usage guide. *BioTechniques*, *50*(2), 98–115.

Pfanner N, Warscheid B, & Wiedemann N. Mitochondrial proteins: from biogenesis to functional networks. , 20 Nature Reviews Molecular Cell Biology § (2019).

Poston CN, Krishnan SC, & Bazemore-Walker CR. (2013). In-depth proteomic analysis of mammalian mitochondria-associated membranes (MAM). *Journal of Proteomics*, *79*, 219–230.

Potting C, Crochemore C, Moretti F, Nigsch F, Schmidt I, Manneville C, Carbone W, Knehr J, DeJesus R, Lindeman A, Maher R, Russ C, McAllister G, Reece-Hoyes JS, Hoffman GR, Roma G, Müller M, … Helliwell SB. (2018). Genome-wide CRISPR screen for PARKIN regulators reveals transcriptional repression as a determinant of mitophagy. *Proceedings of the National Academy of Sciences of the United States of America*, *115*(2), E180–E189.

Potting C, Tatsuta T, König T, Haag M, Wai T, Aaltonen MJ, & Langer T. (2013). TRIAP1/PRELI complexes prevent apoptosis by mediating intramitochondrial transport of phosphatidic acid. *Cell Metabolism*, *18*(2), 287–295.

Priesnitz C, & Becker T. (2018). Pathways to balance mitochondrial translation and protein import. *Genes & Development*, *32*(19–20), 1285–1296.

Quirós PM, Prado MA, Zamboni N, D'Amico D, Williams RW, Finley D, Gygi SP, & Auwerx J. (2017). Multi-omics analysis identifies ATF4 as a key regulator of the mitochondrial stress response in mammals. *The Journal of Cell Biology*, *216*(7), 2027–2045.

Rasool S, Soya N, Truong L, Croteau N, Lukacs GL, & Trempe J. (2018). PINK1 autophosphorylation is required for ubiquitin recognition. *EMBO Reports*, *19*(4).

Rath S, Sharma R, Gupta R, Ast T, Chan C, Durham TJ, Goodman RP, Grabarek Z, Haas ME, Hung WHW, Joshi PR, Jourdain AA, Kim SH, Kotrys A V., Lam SS, McCoy JG, Meisel JD, … Mootha VK. (2021). MitoCarta3.0: an updated mitochondrial proteome now with sub-organelle localization and pathway annotations. *Nucleic Acids Research*, *49*(D1), D1541–D1547.

Redza-Dutordoir M, & Averill-Bates DA. (2016). Activation of apoptosis signalling pathways by reactive oxygen species. *Biochimica et Biophysica Acta*, *1863*(12), 2977–2992.

Richter F, Dennerlein S, Nikolov M, Jans DC, Naumenko N, Aich A, MacVicar T, Linden A, Jakobs S, Urlaub H, Langer T, & Rehling P. (2019). ROMO1 is a constituent of the human presequence translocase required for YME1L protease import. *The Journal of Cell Biology*, *218*(2), 598–614.

Riggs CL, Kedersha N, Ivanov P, & Anderson P. (2020). Mammalian stress granules and P bodies at a glance. *Journal of Cell Science*, *133*(16).

Rockel JS, & Kapoor M. (2016). Autophagy: controlling cell fate in rheumatic diseases. *Nature Reviews Rheumatology 2016 12:9*, *12*(9), 517–531.

Roger AJ, Muñoz-Gómez SA, & Kamikawa R. (2017). The Origin and Diversification of Mitochondria. *Current Biology : CB*, *27*(21), R1177–R1192.

Rohani M, Razmeh S, Shahidi GA, & Orooji M. (2018). A Pilot Trial of Deferiprone in Pantothenate Kinase-Associated Neurodegeneration Patients. *Neurology International 2017, Vol. 9, Pages 79-81*, *9*(4), 79–81.

Ross CA, & Poirier MA. (2004). Protein aggregation and neurodegenerative disease. *Nature Medicine*, *10*(7), S10.

Rual J-F, Ceron J, Koreth J, Hao T, Nicot A-S, Hirozane-Kishikawa T, Vandenhaute J, Orkin SH, Hill DE, van den Heuvel S, & Vidal M. (2004). Toward improving Caenorhabditis elegans phenome mapping with an ORFeome-based RNAi library. *Genome Research*, *14*(10B), 2162–2168.

Ryu D, Mouchiroud L, Andreux PA, Katsyuba E, Moullan N, Nicolet-Dit-Félix AA, Williams EG, Jha P, Lo Sasso G, Huzard D, Aebischer P, Sandi C, Rinsch C, & Auwerx J. (2016). Urolithin A induces mitophagy and prolongs lifespan in C. elegans and increases muscle function in rodents. *Nature Medicine 2016 22:8*, *22*(8), 879–888.

Sarraf SA, Shah H V., Kanfer G, Pickrell AM, Holtzclaw LA, Ward ME, & Youle RJ. (2020). Loss of TAX1BP1-Directed Autophagy Results in Protein Aggregate Accumulation in the Brain. *Molecular Cell*, *80*(5), 779-795.e10.

Sauvé V, Sung G, Soya N, Kozlov G, Blaimschein N, Miotto LS, Trempe J-F, Lukacs GL, & Gehring K. (2018). Mechanism of parkin activation by phosphorylation. *Nature Structural & Molecular Biology 2018 25:7*, *25*(7), 623–630.

Schäfer JA, Bozkurt S, Michaelis JB, Klann K, & Münch C. (2022). Global mitochondrial protein import proteomics reveal distinct regulation by translation and translocation machinery. *Molecular Cell*, *82*(2), 435-446.e7.

Schmidt O, Pfanner N, & Meisinger C. (2010). Mitochondrial protein import: from proteomics to functional mechanisms. *Nature Reviews. Molecular Cell Biology*, *11*(9), 655–667.

Schulz C, Lytovchenko O, Melin J, Chacinska A, Guiard B, Neumann P, Ficner R, Jahn O, Schmidt B, & Rehling P. (2011). Tim50's presequence receptor domain is essential for signal driven transport across the TIM23 complex. *Journal of Cell Biology*, *195*(4), 643–656.

Schulz C, & Rehling P. (2014). Remodelling of the active presequence translocase drives motor-dependent mitochondrial protein translocation. *Nature Communications*, *5*, 4349.

Schulz C, Schendzielorz A, & Rehling P. (2015). Unlocking the presequence import pathway. *Trends in Cell Biology*, *25*(5), 265–275.

Shaltouki A, Hsieh CH, Kim MJ, & Wang X. (2018). Alpha-synuclein delays mitophagy and targeting Miro rescues neuron loss in Parkinson's models. *Acta Neuropathologica*, *136*(4), 607–620.

Shamas-Din A, Brahmbhatt H, Leber B, & Andrews DW. (2011). BH3-only proteins: Orchestrators of apoptosis. *Biochimica et Biophysica Acta (BBA) - Molecular Cell Research*, *1813*(4), 508–520.

Shang L, Chen S, Du F, Li S, Zhao L, & Wang X. (2011). Nutrient starvation elicits an acute autophagic response mediated by Ulk1 dephosphorylation and its subsequent dissociation from AMPK. *Proceedings of the National Academy of Sciences of the United States of America*, *108*(12), 4788–4793.

Shannon P, Markiel A, Ozier O, Baliga NS, Wang JT, Ramage D, Amin N, Schwikowski B, & Ideker T. (2003). Cytoscape: a software environment for integrated models of biomolecular interaction networks. *Genome Research*, *13*(11), 2498–2504.

Shetty T, Sishtla K, Park B, Repass MJ, & Corson TW. (2020). Heme Synthesis Inhibition Blocks Angiogenesis via Mitochondrial Dysfunction. *IScience*, *23*(8), 101391.

Shiba-Fukushima K, Arano T, Matsumoto G, Inoshita T, Yoshida S, Ishihama Y, Ryu K-Y, Nukina N, Hattori N, & Imai Y. (2014). Phosphorylation of Mitochondrial Polyubiquitin by PINK1 Promotes Parkin Mitochondrial Tethering. *PLOS Genetics*, *10*(12), e1004861.

Shimura H, Hattori N, Kubo SI, Mizuno Y, Asakawa S, Minoshima S, Shimizu N, Iwai K, Chiba T, Tanaka K, & Suzuki T. (2000). Familial Parkinson disease gene product, parkin, is a ubiquitin-protein ligase. *Nature Genetics*, *25*(3), 302–305.

Shin C-S, Meng S, Garbis SD, Moradian A, Taylor RW, Sweredoski MJ, Lomenick B, & Chan DC. (2021). LONP1 and mtHSP70 cooperate to promote mitochondrial protein folding. *Nature Communications*, *12*(1), 265.

Shiota T, Imai K, Qiu J, Hewitt VL, Tan K, Shen H-H, Sakiyama N, Fukasawa Y, Hayat S, Kamiya M, Elofsson A, Tomii K, Horton P, Wiedemann N, Pfanner N, Lithgow T, & Endo T. (2015). Molecular architecture of the active mitochondrial protein gate. *Science (New York, N.Y.)*, *349*(6255), 1544–1548.

Sian-Hulsmann J, & Riederer P. (2020). The role of alpha-synuclein as ferrireductase in neurodegeneration associated with Parkinson's disease. *Journal of Neural Transmission 2020 127:5*, *127*(5), 749–754.

Siekevitz P. (1957). Powerhouse of the Cell. *Scientific American*, *197*(1), 131–144.

Sjöstrand FS. (1953). Electron Microscopy of Mitochondria and Cytoplasmic Double Membranes: Systems of Double Membranes in the Cytoplasm of Certain Tissue Cell. *Nature*, *171*(4340), 31–32.

Song J, Herrmann JM, & Becker T. (2021). Quality control of the mitochondrial proteome. *Nature Reviews. Molecular Cell Biology*, *22*(1), 54–70.

Srinivasula SM, Ahmad M, Fernandes-Alnemri T, & Alnemri ES. (1998). Autoactivation of Procaspase-9 by Apaf-1-Mediated Oligomerization. *Molecular Cell*, *1*(7), 949–957.

Suen DF, Narendra DP, Tanaka A, Manfredi G, & Youle RJ. (2010). Parkin overexpression selects against a deleterious mtDNA mutation in heteroplasmic cybrid cells. *Proceedings of the National Academy of Sciences of the United States of America*, *107*(26), 11835–11840.

Swenson SA, Moore CM, Marcero JR, Medlock AE, Reddi AR, & Khalimonchuk O. (2020). From Synthesis to Utilization: The Ins and Outs of Mitochondrial Heme. *Cells*, *9*(3).

Szargel R, Shani V, Elghani FA, Mekies LN, Liani E, Rott R, & Engelender S. (2016). The PINK1, synphilin-1 and SIAH-1 complex constitutes a novel mitophagy pathway. *Human Molecular Genetics*, *25*(16), 3476–3490.

Szczepanowska K, Maiti P, Kukat A, Hofsetz E, Nolte H, Senft K, Becker C, Ruzzenente B, Hornig-Do H-T, Wibom R, Wiesner RJ, Krüger M, & Trifunovic A. (2016). CLPP coordinates mitoribosomal assembly through the regulation of ERAL1 levels. *The EMBO Journal*, *35*(23), 2566–2583.

Tan S, & Wong E. (2017). Kinetics of Protein Aggregates Disposal by Aggrephagy. *Methods in Enzymology*, *588*, 245–281.

Thomas PD, Campbell MJ, Kejariwal A, Mi H, Karlak B, Daverman R, Diemer K, Muruganujan A, & Narechania A. (2003). PANTHER: A library of protein families and subfamilies indexed by function. *Genome Research*, *13*(9), 2129–2141.

Tian H-F, Feng J-M, & Wen J-F. (2012). The evolution of cardiolipin biosynthesis and maturation pathways and its implications for the evolution of eukaryotes. *BMC Evolutionary Biology*, *12*(1), 32.

Till A, Lakhani R, Burnett SF, & Subramani S. (2012). Pexophagy: the selective degradation of peroxisomes. *International Journal of Cell Biology*, *2012*, 512721.

Timmons L, Court DL, & Fire A. (2001). Ingestion of bacterially expressed dsRNAs can produce specific and potent genetic interference in Caenorhabditis elegans. *Gene*, *263*(1–2), 103–112.

Ting S-YY, Yan NL, Schilke BA, & Craig EA. (2017). Dual interaction of scaffold protein Tim44 of mitochondrial import motor with channel-forming translocase subunit Tim23. *ELife*, *6*(April).

Tucker K, & Park E. (2019). Cryo-EM structure of the mitochondrial protein-import channel TOM complex at near-atomic resolution. *Nature Structural & Molecular Biology*, *26*(12), 1158–1166.

Tyanova S, Temu T, Sinitcyn P, Carlson A, Hein MY, Geiger T, Mann M, & Cox J. (2016). The Perseus computational platform for comprehensive analysis of (prote)omics data. *Nature Methods*, *13*(9), 731–740.

Valente EMEM, Abou-Sleiman PM, Caputo V, Muqit MMKK, Harvey K, Gispert S, Ali Z, Del Turco D, Bentivoglio AR, Healy DG, Albanese A, Nussbaum R, González-Maldonado R, Deller T, Salvi S, Cortelli P, Gilks WP, … Wood NW. (2004). Hereditary early-onset Parkinson's disease caused by mutations in PINK1. *Science*, *304*(5674), 1158–1160.

van der Laan M, Wiedemann N, Mick DU, Guiard B, Rehling P, & Pfanner N. (2006). A role for Tim21 in membrane-potential-dependent preprotein sorting in mitochondria. *Current Biology : CB*, *16*(22), 2271–2276.

Van Houten B, Woshner V, & Santos JH. (2006). Role of mitochondrial DNA in toxic responses to oxidative stress. *DNA Repair*, *5*(2), 145–152.

Vance JE. (2014). MAM (mitochondria-associated membranes) in mammalian cells: Lipids and beyond. *Biochimica et Biophysica Acta (BBA) - Molecular and Cell Biology of Lipids*, *1841*(4), 595–609.

Vaquer-Alicea J, & Diamond MI. (2019). Propagation of protein aggregation in neurodegenerative diseases. *Annual Review of Biochemistry*, *88*, 785–810.

Vattem KM, & Wek RC. (2004). Reinitiation involving upstream ORFs regulates ATF4 mRNA translation in mammalian cells. *Proceedings of the National Academy of Sciences*, *101*(31), 11269–11274.

Vig S, Lambooij JM, Zaldumbide A, & Guigas B. (2021). Endoplasmic Reticulum-Mitochondria Crosstalk and Beta-Cell Destruction in Type 1 Diabetes. *Frontiers in Immunology*, *12*, 1271.

Villa E, Proïcs E, Rubio-Patiño C, Obba S, Zunino B, Bossowski JP, Rozier RM, Chiche J, Mondragón L, Riley JS, Marchetti S, Verhoeyen E, Tait SWG, & Ricci J-E. (2017). Parkin-Independent Mitophagy Controls Chemotherapeutic Response in Cancer Cells. *Cell Reports*, *20*(12), 2846–2859.

Violot S, Carpentier P, Blanchoin L, & Bourgeois D. (2009). Reverse pH-dependence of chromophore protonation explains the large Stokes shift of the red fluorescent protein mKeima. *Journal of the American Chemical Society*, *131*(30), 10356–10357.

Vives-Bauza C, Zhou C, Huang Y, Cui M, de Vries RLA, Kim J, May J, Tocilescu MA, Liu W, Ko HS, Magrane J, Moore DJ, Dawson VL, Grailhe R, Dawson TM, Li C, Tieu K, & Przedborski S. (2010). PINK1-dependent recruitment of Parkin to mitochondria in mitophagy. *Proceedings Of The National Academy Of Sciences Of The United States Of America*, *107*(1), 378–383.

Vögtle F-NN, Wortelkamp S, Zahedi RP, Becker D, Leidhold C, Gevaert K, Kellermann J, Voos W, Sickmann A, Pfanner N, & Meisinger C. (2009). Global Analysis of the Mitochondrial N-Proteome Identifies a Processing Peptidase Critical for Protein Stability. *Cell*, *139*(2), 428–439.

Wanderoy S, Tabitha Hees J, Klesse R, Edlich F, & Harbauer AB. (2020). Kill one or kill the many: Interplay between mitophagy and apoptosis. *Biological Chemistry*, *402*(1), 73–88.

Wang C, & Youle RJ. (2009, December 1). The role of mitochondria in apoptosis. *Annual Review of Genetics*, Vol. 43, pp. 95–118. NIH Public Access.

Wang W, Chen X, Zhang L, Yi J, Ma Q, Yin J, Zhuo W, Gu J, & Yang M. (2020). Atomic structure of human TOM core complex. *Cell Discovery*, *6*(1), 67.

Wang X, & Chen XJ. (2015). A cytosolic network suppressing mitochondria-mediated proteostatic stress and cell death. *Nature*, *524*(7566), 481–484.

Wang Y, Xu E, Musich PR, & Lin F. (2019). Mitochondrial dysfunction in neurodegenerative diseases and the potential countermeasure. *CNS Neuroscience & Therapeutics*, *25*(7), 816–824.

Wei Y, Chiang WC, Sumpter R, Mishra P, & Levine B. (2017). Prohibitin 2 Is an Inner Mitochondrial Membrane Mitophagy Receptor. *Cell*, *168*(1–2), 224-238.e10.

Weidberg H, Shvets E, & Elazar Z. (2011). Biogenesis and cargo selectivity of autophagosomes. *Annual Review of Biochemistry*, *80*, 125–156.

Weinhäupl K, Lindau C, Hessel A, Wang Y, Schütze C, Jores T, Melchionda L, Schönfisch B, Kalbacher H, Bersch B, Rapaport D, Brennich M, Lindorff-Larsen K, Wiedemann N, & Schanda P. (2018). Structural Basis of Membrane Protein Chaperoning through the Mitochondrial Intermembrane Space. *Cell*, *175*(5), 1365-1379.e25.

West AP, Shadel GS, & Ghosh S. (2011, May 20). Mitochondria in innate immune responses. *Nature Reviews Immunology*, Vol. 11, pp. 389–402. Nature Publishing Group.

Westphal D, Kluck RM, & Dewson G. (2013). Building blocks of the apoptotic pore: how Bax and Bak are activated and oligomerize during apoptosis. *Cell Death & Differentiation 2014 21:2*, *21*(2), 196–205.

Wickham H. (2019). stringr: Simple, Consistent Wrappers for Common String Operations. R package version 1.4.0. *Cran*.

Wickham H, Averick M, Bryan J, Chang W, McGowan L, François R, Grolemund G, Hayes A, Henry L, Hester J, Kuhn M, Pedersen T, Miller E, Bache S, Müller K, Ooms J, Robinson D, … Yutani H. (2019). Welcome to the Tidyverse. *Journal of Open Source Software*, *4*(43), 1686.

Wilke CO. (2020). ggridges: Ridgeline Plots in "ggplot2" R package version 0.5.2. *Cran*.

Williams CC, Jan CH, & Weissman JS. (2014). Targeting and plasticity of mitochondrial proteins revealed by proximity-specific ribosome profiling. *Science (New York, N.Y.)*, *346*(6210), 748–751.

Williamson CD, Wong DS, Bozidis P, Zhang A, Colberg-Poley AM, Colberg-Poley AM, & Colberg-Poley AM. (2015). Isolation of Endoplasmic Reticulum, Mitochondria, and Mitochondria-Associated Membrane and Detergent Resistant Membrane Fractions from Transfected Cells and from Human Cytomegalovirus-Infected Primary Fibroblasts. *Current Protocols in Cell Biology*, *68*(1), 3.27.1-3.27.33.

Wirth M, Karaca S, Wenzel D, Ho L, Tishkoff D, Lombard DB, Verdin E, Urlaub H, Jedrusik-Bode M, & Fischle W. (2013). Mitochondrial SIRT4-type proteins in Caenorhabditis elegans and mammals interact with pyruvate carboxylase and other acetylated biotin-dependent carboxylases. *Mitochondrion*, *13*(6), 705–720.

Wrobel L, Topf U, Bragoszewski P, Wiese S, Sztolsztener ME, Oeljeklaus S, Varabyova A, Lirski M, Chroscicki P, Mroczek S, Januszewicz E, Dziembowski A, Koblowska M, Warscheid B, & Chacinska A. (2015). Mistargeted mitochondrial proteins activate a proteostatic response in the cytosol. *Nature*, *524*(7566), 485–488.

Xiao B, Deng X, Lim GGYY, Xie S, Zhou ZD, Lim K-LL, & Tan E-KK. (2017). Superoxide drives progression of Parkin/PINK1-dependent mitophagy following translocation of Parkin to mitochondria. *Cell Death & Disease*, *8*(10), e3097–e3097.

Xie J, Marusich MF, Souda P, Whitelegge J, & Capaldi RA. (2007). The mitochondrial inner membrane protein mitofilin exists as a complex with SAM50, metaxins 1 and 2, coiled-coil-helix coiled-coil-helix domain-containing protein 3 and 6 and DnaJC11. *FEBS Letters*, *581*(18), 3545–3549.

Yablonska S, Ganesan V, Ferrando LM, Kim J, Pyzel A, Baranova O V., Khattar NK, Larkin TM, Baranov S V., Chen N, Strohlein CE, Stevens DA, Wang X, Chang Y-F, Schurdak ME, Carlisle DL, Minden JS, & Friedlander RM. (2019). Mutant huntingtin disrupts mitochondrial proteostasis by interacting with TIM23. *Proceedings of the National Academy of Sciences of the United States of America*, *116*(33), 16593–16602.

Yan C, Gong L, Chen L, Xu M, Abou-Hamdan H, Tang M, Désaubry L, & Song Z. (2020). PHB2 (prohibitin 2) promotes PINK1-PRKN/Parkin-dependent mitophagy by the PARL-PGAM5-PINK1 axis. *Autophagy*, *16*(3), 419–434.

Yano H, Baranov S V, Baranova O V, Kim J, Pan Y, Yablonska S, Carlisle DL, Ferrante RJ, Kim AH, & Friedlander RM. (2014). Inhibition of mitochondrial protein import by mutant huntingtin. *Nature Neuroscience*, *17*(6), 822–831.

Yoo SH, Kim HY, Rho JH, Jeong SY, Yun J, Yun I, Park HT, & Yoo YH. (2015). Targeted inhibition of mitochondrial Hsp90 induces mitochondrial elongation in Hep3B hepatocellular carcinoma cells undergoing apoptosis by increasing the ROS level. *International Journal of Oncology*, *47*(5), 1783–1792.

Yorimitsu T, & Klionsky D. (2005). Autophagy: molecular machinery for self-eating. *Cell Death and Differentiation*, *12*(Suppl 2), 1542.

Young JC, Hoogenraad NJ, & Hartl FU. (2003). Molecular chaperones Hsp90 and Hsp70 deliver preproteins to the mitochondrial import receptor Tom70. *Cell*, *112*(1), 41–50.

Zhao Q, Wang J, Levichkin I V., Stasinopoulos S, Ryan MT, & Hoogenraad NJ. (2002). A mitochondrial specific stress response in mammalian cells. *The EMBO Journal*, *21*(17), 4411.

Zhao W, Shi F, Guo Z, Zhao J, Song X, & Yang H. (2018). Metabolite of ellagitannins, urolithin A induces autophagy and inhibits metastasis in human sw620 colorectal cancer cells. *Molecular Carcinogenesis*, *57*(2), 193.

Zick M, Rabl R, & Reichert AS. (2009). Cristae formation—linking ultrastructure and function of mitochondria. *Biochimica et Biophysica Acta (BBA) - Molecular Cell Research*, *1793*(1), 5–19.

Zimorski V, Ku C, Martin WF, & Gould SB. (2014). Endosymbiotic theory for organelle origins. *Current Opinion in Microbiology*, *22*, 38–48.

Zurita Rendón O, Shoubridge EA, Rendón OZ, & Shoubridge EA. (2018). LONP1 Is Required for Maturation of a Subset of Mitochondrial Proteins, and Its Loss Elicits an Integrated Stress Response. *Molecular and Cellular Biology*, *38*(20), 1–17.

7 Publication list

7.1 FIRST-/SHARED FIRST-AUTHORSHIP PUBLICATIONS

Large parts of the research presented in this work have been published in the following research article:

Michaelis JB, Brunstein MB, Bozkurt S, Alves L, Wegner M, Kaulich M, Pohl C & Münch C (**2022**). Protein import motor complex reacts to mitochondrial misfolding by reducing protein import and activating mitophagy. *Nat. Comm* (**resubmitted after revision**, 01-2022)

Schäfer JA, Bozkurt S, **Michaelis JB**, Klann K, & Münch C. (**2022**). Global mitochondrial protein import proteomics reveal distinct regulation by translation and translocation machinery. *Molecular Cell*, *82*(2), 435-446.e7.

7.2 CO-AUTHORSHIP PUBLICATIONS RELATED TO THIS PROJECT

Li X, Straub J, Medeiros TC, Mehra C, den Brave F, Peker E, Atanassov I, Stillger K, **Michaelis JB**, Burbridge E, Adrain C, Münch C, Riemer J, Becker T, & Pernas LF. (**2022**). Mitochondria shed their outer membrane in response to infection-induced stress. *Science (New York, N.Y.)*, *375*(6577), eabi4343.

Poluzzi C, Nastase MV, Zeng-Brouwers J, Roedig H, Hsieh LTH, **Michaelis JB**, Buhl EM, Rezende F, Manavski Y, Bleich A, Boor P, Brandes RP, Pfeilschifter J, Stelzer EHK, Münch C, Dikic I, Brandts C, … Schaefer L. (**2019**). Biglycan evokes autophagy in macrophages via a novel CD44/Toll-like receptor 4 signaling axis in ischemia/reperfusion injury. *Kidney International*, *95*(3), 540–562.

Meyer N, Zielke S, **Michaelis JB**, Linder B, Warnsmann V, Rakel S, Osiewacz HD, Fulda S, Mittelbronn M, Münch C, Behrends C, & Kögel D. (**2018**). AT 101 induces early mitochondrial dysfunction and HMOX1 (heme oxygenase 1) to trigger mitophagic cell death in glioma cells. *Autophagy*, *14*(10), 1693–1709.

8 Contributions of co-workers

Except where stated otherwise by reference or acknowledgment, the work presented was generated by myself, Jonas Benjamin Michaelis between 2017 and 2021 under the supervision of my advisors during my doctoral studies. All contributions from colleagues are explicitly referenced in the thesis. The material listed below was obtained in the context of collaborative research:

Figure 14: Genome-wide CRISPR/Cas9 screen identifies protein import gene depletion as driver for mitophagy. Martin Wegner (Kaulich group, Goethe Universität Frankfurt) supported me during the steps of next generation sequencing sample preparation. He handled the next generation sequencing machine and raw data analysis, including cropping of sequencing results and enrichment analysis via the MAGeCK algorithm. I established the reporter cell line, FACS approach, DNA sample preparation for FACS-sorted samples, performed the functional data analysis and final visualization of the data sets. The data will be published in Michaelis et al 2022 (in revision, 2022-01).

Figure 15: Mitophagy CRISPR/Cas9 screen identified novel PINK1-mitophagy-essential genes. Martin Wegner (Kaulich group, Goethe Universität Frankfurt) supported me during the steps of next generation sequencing sample preparation. He handled the next generation sequencing machine and raw data analysis, including cropping of sequencing results and enrichment analysis via the MAGeCK algorithm. I established the reporter cell line, FACS approach, DNA sample preparation for FACS-sorted samples, performed the functional data analysis and final visualization of the data sets.

Figure 17: Loss of PAM components induced mitophagy in *C.elegans*. Collaboration partner Ludovico Alves (Pohl/Eimer group, Goethe Universität Frankfurt). Ludovico Alves performed RNAi experiments of *C.elegans,* microscopy and data analysis. The initial idea to analyze PAM protein import components for their effect in *C.elegans* came from Christian Münchs and me. The data will also be published in Michaelis et al 2022 (in revision, 2022-01).

Figure 21: Mitochondrial protein import reduction is accompanied by mitophagy without the necessity for mitochondrial membrane depolarization. Collaboration partner Süleyman Bozkurt (Münch group,

Goethe Universität Frankfurt) performed TMRE and mePROD^{mt} measurements based on my established protocol. I analyzed and visualized the data. Data will also be published in Michaelis et al 2022 (in revision, 2022-01).

Figure 27: PAM complex sequestered from TIM translocon upon protein folding stress. Collaboration partner Melinda Brunstein (Münch group, Goethe Universität Frankfurt) performed IP-biotin enrichment experiments after the TurboID-proximity labeling and prepared the mass spectrometry samples. I cloned, established the cell line, the experimental idea, performed the experiment in cell culture, harvested the cells and analyzed the data. The data will also be published in Michaelis et al 2022 (in revision, 2022-01).

Figure 28: Upon mitochondrial proteome perturbation, the PAM complex sequestered from the TIM translocon and enriched in the insoluble fraction. Collaboration partner Melinda Brunstein (Münch group, Goethe Universität Frankfurt). Data sets from figure 27, were used in further analysis and clustering by me.

Figure 30: Mitochondrial isolation and organelle-specific SILAC-boosting allows monitoring of mitochondrial translation and protein import. Collaboration partner Süleyman Bozkurt (Münch group, Goethe Universität Frankfurt) used my established protocol to purify mitochondria and performed label-free quantification proteomics on it. I analyzed this data set to show mitochondrial enrichment and visualize which other cellular components were present. Süleyman Bozkurt also used my established mePROD^{mt} protocol to measure the amount of mitochondrial heavy labeled peptides in a two hour SILAC-labeled HeLa mitochondrial extract. He visualized the data as bar graph, as shown in the figure. Data was published in Schäfer, Bozkurt, Michaelis et al 2022.

Figure 35: Compartment selective signal enhancing of translation measurements allows to measure mitochondrial and whole cell translation. Collaboration partner Süleyman Bozkurt (Münch group, Goethe Universität Frankfurt) performed one cell culture experiment and prepared pulsed-SILAC

proteomic samples. He visualized the data as bar graph, as shown in the figure. The workflow and idea were my contribution. Data was published in Schäfer, Bozkurt, Michaelis et al 2022.

Figure 36: CCCP modulates mitochondrial protein import by translation- and import-driven regulation. Jasmin Schäfer and Süleyman Bozkurt (Münch group, Goethe Universität Frankfurt) Jasmin Schäfer performed the data analysis and visualization. Süleyman Bozkurt reloaded my proteomic samples a second time on mass spectrometer. I performed the experiment in cell culture and prepared the proteomic samples. Data was published in Schäfer, Bozkurt, Michaelis et al 2022.

Figure 37: Outer mitochondrial membrane and inter-membrane space protein uptake is regulated by the translation rate. Jasmin Schäfer and Süleyman Bozkurt (Münch group, Goethe Universität Frankfurt) Jasmin Schäfer performed the data analysis and visualization. Süleyman Bozkurt reloaded my proteomic samples a second time on mass spectrometer. I performed the experiment in cell culture and prepared the proteomic samples. The final network representation was also done by me. The data was published in Schäfer, Bozkurt, Michaelis et al 2022.

Hannah Mende (Müller group, Goethe Universität Frankfurt) brought up the idea to use the HaloTag-technology for pulsed-labelling and combine it with mitochondrial extraction. This method was then established by me and used as validation for mePROD^{mt} (Figure 33). Georg Tascher (SFB1177 Z01 *proteomics unit*, Goethe Universität Frankfurt) handled most of the mass spectrometry machine work with technical assistance of Martin Adrian-Allgood (Münch group, Goethe Universität Frankfurt). The development of mePROD^{mt} (see Chapter "4.3 Development of a measurement for global mitochondrial protein import") was built on the previous work of Kevin Klann (Münch group, Goethe Universität Frankfurt). He also supported the project by scientific discussions.

9 Supplements

Supplementary table 1: Most enriched genetic deletions which induced mitophagy in CRISPR/Cas9 screen. Data filtered for 1000-fold p<0.05 enriched candidates with at least three enriched gRNAs. HeLa FlpIn mt-*mKEIMA* with inducible *PRKN* expression used. Cells sorted eight days after gRNA library transduction by FACS and compared to unsorted population.

Gene ID	log_{10} sorted/total population	RRA score	p-value	gRNAs enriched
UROD	6.401	3.74E-11	2.46E-07	4
RFC3	6.049	9.99E-08	1.72E-06	3
TCEB2	5.453	5.14E-08	1.23E-06	4
SAMM50	5.053	3.97E-06	1.35E-05	3
DNAJC11	4.811	1.42E-09	2.46E-07	4
GRPEL1	4.538	9.66E-06	3.99E-05	4
RPL17	4.268	6.64E-06	2.53E-05	4
LONP1	4.260	4.37E-06	1.45E-05	4
TELO2	4.127	2.34E-07	2.22E-06	4
VPS13D	4.074	4.43E-06	1.45E-05	4
TUBGCP2	4.068	8.75E-05	3.42E-04	3
TUFM	3.901	3.23E-04	1.18E-03	4
PMPCB	3.883	1.91E-04	7.20E-04	4
EXT1	3.853	2.81E-04	1.03E-03	3
MED30	3.725	5.12E-04	1.91E-03	3
PHF5A	3.717	2.67E-05	1.12E-04	3
HSPA8	3.709	1.35E-04	5.17E-04	3
ANAPC11	3.658	4.52E-05	1.81E-04	4
ORC6	3.600	3.63E-04	1.33E-03	3
KRCC1	3.578	1.52E-04	5.87E-04	3

ELOC	3.570	7.60E-04	2.78E-03	3
PINK1	3.562	5.27E-04	1.97E-03	3
TOMM40	3.555	3.18E-04	1.16E-03	3
NCBP1	3.543	1.47E-03	5.32E-03	3
PLRG1	3.498	2.89E-04	1.06E-03	3
KIF22	3.494	2.49E-04	9.24E-04	3
TUBD1	3.487	8.56E-05	3.36E-04	3
MYC	3.463	7.66E-06	2.93E-05	3
HSPA9	3.442	5.83E-03	2.01E-02	3
BUB1	3.439	1.41E-04	5.45E-04	3
POLRMT	3.435	3.31E-05	1.33E-04	3
C11orf74	3.422	5.16E-04	1.92E-03	3
PISD	3.375	9.49E-05	3.62E-04	4
FECH	3.372	2.53E-05	1.07E-04	4
PRKDC	3.343	7.13E-06	2.76E-05	3
POLE	3.333	8.11E-04	2.96E-03	3
OR8B4	3.295	4.96E-04	1.84E-03	3
EIF3I	3.294	1.24E-03	4.55E-03	3
C1D	3.253	7.73E-04	2.83E-03	3
VHL	3.253	3.34E-04	1.22E-03	4
RBBP4	3.252	4.51E-04	1.67E-03	3
PLEKHA3	3.250	1.52E-03	5.50E-03	4
UBE2U	3.249	2.47E-04	9.19E-04	4
NME3	3.231	6.25E-04	2.32E-03	3
IFIT5	3.224	1.28E-03	4.70E-03	3
POLD3	3.206	8.40E-04	3.07E-03	3

TBL3	3.189	1.55E-03	5.61E-03	3
TRAPPC1	3.174	4.14E-03	1.45E-02	4
DYX1C1	3.172	7.65E-04	2.80E-03	3
ZNF493	3.170	5.83E-04	2.16E-03	3
TPM3	3.167	6.07E-04	2.25E-03	3
ZBTB18	3.158	2.88E-03	1.02E-02	3
CTR9	3.156	2.04E-05	8.24E-05	4
CD109	3.138	2.19E-03	7.86E-03	3
CRHR1	3.125	7.31E-04	2.69E-03	4
RAB30	3.105	8.90E-04	3.26E-03	4
APTX	3.094	4.02E-04	1.47E-03	3
KAT2A	3.079	1.40E-03	5.10E-03	3
AFG3L2	3.078	2.17E-04	8.11E-04	3
TIMM13	3.051	1.40E-03	5.11E-03	4
DAGLA	3.051	4.53E-03	1.58E-02	3
NAA50	3.048	6.33E-03	2.18E-02	3
OMA1	3.037	1.72E-03	6.21E-03	3
KIAA1024	3.036	1.62E-03	5.83E-03	3
PLEKHG4B	3.022	2.09E-03	7.50E-03	4
GIMAP8	3.016	3.22E-05	1.31E-04	4
KANSL3	3.005	6.76E-04	2.49E-03	4
MZF1	3.002	3.21E-04	1.17E-03	3

Supplementary table 2: GTPP does not significantly increase HSPD1 or HSPE1 in whole cell or mitochondria. Total protein quantification of pulsed-SILAC labeled cells, which were treated for 6h with GTPP. The whole cell proteome was generated from whole cell lysates and the mitochondrial proteome by the crude extraction of mitochondria. Statistical significance was calculated by two-sided unpaired t-testing for n=3 replicates.

	GENE SYMBOL	LOG_2 GTPP/ DMSO	P-VALUE
WHOLE CELL PROTEOME	*HSPE1*	-0.040	0.280
	HSPD1	0.009	0.811
MITOCHONDRIAL PROTEOME	*HSPE1*	-0.307	0.256
	HSPD1	-0.203	0.399

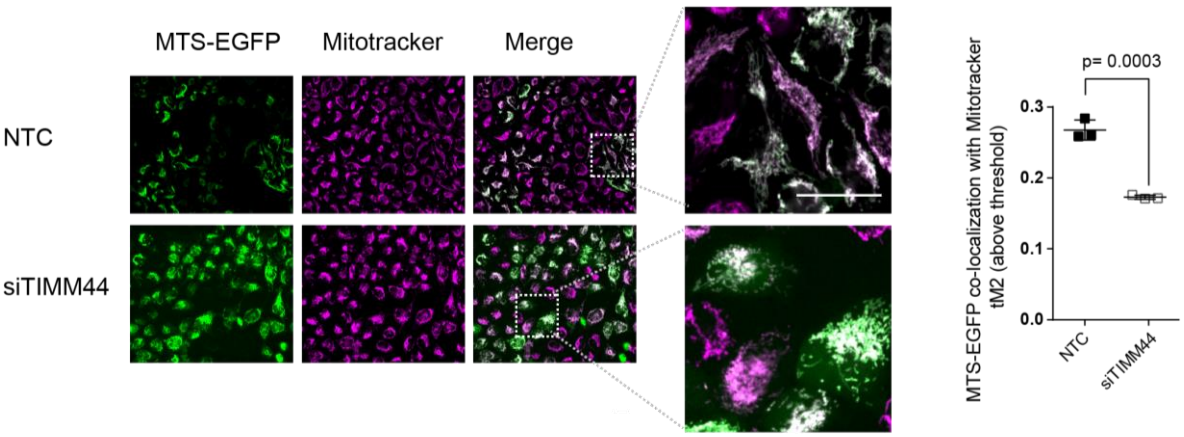

Supplementary Figure 1: *TIMM44* depletion decreases matrix-targeted protein import. HeLa FlpIn TRex cells with inducible *MTS-EGFP* and *PRKN* expression were treated with *TIMM44* or *NTC* siRNA for 96 h. Dox was added 15 h before microscopy (to induce *MTS-EGFP* and *PRKN*). Mitochondrial localization of EGFP was analyzed via staining with Mitotracker Deep Red FM and live cell imaging. Scale bar 25 µm. The NTC is the same as in Figure 19C.

10 Acknowledgement

I would like to first thank Christian, my direct supervisor for the last five years. We worked together on projects that eventually led to this thesis and several publications. Thank you for the freedom and trust you put in me to pursue my ideas, to establish novel experiments and to write my publications. These were not easy tasks, but I have grown as a person and as a scientist.

This process would not have been possible without the support of my friends and family. Therefore, big thanks go to my colleagues from the Münch, Müller and Bremm group; for many discussions of my data, company on long work days and support during experiments. Here I would like to mention especially Hannah, Jasmin, Mila, Verena and Süleyman. Thanks also go to all other colleagues from the IBCII, Kaulich and Dikic group for a good work environment. Furthermore, I would like to thank all collaboration partners and co-authors, who also set me up broadly in terms of topics and took work off my hands, here I would especially like to mention Ludovico Alves, Martin Wegner, Melinda Brunstein, Jasmin Schäfer, Süleyman Bozkurt, Christian Pohl, Manuel Kaulich, Nina Meyer and Donat Kögel.

I would also like to thank Prof. Dr. Volker Dötsch for evaluating this work. I would also like to thank all other members of the examination board for their time and interest in my work, as well as my thesis advisory committee.

Big thanks also go to my girlfriend Linda, who supported me especially in the process of writing, took a lot of other work off my hands and also proofread this thesis. I know I often had little time for us, so thank you for your understanding and patience.

Furthermore, I don't want to forget my colleagues Hannah Mende, Alexandra Hertel, Rebecca George Tharyan and Jasmin Schäfer, who took the time to read my thesis and provided me with many helpful comments.

In addition, thanks also go to the SFB1177 for Autophagy, which funded my position during the project, and the proteomics unit with especially Georg Tascher, who made many mass spectrometric measurements possible.

Without all of you, I would not have been able to complete this work.

Thank you all for that!